1. Report No. FHWA/TX-04/0-1896-1	2. Government Accession No.	3. Recipient's Catalog No.
4. Title and Subtitle Field Measurements of Diaphragm and Top Lateral Members of Three Trapezoidal Composite Box Girder Bridges		5. Report Date December 2002
		6. Performing Organization Code
7. Author(s) Benjamin A. Cheplak, Matthew A. Memberg, Karl H. Frank, and Joseph A. Yura		8. Performing Organization Report No. Research Report 0-1896-1
9. Performing Organization Name and Address Center for Transportation Research The University of Texas at Austin 3208 Red River, Suite 200 Austin, TX 78705-2650		10. Work Unit No. (TRAIS)
		11. Contract or Grant No. Research Project 0-1896
12. Sponsoring Agency Name and Address Texas Department of Transportation Research and Technology Implementation Office P.O. Box 5080 Austin, TX 78763-5080		13. Type of Report and Period Covered Research Report
		14. Sponsoring Agency Code

15. Supplementary Notes

Project conducted in cooperation with the U.S. Department of Transportation, Federal Highway Administration, and the Texas Department of Transportation.

16. Abstract

The results of field tests on three trapezoidal box girder bridges are presented. The study concentrated on the measurement of the strains in the external and internal diaphragms and the top laterals of the boxes. The strains were collected when the girders were loaded by a crane lifting up on the girders before placement of the deck, during the casting of the deck, and under truck loading after hardening of the deck. The measured results were compared with a three-dimensional finite element model of the bridge. The measured forces in the diaphragms were very low and generally much lower than predicted from the finite element analysis. This was partially due to the flexibility of the connections to the girder and the connection of the diaphragms to flanges in the model. The forces in the top laterals, which are used to produce a semi-closed section prior to hardening of the deck, were much smaller then predicted by the non-composite finite element model. The concrete deck hardened during the concrete placement and within hours after placement was acting compositely with the steel girder. The external diaphragms and the top lateral forces were very small during the truck load tests of the composite bridge. The stiff slab provided a closed section that replaced the structural function of the top laterals and provided a continuous connection between the girder that eliminated the structural function of the external diaphragms.

17. Key Words box girders, diaphragm, lateral systems, field tests, composite bridges	18. Distribution Statement No restrictions. This document is available to the public through the National Technical Information Service, Springfield, Virginia 22161.		
19. Security Classif. (of report) Unclassified	20. Security Classif. (of this page) Unclassified	21. No. of pages 126	22. Price

Form DOT F 1700.7 (8-72)   Reproduction of completed page authorized

Field Measurements of Diaphragm and Top Lateral Members of Three Trapezoidal Composite Box Girder Bridges

by

Benjamin A. Cheplak, Matthew A. Memberg,
Karl H. Frank, and Joseph A. Yura

Research Report 0-1896-1

Research Project 0-1896

FIELD MONITORING OF TRAPEZOIDAL STEEL BOX BEAMS

ACKNOWLEDGEMENTS

DISCLAIMER

NOT INTENDED FOR CONSTRUCTION,

PERMIT, OR BIDDING PURPOSES

K. H. Frank, P.E, Texas No. 48953

J. A. Yura, P.E, Texas No. 29859

Research Supervisors

TABLE OF CONTENTS

LIST OF FIGURES

LIST OF TABLES

SUMMARY

The results of field tests on three trapezoidal box girder bridges are presented. The study concentrated on the measurement of the strains in the external and internal diaphragms and the top laterals of the boxes. The strains were collected when the girders were loaded by a crane lifting up on the girders before placement of the deck, during the casting of the deck, and under truck loading after hardening of the deck. The measured results were compared with a three-dimensional finite element model of the bridge. The measured forces in the diaphragms were very low and generally much lower than predicted from the finite element analysis. This was partially due to the flexibility of the connections to the girder and the connection of the diaphragms to flanges in the model. The forces in the top laterals, which are used to produce a semi-closed section prior to hardening of the deck, were much smaller then predicted by the non-composite finite element model. The concrete deck hardened during the concrete placement and within hours after placement was acting compositely with the steel girder. The external diaphragms and the top lateral forces were very small during the truck load tests of the composite bridge. The stiff slab provided a closed section that replaced the structural function of the top laterals and provided a continuous connection between the girder that eliminated the structural function of the external diaphragms.

CHAPTER 1:
INTRODUCTION

1.1 BACKGROUND

Trapezoidal steel box girders are often used for curved bridges due to their high torsional rigidity and aesthetic appeal. A conventional twin box girder system is designed with a cast-in-place concrete deck. The deck acts compositely with the steel U-shaped girders through the use of shear studs on the top flanges of the girders. This adds significant stiffness to the bridge as it completes two closed box girders. Figure 1.1 shows the cross section of a trapezoidal box girder system.
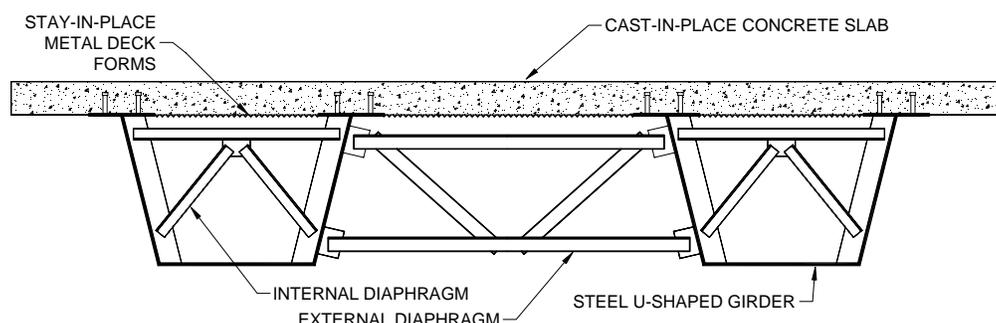
Figure 1.1 Cross section of Trapezoidal Box Girder System

For stability during construction, the top flanges of each girder require bracing. Also, to limit twisting distortions between one box girder and the other during construction, external cross frames or diaphragms are often temporarily installed between the girders at intermediate points along the span. The forces in the top lateral bracing and external diaphragms were investigated during this study.

1.2 BRIDGES UNDER STUDY

Trapezoidal steel box girders were used for the addition of overpasses at the intersection of IH-35 and US 290 in Austin, TX. The overpasses were erected over heavy traffic and required sharp curves with long spans. Each overpass uses concrete U-beams for the straight on-ramps and steel box girders for the curved portions. The Texas Department of Transportation (TxDOT) designed the girders and the contractor, J. D. Abrams, Inc., was responsible for the construction of the interchange. Trinity Industries, Inc. fabricated the steel girders in Houston, TX.

The overpasses chosen for this study were Direct Connect Z, which connects eastbound RM 2222 with southbound IH-35; Direct Connect K, which connects southbound IH-35 with eastbound US 290; and Direct Connect Y, which connects northbound IH-35 with eastbound US 290. These overpasses are shown in Figure 1.2.
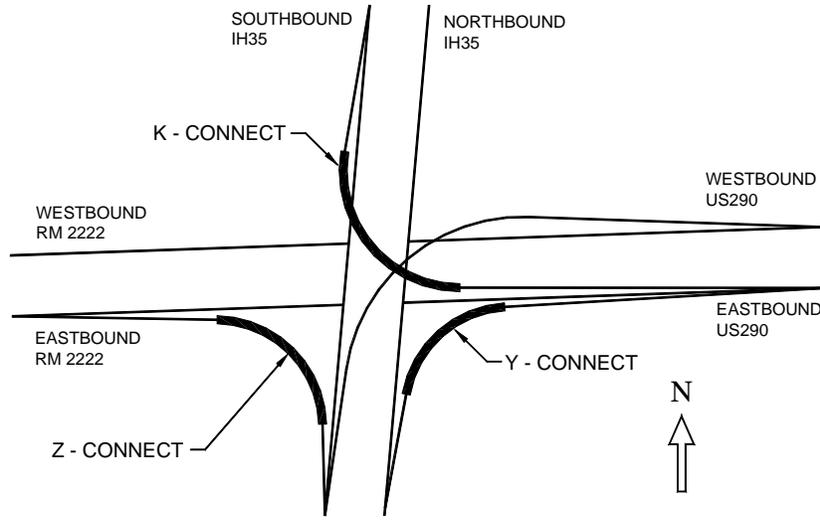
Figure 1.2 Site Location

1.2.1   Z-Connect Dimensions

The steel portion of Z-connect consists of one three-span bridge followed by a two-span bridge. The three-span bridge was under investigation and is shown below in Figure 1.3. The top laterals, internal diaphragms, and external diaphragms can be seen in Figure 1.4. The symmetrical bridge has two side spans of about 150 ft in length and a middle span of 190 ft. The radius of the centerline of the bridge is 450 ft.

Figure 1.5 shows the dimensions of the girder cross section. The top and bottom flanges vary in thickness along the length of the bridge (Appendix A). Internal diaphragms (Figure 1.6), which prevent warping of the trapezoidal cross section of the girder due to torsion, are spaced approximately every 20 feet. Solid plates with stiffeners are used as internal diaphragms at the end piers. Plates with access holes and stiffeners are located at the intermediate piers (Figure 1.7).

A top lateral truss fastened to the top flanges of each girder was used to increase the torsional stiffness of the steel section during construction. This truss system forms a "quasi-closed" box section. The top laterals (Figure 1.) are WT7x21.5 sections and are designed to resist torsion. These members also have stresses due to bending although these stresses are not considered in design (Fan and Helwig, 1999).
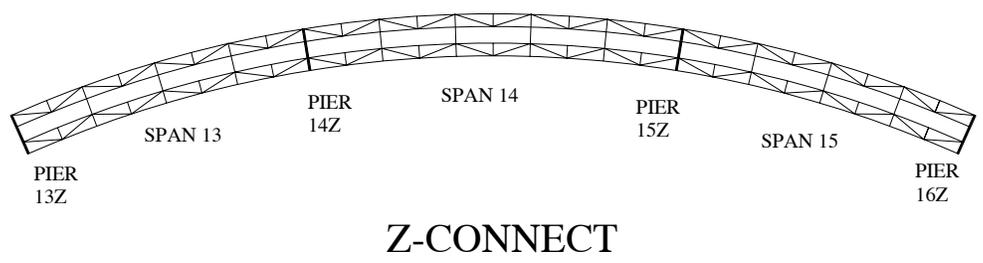
Figure 1.3 Plan View of Bridge under Study
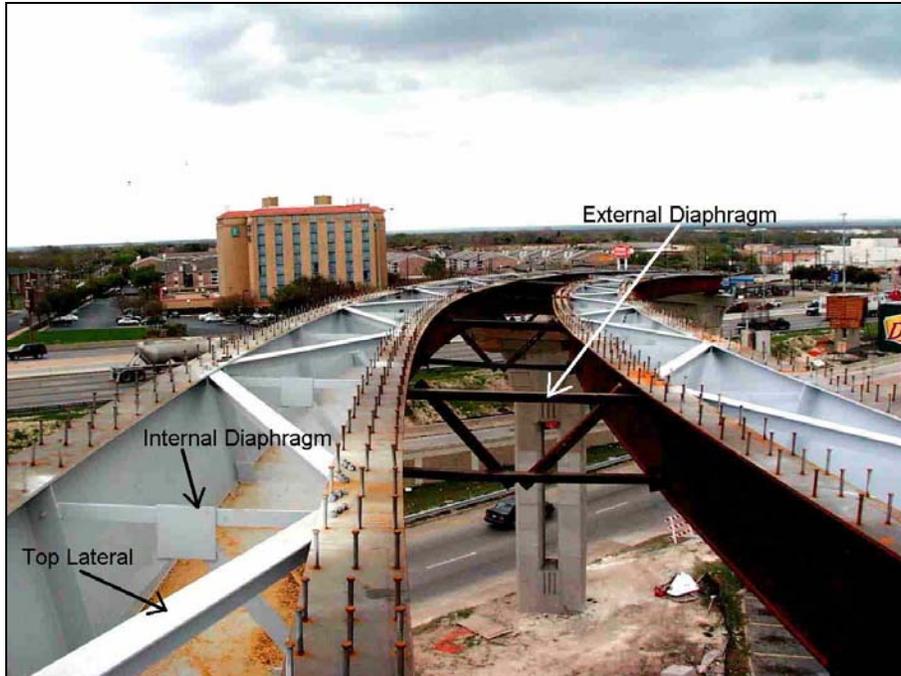
Figure 1.4 Picture of Z-Connect During Construction
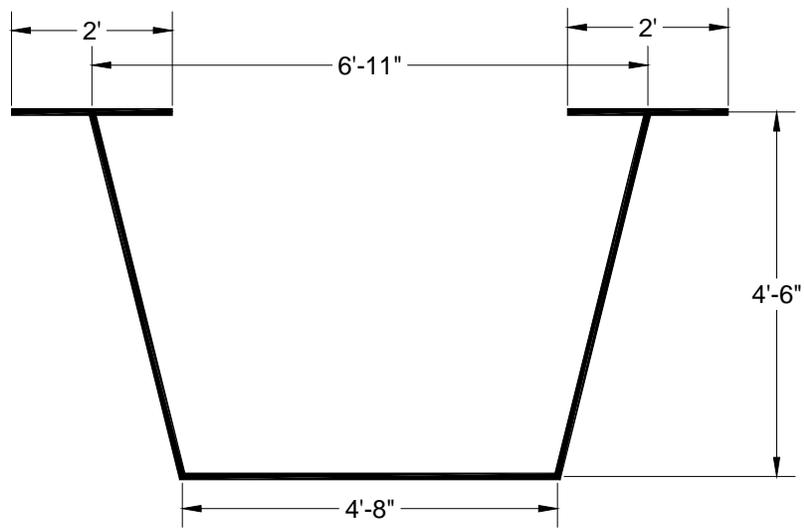
Figure 1.5 Girder Cross Section
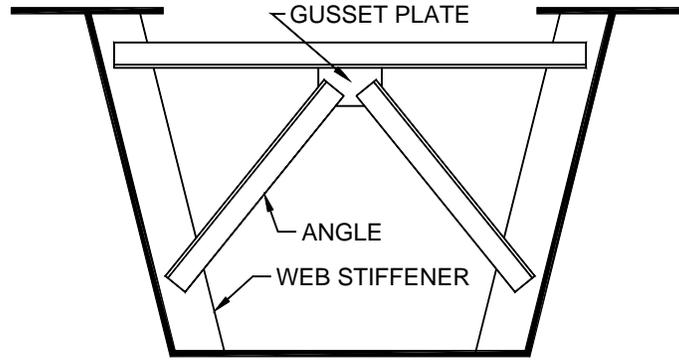
Figure 1.6 Intermediate Internal Diaphragm
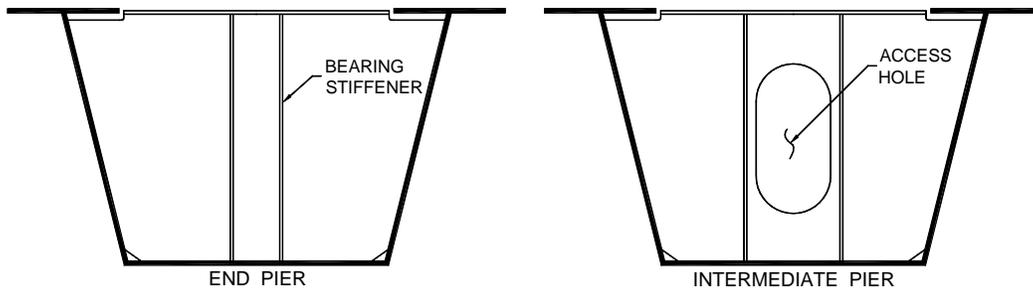
Figure 1.7 End and Pier Diaphragms

1.2.2   Erection Procedure

Each girder was delivered to the site in 90-110 ft sections. The beam sections for each girder were erected according to their piece number shown in Figure 1.8. Field splices were bolted as the girders were supported by a combination of shore towers and cranes. Pier diaphragms and intermediate external diaphragms were installed after the inner and outer girders were in place. The intermediate external diaphragms were attached at every other internal diaphragm location (approximately 40 feet) to control distortions between the two girders during the concrete pour. All external diaphragms between piers were removed after the concrete deck hardened for aesthetic reasons and fatigue concerns.
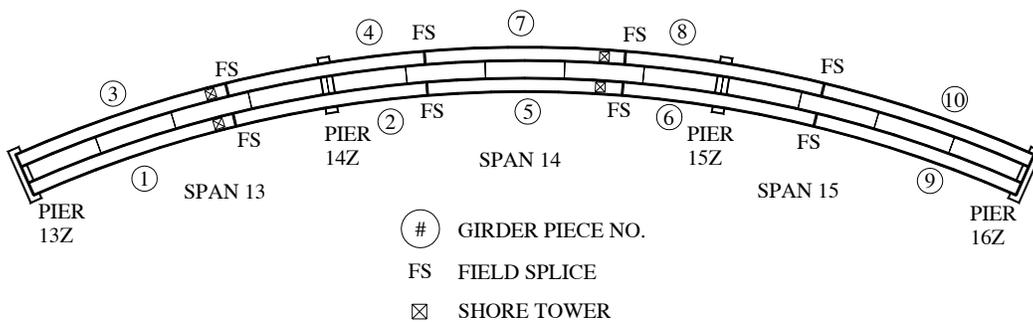
Figure 1.8 Bridge Assembly Sequence

1.2.3   K-Connect Dimensions

The steel portion of K-Connect has three spans with a radius of curvature of approximately 575 feet at the centerline of the cross-section. The curved portion of the bridge is symmetric; end spans 17 and 19 are of equal length. Figure 1.9 shows the bridge in plan view.

The locations of the internal diaphragms, top lateral bracing, and external diaphragms are also shown in Figure 1.9. The internal diaphragms are spaced approximately every 16 feet. The location of an internal diaphragm is also known as a panel point. The external diaphragms, made up of L5x5x^1/$_2$ members were placed at every other panel point. WT8x33.5 members were used for all top lateral bracing. As in Z-Connect, solid plates with stiffeners are used as internal diaphragms at the end piers, and plates with access holes and stiffeners are located at the intermediate piers. Figure 1.10 shows the dimensions of the girder cross-section. The girders were erected by a similar procedure as in Z-Connect.
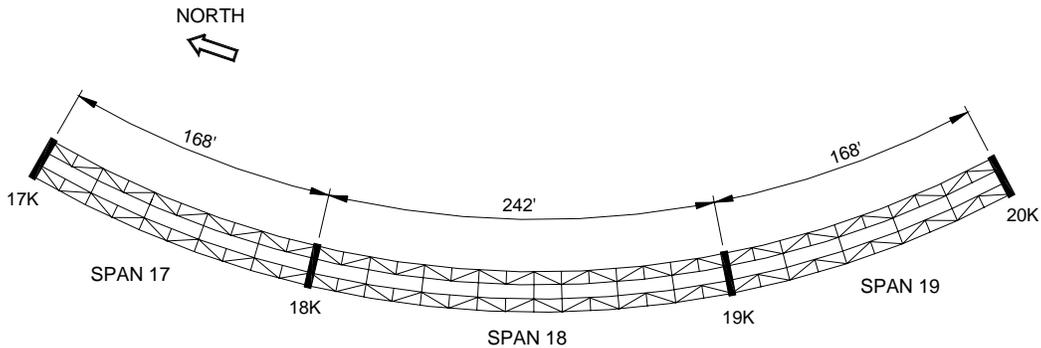
Figure 1.9 Bridge K Dimensions
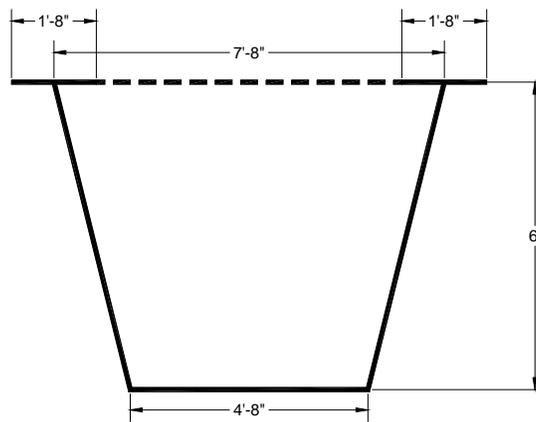
Figure 1.10 K Girder Dimensions

1.2.4   Y-Connect Dimensions

The steel portion of Y-Connect consists of four spans and has a straight portion and a curved portion with a radius of curvature of approximately 460 feet at the centerline of the cross-section. End spans 1 and 4 are of equal length, and middle spans 2 and 3 have equivalent length. The curved portion begins in the middle of span 2. Figure 1.11 shows the bridge in plan view.

The locations of the internal diaphragms, top lateral bracing, and external diaphragms are also shown in Figure 1.11. The internal diaphragms are spaced approximately every 17 feet. The external diaphragms, made up of L5x5x$^1/_2$ members were placed at every other panel point. WT8x33.5 members were used for all top lateral bracing. As in Z-Connect, solid plates with stiffeners are used as internal diaphragms at the end piers, and plates with access holes and stiffeners are located at the intermediate piers. Figure 1.12 shows the dimensions of the girder cross-section. The girders were erected by a similar procedure as Connects Z and K.
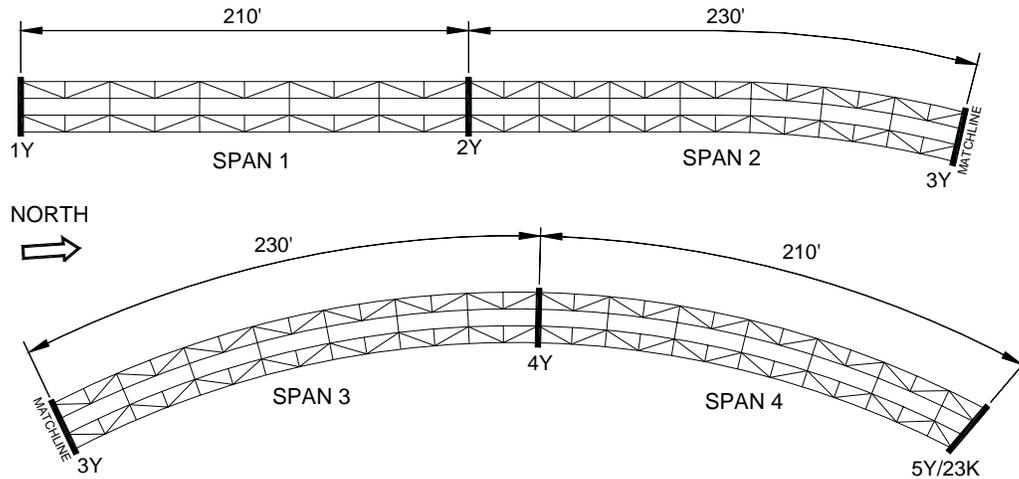
Figure 1.11 Bridge Y Dimensions
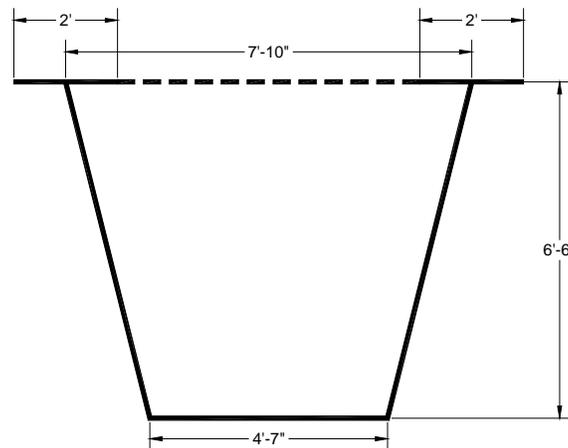
Figure 1.12 Y Girder Dimensions

1.3   EXTERNAL DIAPHRAGM DESIGN

In typical I-girder construction, intermediate cross frames or diaphragms are necessary to control lateral flange bending stresses and to provide stability for the girders. These diaphragms act as primary load-carrying elements due to the interaction of bending and torsion in the girders. Preliminary design equations can be used to estimate the necessary diaphragm spacing using parameters such as span length, girder radius of curvature, and girder flange width (Davidson et al., 1996).

For U-girder design, a combination of internal diaphragms and lateral bracing can be used to control the warping stresses and the stability of the girders (Chen, 1999). These members form the girder into a quasi-closed section. A closed cross section can have over a thousand times greater torsional stiffness than a similar open section, such as an I-girder (Basler and Kollbrunner, 1969). Therefore, intermediate external diaphragms are not as essential as major load-carrying elements on box girders as they are in I-girders. The primary function of these members is to control distortions between the box girders during construction. Trapezoidal box girders have been successfully built with external diaphragms only at the piers (Fan, 1999)

Currently, the AASHTO (American Association of State Highway and Transportation Officials) *Guide Specifications for Horizontally Curved Highway Bridges* (1993) does not require the use of external diaphragms between box girders. There are no provisions for the design of external diaphragms. However, internal diaphragms are specified according to Section 2.28:

> *Intermediate diaphragms or cross frames within each box girder shall be required to limit the normal stresses and the transverse bending stresses due to distortion... The longitudinal spacing and stiffness of such diaphragms, if required, shall be determined using a rational analysis.*

External diaphragms are discussed in the commentary section 10.2.3 of the NCRHP (National Cooperative Highway Research Program) *Recommended Specifications for Steel Curved-Girder Bridges* (1998), which states:

> *External bracing at other than support points is usually not necessary. If analysis shows that the boxes will rotate excessively when the deck is placed, temporary external bracing may be desirable.*

As an additional aid in the design of the external diaphragms, TxDOT engineers referred to section 10 of the Colorado Department of Transportation *Bridge Design Manual*. It recommends the following for box girders:

> *When the radius of curvature, R, is less than 1000 feet, temporary external diaphragms shall be provided at every internal cross frame…. These temporary frames serve to unify the overall action of the steel box girders during deck pouring while also providing additional restraint for temperature effects.*

The diaphragms were designed using angle members since they were the most economical shape. The angle size was determined by satisfying kL/r requirements in AASHTO Guide Specifications.

Finite-element analysis tools capable of modeling the details of the complex geometry and loading of curved girders are available. However, this type of analysis is complicated and is usually costly and time consuming. In addition, further testing and work with finite-element analysis is needed to determine its reliability in predicting the behavior of curved bridges.

1.4 SCOPE

The work presented was part of research project 1896, "Field Monitoring of Steel Trapezoidal Box Girders." The research was funded by TxDOT and mainly focused on the field monitoring of the external diaphragms that connect the two box girders and the top flange lateral bracing system. Forces in the top lateral bracing system were measured and results from these members were used to establish the distribution of forces between the two girders.

The field testing research was conducted in conjunction with analytical work using a finite element model (herein referred to as FEM). The analytical model is described in detail in Section 1.5. Forces were measured in the external diaphragms and were compared with the analytical model throughout different loadings during construction. The aim of the research was to provide a better understanding of the

function of the diaphragms and determine their necessity. It is important to minimize the number of external diaphragms due to their added cost for design, fabrication, installation and removal.

For this study, stresses in the external diaphragms and top laterals were monitored through three main loadings on the separate bridges. The first was a full-scale load test conducted on Z-Connect using a crane to lift the girders before the concrete deck was placed. The test setup and results will be discussed in Chapter 3. Chapter 4 will focus on the second loading, the concrete deck placement of Connects Z, K, and Y. The third loading was a live load test performed on Connects Z and K with trucks on the composite girder bridge (Chapter 5).

1.5 ANALYSIS USING FINITE ELEMENT MODEL

1.5.1 Finite Element Model Description

The three bridges were analyzed by a commercially available finite element code called ABAQUS. Three-dimensional models[1] were prepared using the dimensions given in the design drawings. The structural components were modeled with shell, beam, and brick elements. Eight node quadratic shell elements with reduced integration (S8R5) were used to model the top and bottom flanges, webs and pier diaphragms. Four shell elements were used in webs and bottom flanges, whereas two shell elements were used for each top flange. Three dimensional 2-node linear beam elements (B31) were used to model internal diaphragms, external diaphragms, and top lateral bracing members. Three-dimensional 20-node quadratic bricks (C3D20) were used to model the concrete deck. No deformation was allowed between flange and deck.

Eight shell elements were employed between each internal brace locations. One and twenty brick elements were used along the thickness and width of the deck, respectively. All analyses were linear. Figure 1.13 shows a portion of the composite bridge model.

1.5.2 FEM Studies Prior to Construction

Originally, each bridge was designed to have intermediate external diaphragms installed at every panel point; for example, Z-Connect was designed to have 23 diaphragms installed every 20 feet. Further analysis with the FEM showed that the number of diaphragms in each bridge could be reduced; for Z-Connect, the 23 diaphragms every 20 feet could be reduced to 10 diaphragms at 40 feet (Figure 1.14). There was very little difference in the relative displacements between the girders when using 23 external diaphragms compared to 10 diaphragms. A system using only four external diaphragms was also investigated; relative displacements between the girders significantly increased using this system compared to the 23-diaphragm system. Based upon the analysis results, TxDOT agreed to only install every other diaphragm that was originally designed in each of the four overpasses. This reduction saved construction time and fabrication costs since fewer diaphragms were installed and then removed. The FEM was also used to refine the lengths of each segment during concrete placement to minimize the top lateral forces.

---

[1]Analysis and description of models provided by Cem Topkaya, PhD candidate (2001), The University of Texas at Austin
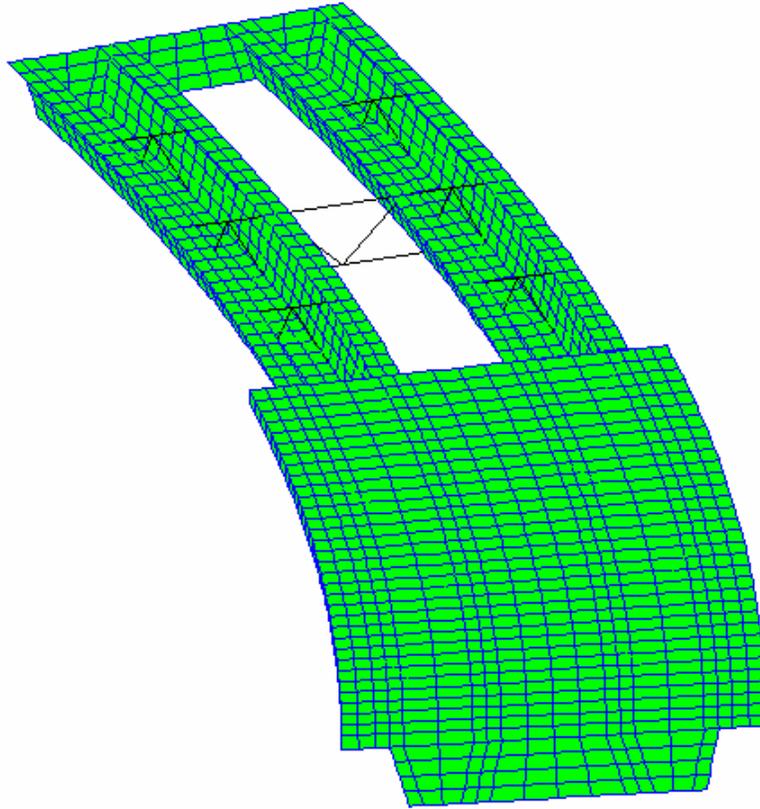
Figure 1.13 Section of Finite Element Model

23 External Diaphragms

10 External Diaphragms
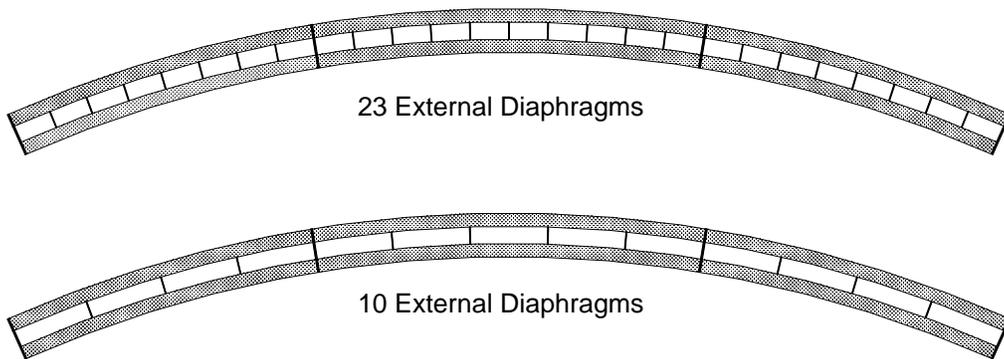
Figure 1.14 Reduction in External Diaphragms in Z-Connect

The FEM was also used to predict the forces in the external diaphragms and top lateral bracing system due to different types of loading, including the field tests. The measured forces are compared to the predicted forces from the FEM.

CHAPTER 2:
INSTRUMENTATION

2.1   INTRODUCTION

This chapter presents the procedures of the field studies conducted during the construction of a curved steel box girder bridge. A description of the data acquisition system, calibration of the system, and results from lab tests will be discussed in this chapter. The reliability of the data that was collected from the field study will also be discussed.

2.2   DATA ACQUISITION SYSTEM

The majority of the field data was measured using a Campbell Scientific 21X Micrologger and a 23X Micrologger. Several AM416 Multiplexers were connected to the 21X and 23X in the field to increase the number of channels that could be read. 12-volt deep-cycle marine batteries that were charged by solar panels powered the systems. In series with the solar panels, regulators were installed to insure that the batteries were not overcharged. Since the systems were not always easily accessible, modems and cell phones were connected to the dataloggers. This setup allowed for data to be collected using cellular communication from a remote site. The modems were activated at specified times for short intervals to prevent excessive power drain. A schematic of the basic system is shown in Figure 2.1.
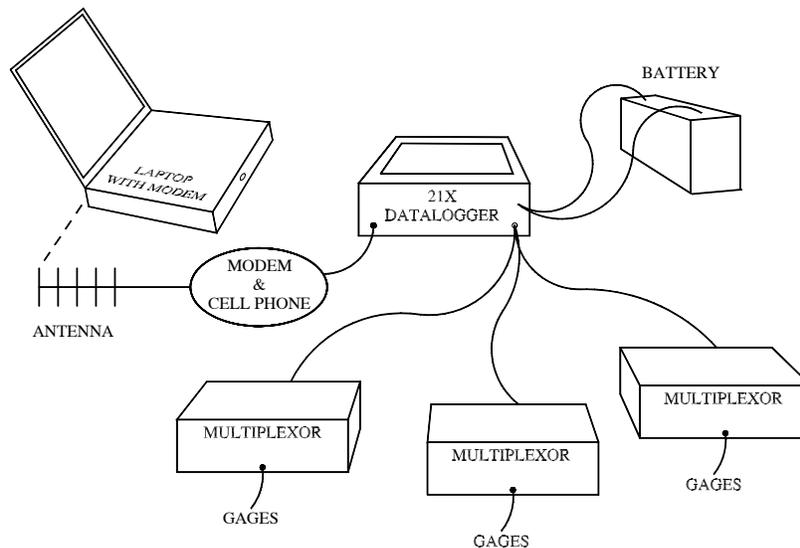
Figure 2.1 Overview of Data Acquisition System

A multiplexer can read up to 16 different channels sequentially. All of the measurements in the study were taken by strain gages that were temperature compensated for steel. After bonded to the steel, the gage's resistance changes in proportion to the strain in the member. The gage is wired in a full bridge configuration (Figure 2.2) with three precision resistors. If an excitation is applied to the full bridge, a change in gage resistance will change the voltage across the bridge. The 21X and 23X record an output voltage, V_o, divided by the bridge excitation, V_{exc}. The strain, ε, can then be calculated using the equation $\varepsilon = 4 \times V_o \div (GF \times V_{exc})$, where GF is the gage factor.
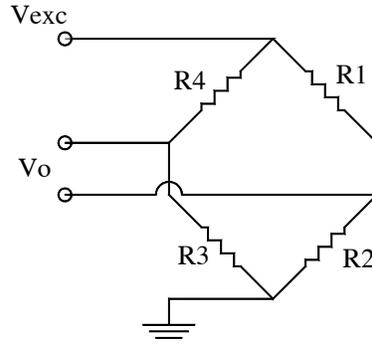
Figure 2.2 Full Bridge Configuration

Since the gages are temperature compensated, the strain in the steel due to temperature changes will produce little or no change in gage resistance and therefore no apparent strain. If the steel changes temperature and is not allowed to expand or contract accordingly, then an apparent strain will be read in the gage.

Since the gages would be exposed to the elements for a long period of time, wax and sealant were applied to the gage as weather protection. Also, mechanical protection such as plywood, steel angle, and steel plate surrounded the instrumentation to prevent damage during the erection of the bridges (Figure 2.3 and Figure 2.4).
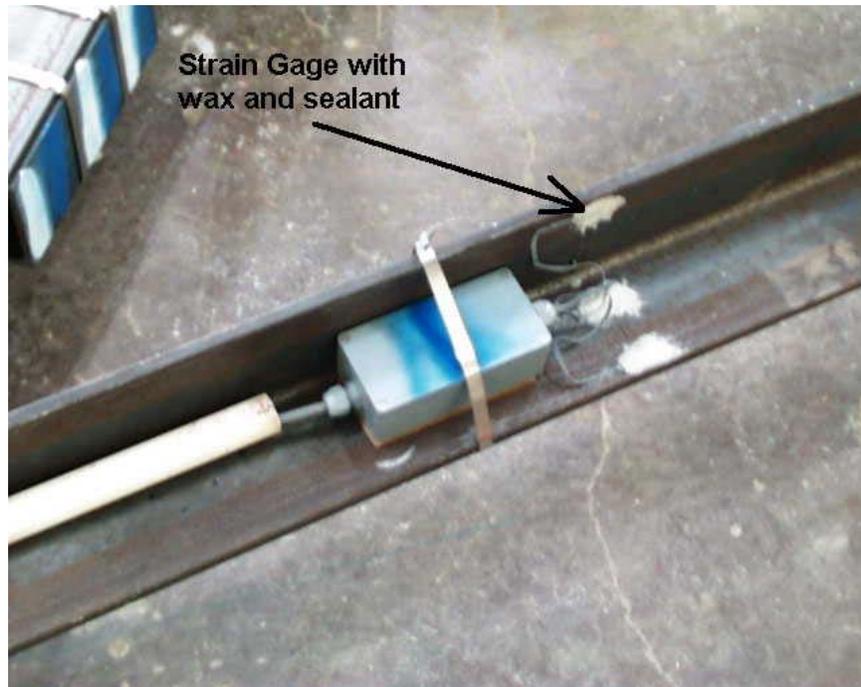
Figure 2.3 Installed Gages on Angle Member

Figure 2.4 Instrumentation Protection

2.3   LAB TEST ON ANGLE MEMBER

Using the common assumption in mechanics that plane sections remain plane, the axial force and biaxial bending moments in a member can be calculated with a minimum of three strain measurements at a cross section. Lab tests were performed on angle members to determine a reliable strain gage configuration. Eight strain gages were installed on a 5ft long L5x5x3/8 member as shown in Figure 2.5. This member is similar to the angles used on the external diaphragms (L5x5x1/2).
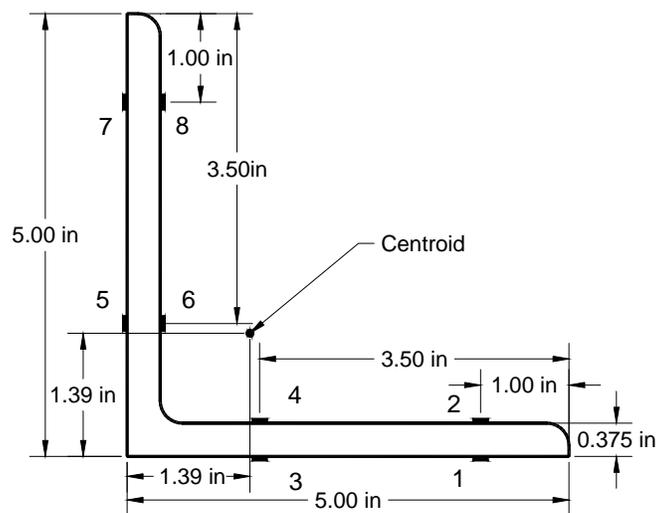
Figure 2.5 Strain Gage Configuration of Angle for Lab Test

13

Steel tabs were welded to the outside of one angle leg at both ends that could fit into the test machine grips. The angle was loaded eccentrically, simulating the angle connection on the external diaphragm. The gaged cross section was located at the mid length of the angle to prevent shear lag from the loaded tabs at the ends of the angle from affecting the strain readings. The strain measurements from the tests were used to calculate the axial force in the member. The measured axial force was then compared to the load cell from the testing machine.

Since it is assumed that plane sections remain plane, the strain at the centroid of the angle, $\varepsilon_{centroid}$, was calculated by forming a plane with the combination of three strain measurements. The formula used for this calculation was $\varepsilon_i = a \times x_i + b \times y_i + c$, where x_i and y_i are the Cartesian coordinates of any point i on the cross section measured from the heel of the angle. The constants a, b, and c can be solved for simultaneously with the coordinates of three gages and their corresponding strain readings. Once the constants are found, the strain at the centroid can be found using the previous equation and the coordinates of the centroid. The axial force, P, can then be calculated using the formula $P = \varepsilon_{centroid} \times E \times A$, where E is the modulus of elasticity (29000ksi for steel) and A is the cross sectional area of the member. An example of this calculation is shown in Appendix B.

A typical graph from the load test is shown below in Figure 2.6. If the angle remains linear-elastic, the measured load (y-axis) should always be equal to the applied load (x-axis) creating a line of slope 1.0. The plot in Figure 2.6 has a slope relatively close to 1.0, but the trendline is offset and crosses the y-axis above zero. The reason for this is uncertain, but it is probably due to the sensitivity of the testing machine at low loads. Figure 2.7 is a plot of the same data, except the zero reading for the force in the member is taken at an applied load of 5kips. Also, the x-axis is now the change in applied load, as opposed to the applied load. This data correlates much better than the previous plot and results in approximately 3% difference between the measured load in the angle and the applied load from the test machine.
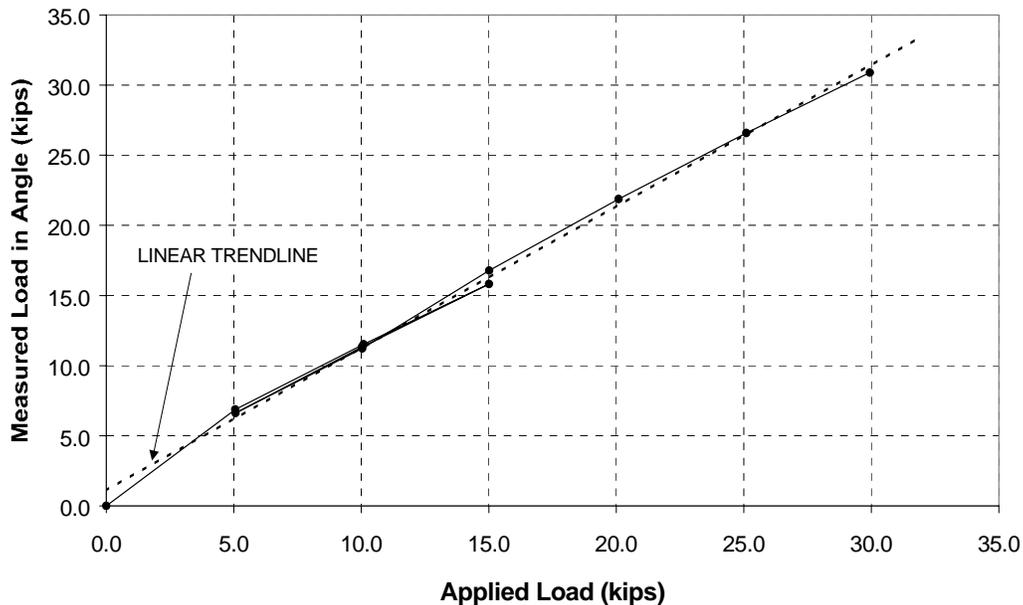
Figure 2.6 Axial Force Measurement of Angle in Lab Test
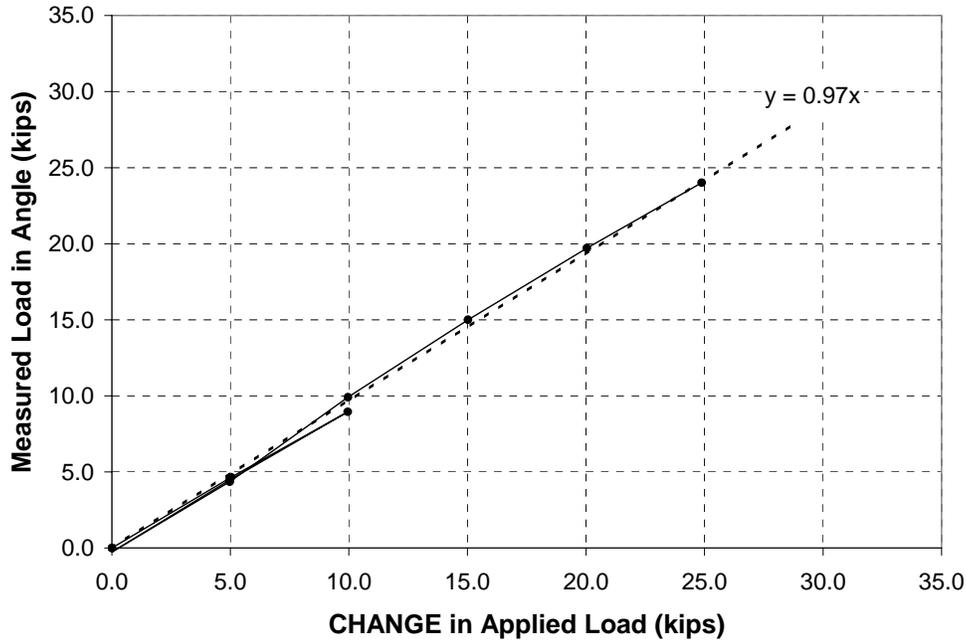
Figure 2.7 Axial Force Measurement of Angle in Lab Test - Adjusted

Using sets of three of the eight gages in different configurations, axial forces were calculated using the method described above. The slopes for each configuration were compared and are shown in Table 2.1. The axial force estimates varied very little between the different gage configurations, although some configurations were slightly more accurate than others. The tests showed that only three gages at a cross section were necessary to accurately predict the axial force on the angle in tension. The gage configuration that was eventually used on the diaphragms is shown in Figure 2.8. Arranging all of the gages on the inside of the legs of the angles made it easier to add mechanical protection to the gages.

Table 2.1 Lab Test Results on Angle Member

	Gage Configuration							
	135	**137**	**157**	**357**	**246**	**248**	**268**	**468**
Slope	1.002	0.990	0.995	0.0984	1.007	0.987	0.999	0.981

2.4   DIAPHRAGM INSTRUMENTATION

2.4.1   Z-Connect

For this study, three external diaphragms on Z-connect were instrumented before they were installed on the bridge. The external diaphragms consist of angle members in a K truss configuration. All five members were instrumented with three strain gages at each cross section as shown in Figure 2.8. Figure 2.9 shows the locations of the instrumented diaphragms along the bridge. After each inner and outer girder was erected, the diaphragms were bolted and then welded to WT stubs that were bolted to the webs of the girders (Figure 2.10). Once the concrete deck hardened, the external diaphragms were removed by flame cutting the WT stubs (Figure 2.11).

The instrumentation setup allowed for one multiplexer to be assigned per diaphragm. Since each multiplexer has 16 available channels and 15 channels were used as gages on the angle members, the last channel was used to read "dummy" gage. This gage was bonded to a steel plate that was placed inside a protective box. The plate would have zero change in stress since it was not attached to any other member. Since it is temperature compensated, the dummy gage should not have a change in resistance, even if the steel plate expands or contracts due to temperature variations. However, the dummy gage did have a slight change in strain measurement, although this change was small compared to strains in the bridge members. The dummy gage readings were subtracted from the other strain measurements since it was assumed that the same small error due to temperature was occurring in each gage.

The disadvantage of the strain gage layout was that there was no redundancy in each angle member. If one gage in a member did not function properly, the other two gages at the cross section were useless. Three strain measurements are needed at a cross section to find the strain at the centroid and the axial force.
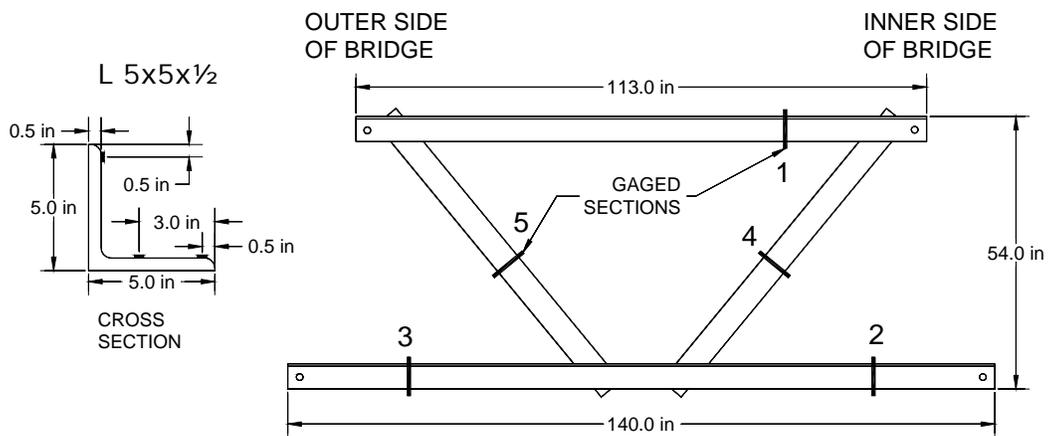
Figure 2.8 Instrumented External Diaphragm
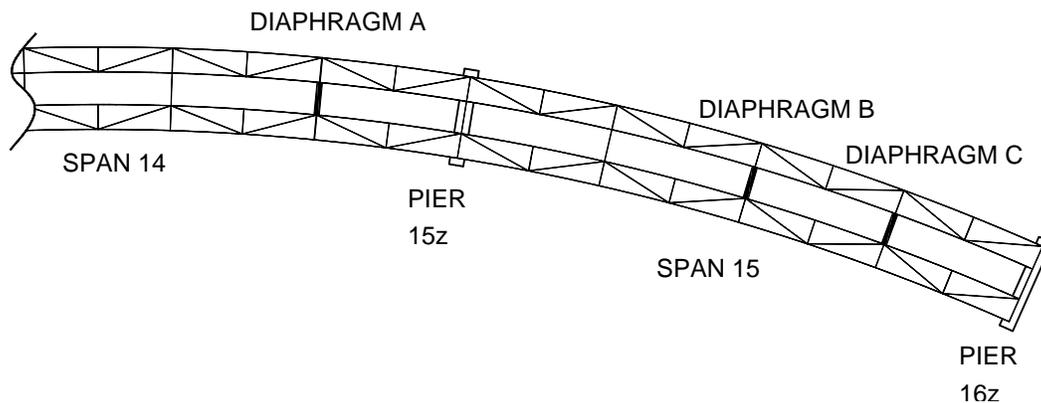
Figure 2.9 Instrumented External Diaphragm Locations

Figure 2.10 Installed External Diaphragms on Z-Connect

Figure 2.11 Flame Cut Removal of External Diaphragms

2.4.2   K-Connect

Two intermediate external cross frames were instrumented in K-Connect. Each external cross frame, or diaphragm, consisted of five members in a K-brace arrangement. Two cross sections per member were

instrumented for redundancy. On the three horizontal members of each frame, the two cross sections had the standard three-gauge configuration for an angle section that is shown in Figure 2.8. On the two diagonal members of each frame, there was one cross section with the three-gauge configuration and one with a four-gauge configuration, which was simply the three-gauge configuration plus an extra gauge. The strain values at each cross section were used to calculate the axial force in the member.

The reason for using the four-gauge configuration for two members of the cross frame is simply because an extra channel was available on the multiplexer. There were two multiplexers per diaphragm, and they each recorded five cross sections. One gauge was added to one of the cross sections of each of the cross frame diagonals in order to make use of the remaining channel in each multiplexer. This also provided extra redundancy. For each of the four total cross sections with the four-gauge configuration, the axial force was calculated using both the three-gauge and four-gauge arrangements. It was found that both methods produced the same value for axial force.

Figure 2.12 shows the dimensions and instrumented cross sections on the diaphragms. Cross sections Aa through Ae were attached to multiplexer A, and cross sections Ba through Be were attached to multiplexer B, and so on. The locations of multiplexers A, B, C, and D are visible in Figure 2.13. Multiplexers A and B were affixed to diaphragm #11, and multiplexers C and D were affixed to diaphragm #18. Locations "a" through "d" from each multiplexer have three-gauge configurations, and location "e" from each multiplexer has a four-gauge configuration.
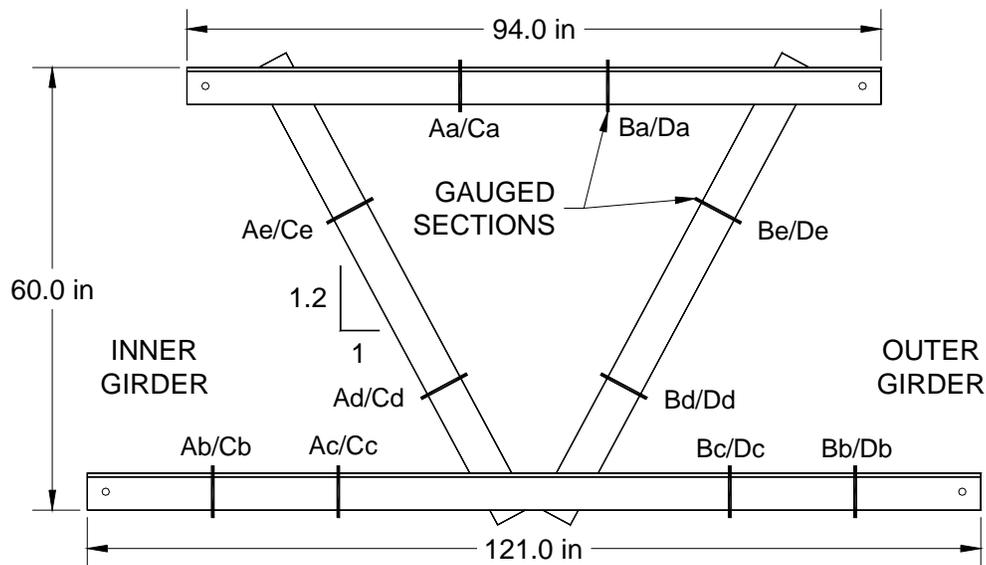
Figure 2.12 Strain Gauge Locations on Instrumented External Diaphragms

A photo of diaphragm #11 is presented in Figure 2.14. This is diaphragm #11. The two gray boxes that are attached to the bottom of the diaphragm diagonals are multiplexers A and B; multiplexer A is on the left, and multiplexer B is on the right. This is the same view as in Figure 2.12. The road that is visible below the bridge is southbound IH-35.
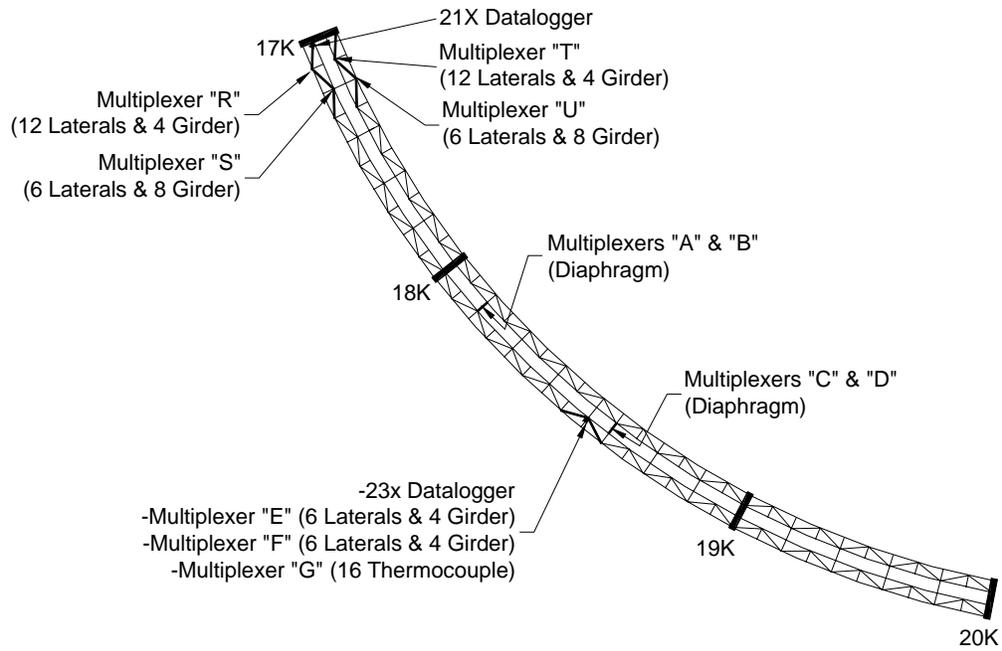
Figure 2.13 Instrumented Locations on K-Connect

Figure 2.14 Intermediate External Diaphragm #11 -- Looking South

19

The reason for using the four-gauge configuration for two diagonal members of the cross frame is simply because an extra channel was available on the multiplexer. There were two multiplexers per diaphragm, and they each recorded five cross sections. One gauge was added to one of the cross sections of each of the cross-frame diagonals in order to make use of the remaining channel in each multiplexer. This also provided extra redundancy. For each of the four total cross sections with the four-gauge configuration, the axial force was calculated using both the three-gauge and four-gauge arrangements. It was found that both methods produced the same value for axial force.

2.5   DIAPHRAGM LAB TEST

Lab tests were performed on two external diaphragms that were used in K-Connect. These diaphragms had slightly different dimensions from the diaphragms on Z-Connect, but the angle sizes were the same and the geometry was very similar. In the lab, the diaphragm was bolted into a column and lifted at its end with an overhead crane equipped with a load cell. Each member had two cross sections instrumented for redundancy (the change in axial force in each member should be constant along its length). The gaged sections and the load test setup are shown in Figure 2.15. Unfortunately due to this setup, a perpendicular load on the diaphragm top chord resulted in a horizontal reaction on the overhead crane. This limited the amount of load that could be applied to the diaphragm since the crane would begin to roll when there was more than 2 kips in the cable.
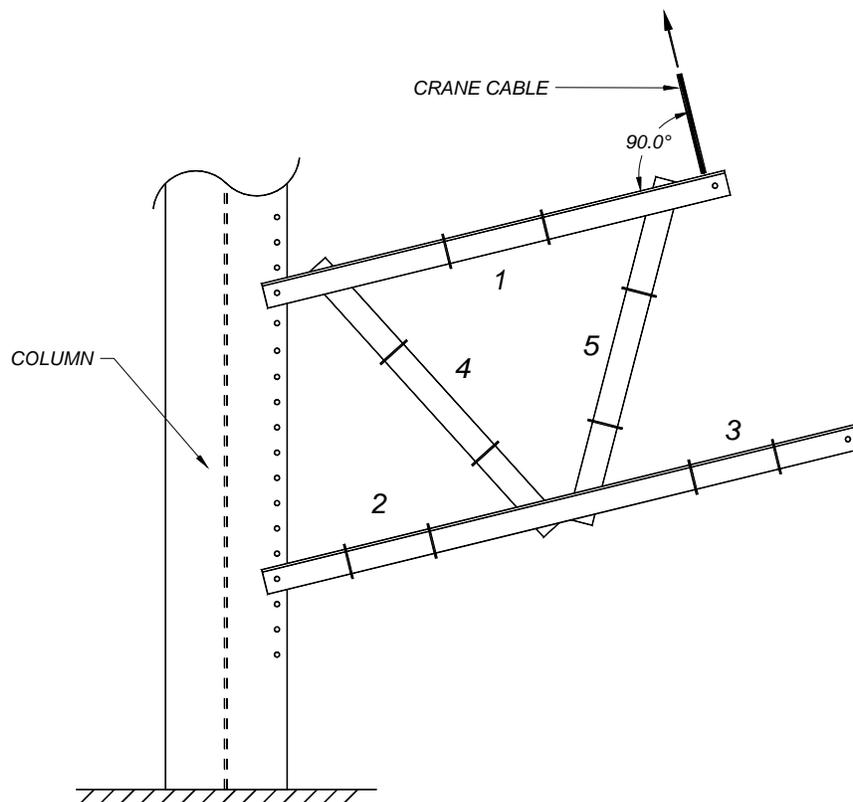
Figure 2.15 Diaphragm Lab Test Setup

2.5.1   Evaluation of the Test Data

Figure 2.16 shows the chord member results, and Figure 2.17 shows the diagonal member results from the first lab test. The load increased in time at approximately 0.5 kip increments. The maximum stresses

during this test were very low however (less than 0.5 ksi). The calculated force is very sensitive at this low stress and the two cross sections on the member are not always equal. In other words, a small error due to noise in the system makes a big difference at this level of stress. In member 1, the axial forces vary by as much as 0.8 kips (0.2 ksi). The axial forces in member 2 are equal at first, but then a small shift occurs midway through loading. This discrepancy shows the sensitivity of the analysis to noise in the system. For example, member 3 is a zero force member in this lab test, but axial forces up to 0.2 kips were measured for this member. At this level of load, 0.2 kips is a measure of the reliability of the axial force measurement from the strains in the member. The diagonals in this lab test show better correlation than the other two members. Also, it is apparent that the compression in one diagonal is almost equal to the tension in the other diagonal as expected.

From the test of the second diaphragm, the chord results (Figure 2.18) and the diagonal results (Figure 2.19), show less correlation between the two cross sections than in the first test. Member 2 shows good correlation between the cross sections, but the other members have a considerable difference. There are significant variations in forces especially in the diagonals during this test. The applied loads during test 2 are a little higher than in test 1, but the stresses in the members are still somewhat low (less than 1 ksi).

Another reason why there may be some discrepancy in the measurements is because there is eccentric shear in the angles that produce some torsion and bending. This causes a large variation in stress along a cross section, so a very small error in the location of the gage can have a large effect on the axial force prediction. During the laboratory load test, for example, a member has a microstrain distribution as shown in Figure 2.20. If gage 1 has a location error of 1/16 in, the axial force calculation for the member changes by 10%.
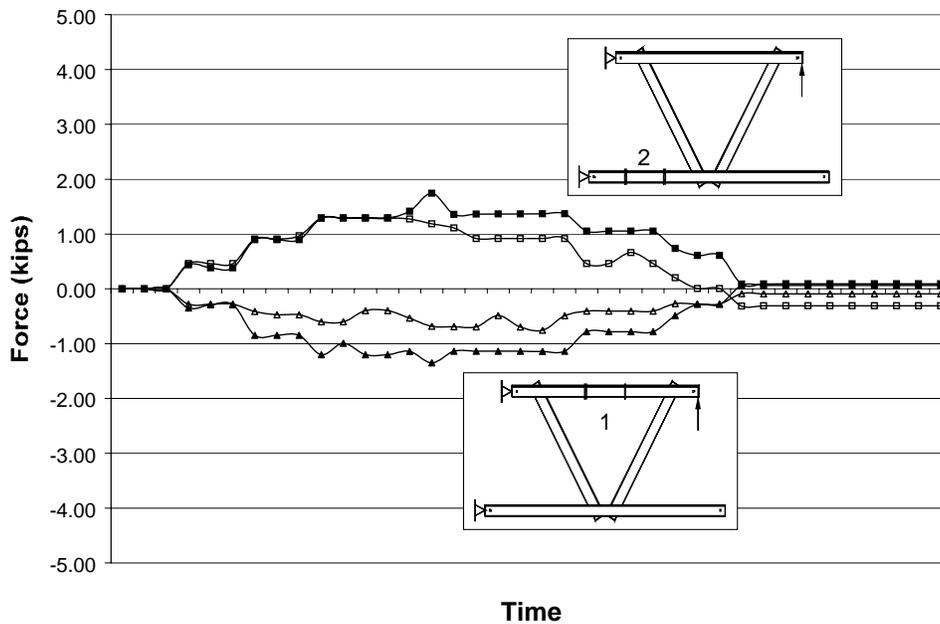
Figure 2.16 Diaphragm Lab Test 1 Results - Chords

21
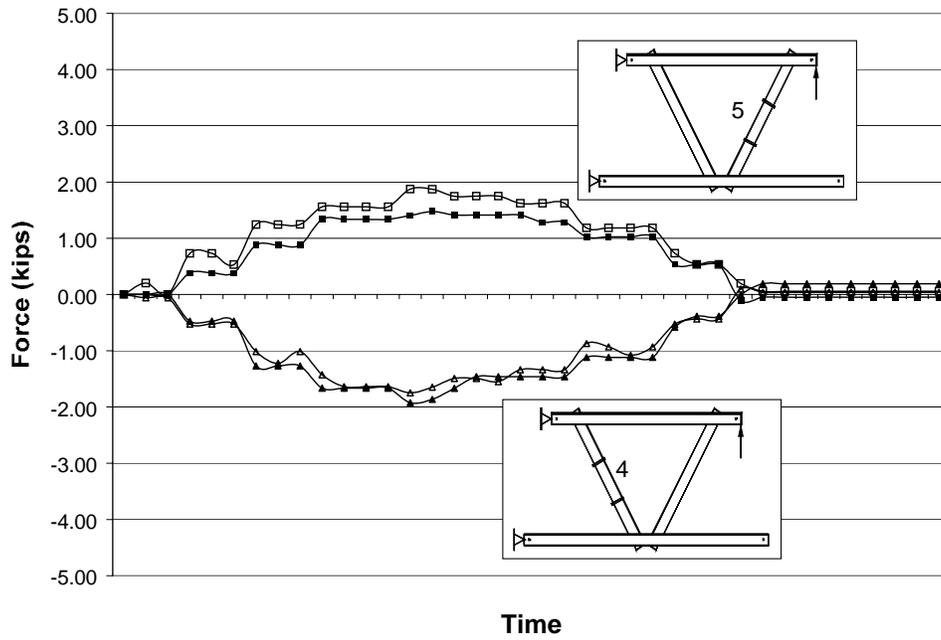
Figure 2.17 Diaphragm Lab Test 1 Results - Diagonals
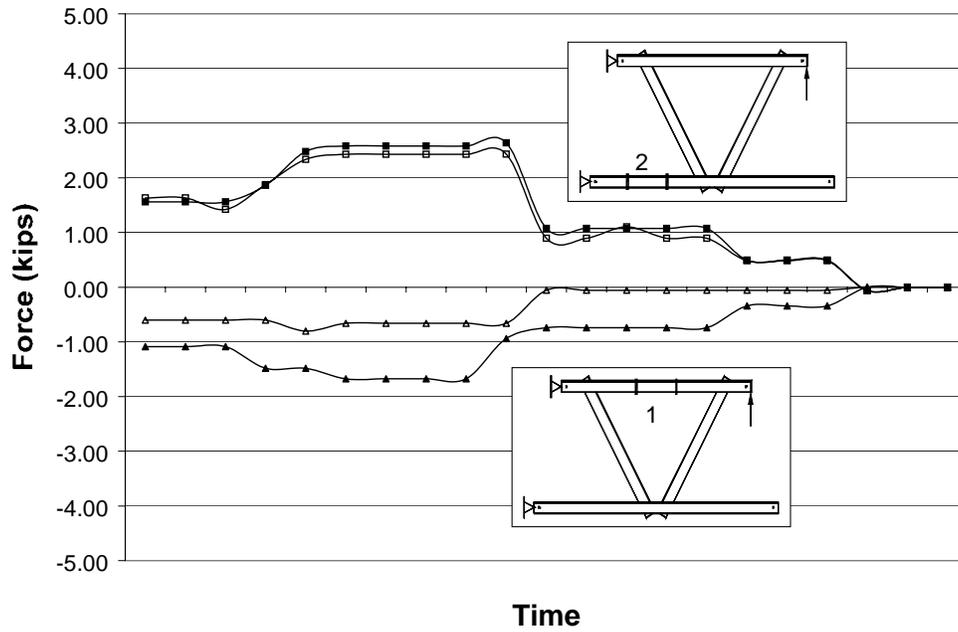
Figure 2.18 Diaphragm Lab Test 2 Results - Chords
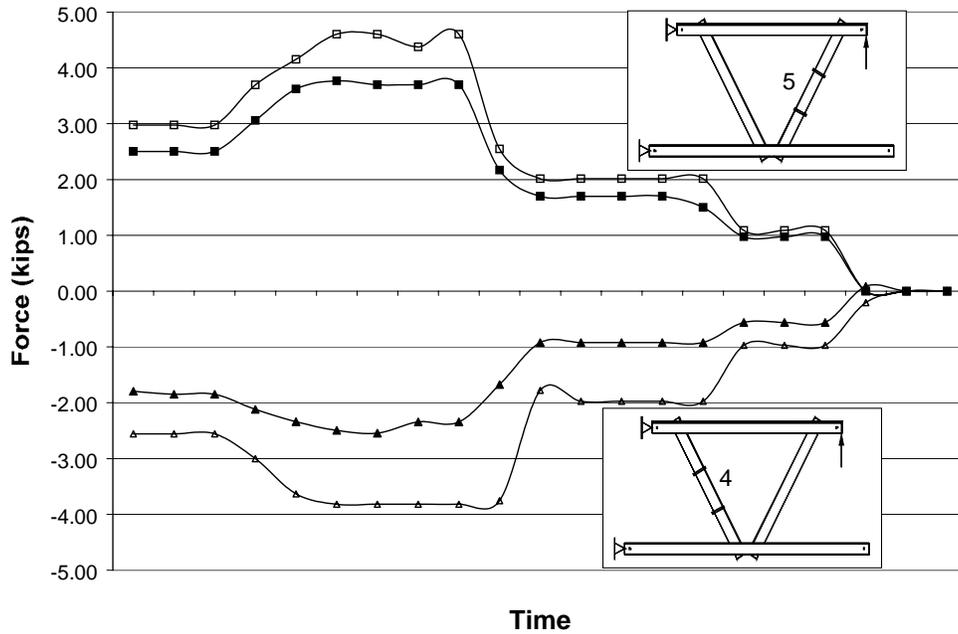
Figure 2.19 Diaphragm Lab Test 2 Results - Diagonals
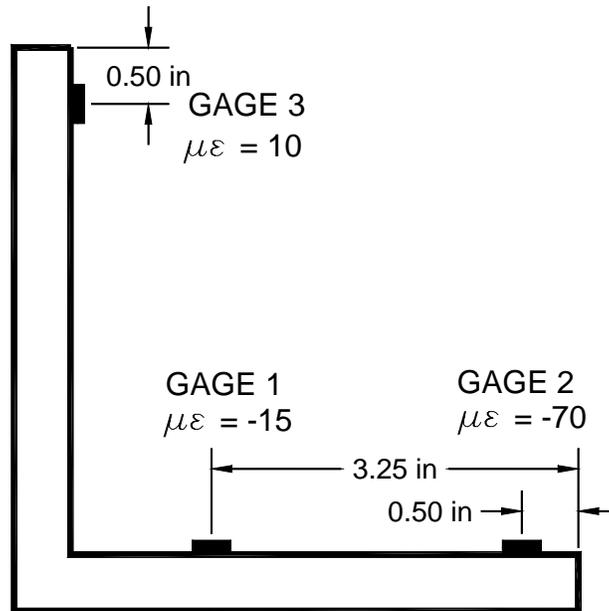
Figure 2.20 Microstrain Distribution along Angle Cross Section

2.5.2   SAP Model of External Diaphragm

To check the accuracy of the axial load measurements during the lab tests, SAP2000, a structural analysis program, was used to model the diaphragm. The diaphragm was modeled as frame elements with rigid

connections since the angles were welded along one leg. The frame would need to be analyzed in 3D if out-of-plane bending moments were to be calculated, but the model was used to primarily to find the member axial forces, so a 2D analysis was used. The connections to the column were modeled as pins (allowed end rotation) since only a single bolt was used for each angle. To some extent the axial forces changed if the column connections were modeled as pins or as fixed. There was considerable change in the axial forces, especially in the diagonals, if the ends of the angles were pinned or fixed. This probably contributes to the difference between the predicted and measured results.

Figure 2.21 shows the results from the SAP analysis for models with different connection stiffness. The connections to the columns were either modeled as pins or semi-fixed. The term "semi-fixed" in this analysis represents the column connection as a 5 in long angle member with the moment of inertia reduced by 90%. The ends of the reduced member were completely fixed. This is an approximation to take into account the small amount of fixity by the tightened bolt. The angle-to-angle connections were modeled as either pins, fixed, or semi-fixed, where "semi-fixed" indicates a 5 in long angle member with the moment of inertia equivalent to one leg of an angle ($I = 5.2$ in^4).

The SAP model forces and the measured axial forces are compared in Figure 2.22. The SAP results are from the model that includes semi-fixed connections at all ends of the angles. The displayed forces in the figure are due to the maximum applied loads on the diaphragms in the lab. The diagonals from test 1 correlate fairly well with the SAP predictions. In test 2, the diagonals do not match up as well and there is also more variation of measured force along the member.

The top chords of both diaphragms have one cross section that correlates well with the predicted forces. The other cross section on these members might have a bad gage, hence the large variation in force measurement. For the bottom chords of both diaphragms, there is little variation in the axial force measurements at both cross sections. However, the predicted forces underestimate the measured forces significantly. To maintain static equilibrium with these small bottom chord forces, a very large moment would be required at the single bolted ends of the angles (Figure 2.23). This is not very realistic and the measured forces are probably underestimating the true force in these members during the test.

2.6 SYSTEM CALIBRATION

Since the research project was constrained by the bridge construction schedule, the data acquisition system had to be quickly installed. The tight schedule did not allow for time to calibrate the system in the lab. Instead, the entire system was calibrated in the field once it was installed.

As mentioned earlier in chapter 1, a load test was performed on the girders before the concrete deck was poured. A crane lifted on the top flanges of the steel girders, creating an upward point load on the curved bridge. During this load test, a majority of the measurements taken by the data acquisition system had an error. The error was discovered shortly after the load test, but the system had to be calibrated first before correcting the problem.

The error occurred in the system because the current capacity of the 21X was exceeded. Some of the five multiplexers had to share the three available ports that were used for the full bridge excitation. Multiplexers A and B shared one, multiplexers C and D shared another, and multiplexer E used the last port by itself. At multiplexers A, B and C, the excitation was applied to all 16 gages on the diaphragms simultaneously, while each channel had an individual signal. All of the full bridges on multiplexer A and B (32 total) were excited at the same time with 2V while one reading was taken. This parallel arrangement of gages resulted in very small total resistance. Since $I = V/R$, where I is the current, V is the voltage, and R is the total resistance, the current required for a certain voltage increases as the resistance decreases. The current capacity of the 21X was exceeded when too many gages were arranged in parallel, resulting in a smaller excitation voltage across the full bridge.
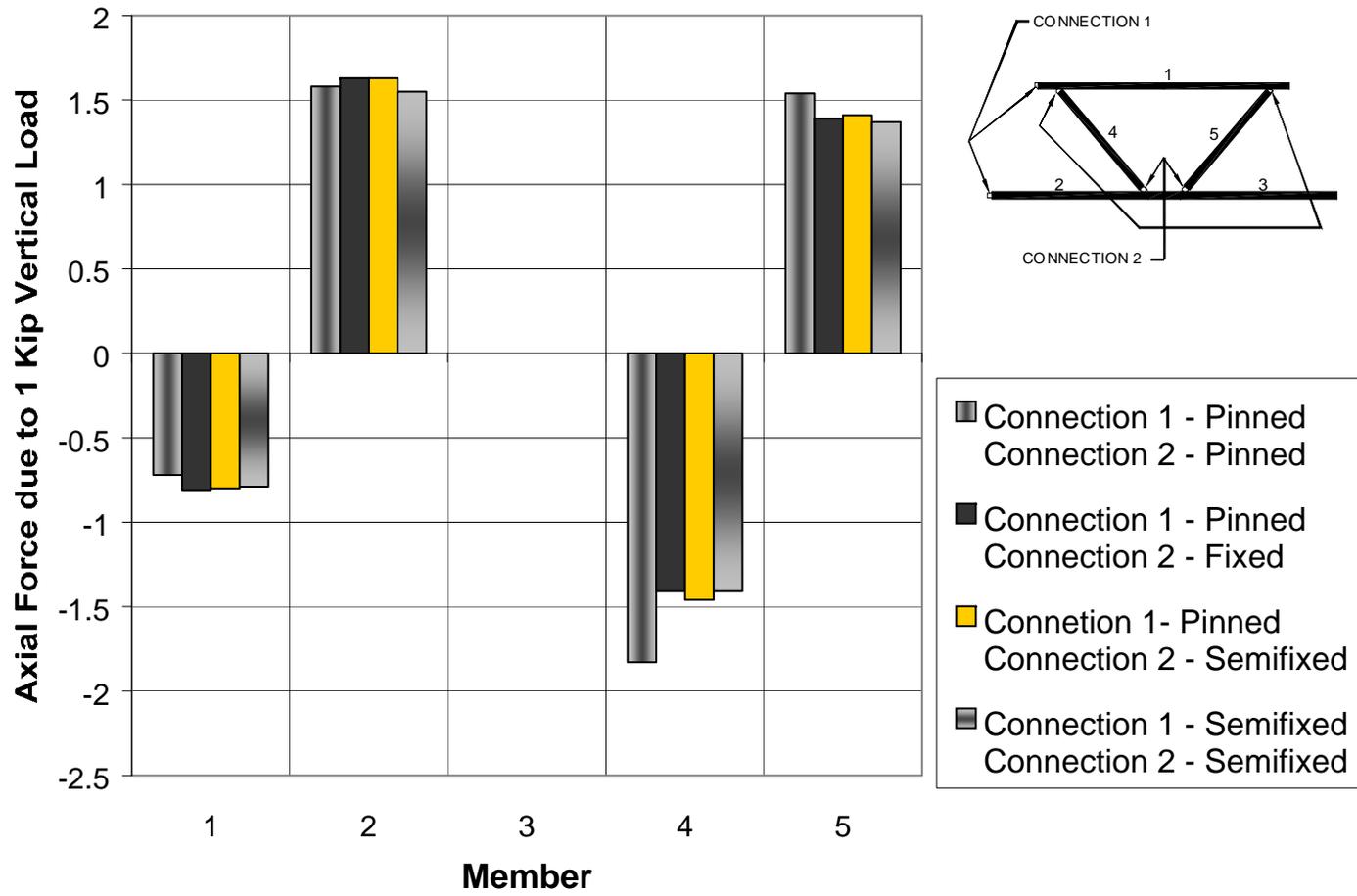
Figure 2.21 SAP Model Results for External Diaphragm

LAB TEST 1
APPLIED LOAD = 1.29KIPS

-0.40 / *-1.06*   **-1.20** / *-1.06*
-1.66 / *-1.86*   **1.56** / *1.87*
-1.64 / *-1.86*   **1.34** / *1.87*
1.29 / *2.12*   **1.29** / *2.12*

MEASURED FORCE
PREDICTED FORCE

LAB TEST 2
APPLIED LOAD = 2.053KIPS

-0.61 / *-1.68*   **-1.68** / *-1.68*
-2.34 / *-2.96*   **3.70** / *2.98*
-3.82 / *-2.96*   **4.38** / *2.98*
2.43 / *3.37*   **2.58** / *3.37*

MEASURED FORCE
PREDICTED FORCE
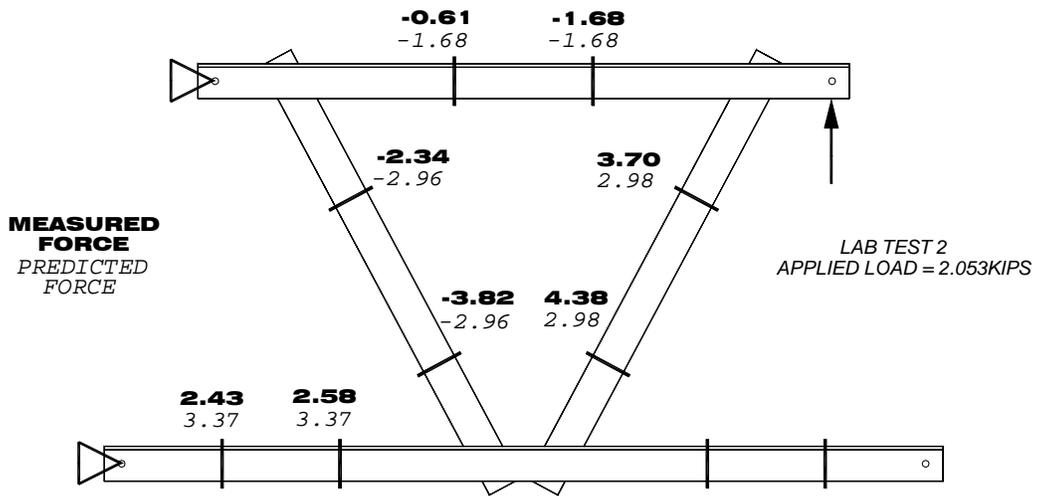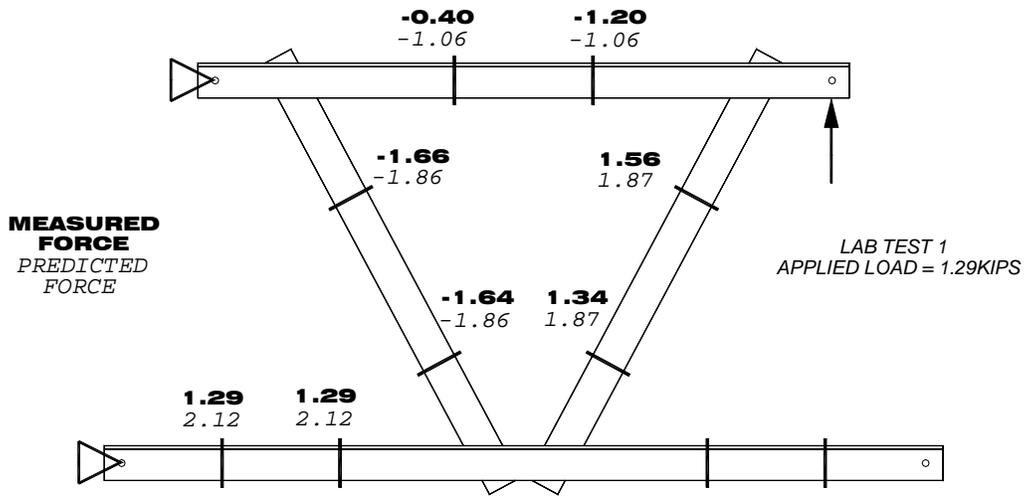
Figure 2.22 Diaphragm Lab Test – Measured VS Predicted Forces

M1 + M2 + 1.29(55) = 1.29(90) ⟹ M1 + M2 = 45 kip-in
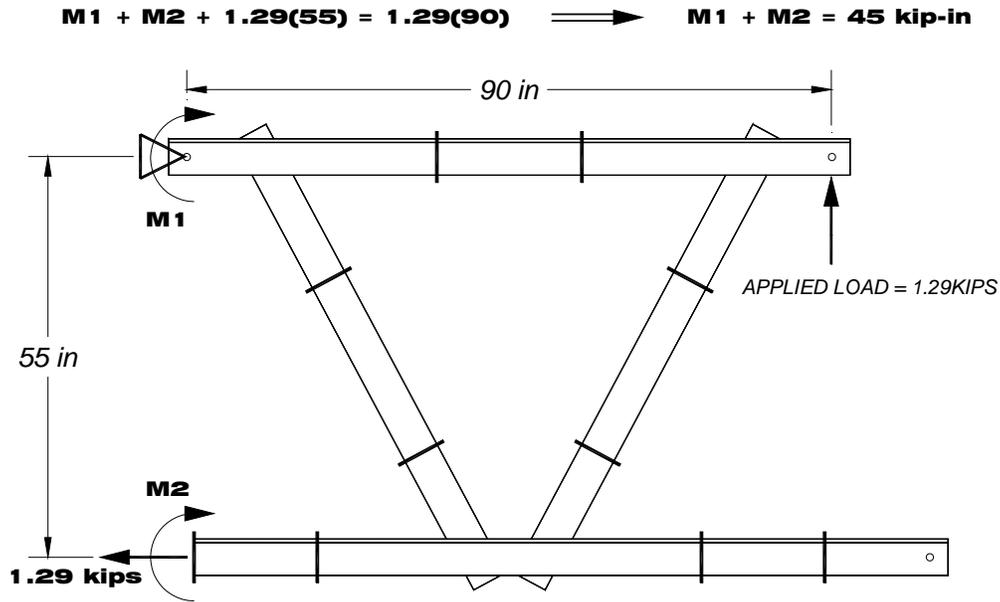
Figure 2.23 Equilibrium Calculation of External Diaphragm

The system was calibrated by checking several channels on each multiplexer with a strain calibrator in place of the full bridge. Each full bridge needed to be replaced instead of only the gage since the completion resistors were not accessible. These calibrations were then used to back out the real strains from the load test data. The system was rewired by using a separate excitation for each member; therefore only 3 gages were excited at the same time. Lab tests discussed in the following section showed that this arrangement would solve the problem. The correction factors were only applied to the results for the crane load test.

2.7   LAB CALIBRATION TEST

Lab tests were also performed on a 21X by hooking up the calibrator in parallel with a variable resistor. This simulated the error in the field and verified the cause of error. The setup and results for the test are shown in Figure 2.24 and Figure 2.25.
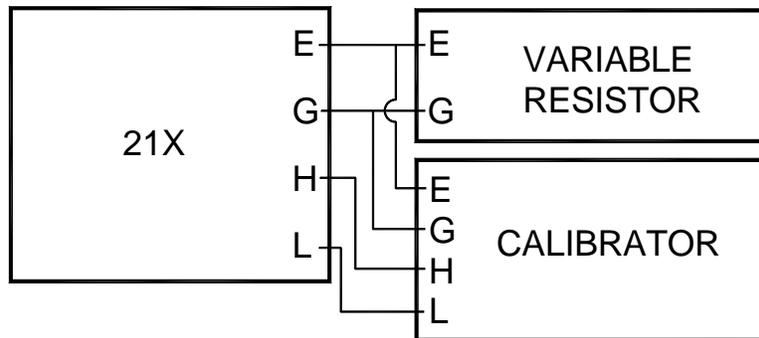
Figure 2.24 Lab Calibration Test Setup
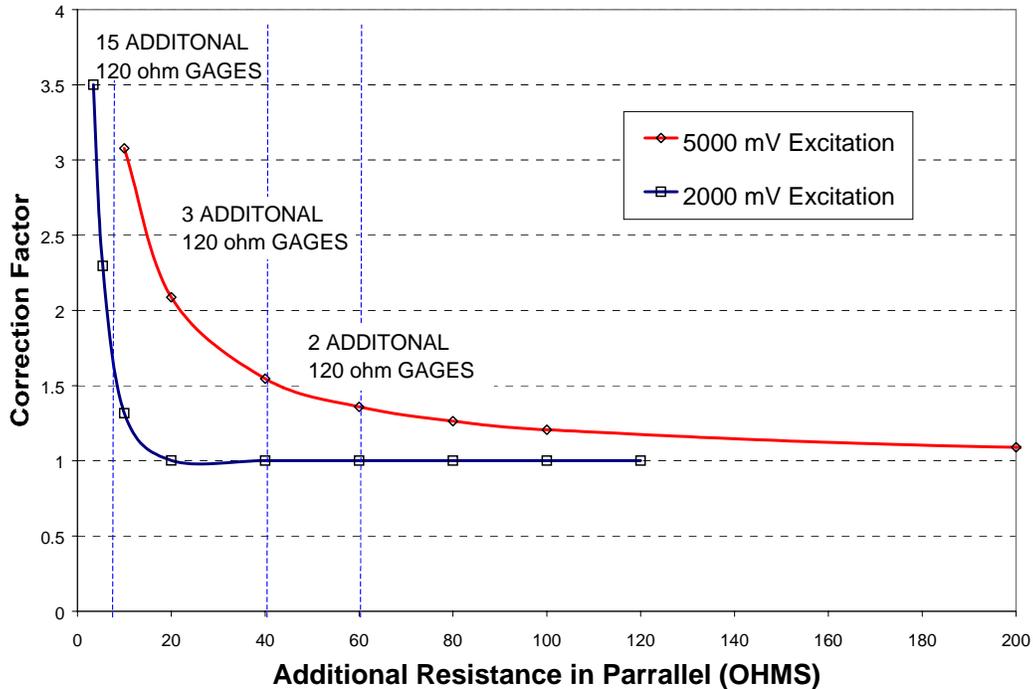
Figure 2.25 Calibration of 21X (120 ohm Gage)

The calibration factors from the lab test correlated very well with the error in the field using the 1550A Strain Indicator Calibrator. This verified that the simultaneous excitation was the source of error in the system. The lab test also showed that applying the correction factors to the field measurements would yield the true strain results. The correction factor varied depending on how many gages were functional at the time of the crane load test. Also, there was no error (Correction Factor = 1) if more than 20ohms of resistance were in parallel when using a 2000mV excitation.

2.8   TOP LATERAL INSTRUMENTATION

2.8.1   Z-Connect

After the girders were erected, strain gages were attached to four top laterals near pier 16z. The first two laterals on the inner girder and the first two laterals on the outer girder were gaged. Each lateral was instrumented at two cross sections with three gages (Figure 2.26). Since the axial force in the laterals should be constant throughout the length of the member, the two gaged cross sections added redundancy to the measurements.

Multiplexer D controlled the outer top lateral gages while multiplexer E was used for the inner top laterals. Unlike the diaphragm multiplexers, the excitation was not commoned for the individual gages for the top laterals. However, since the excitation port on multiplexers C and D was shared, the excitation sent to the outer top laterals was reduced from the resistance of the diaphragm gages. No correction was needed for the inner top laterals since only one gage was excited at a time.

An identical gage configuration for top laterals was used on the opposite side of the bridge. These four laterals (Figure 2.27) were instrumented after the crane load test, but before the concrete pour. The readings for these laterals were taken on a separate 21X system. No correction factors were needed for these laterals.
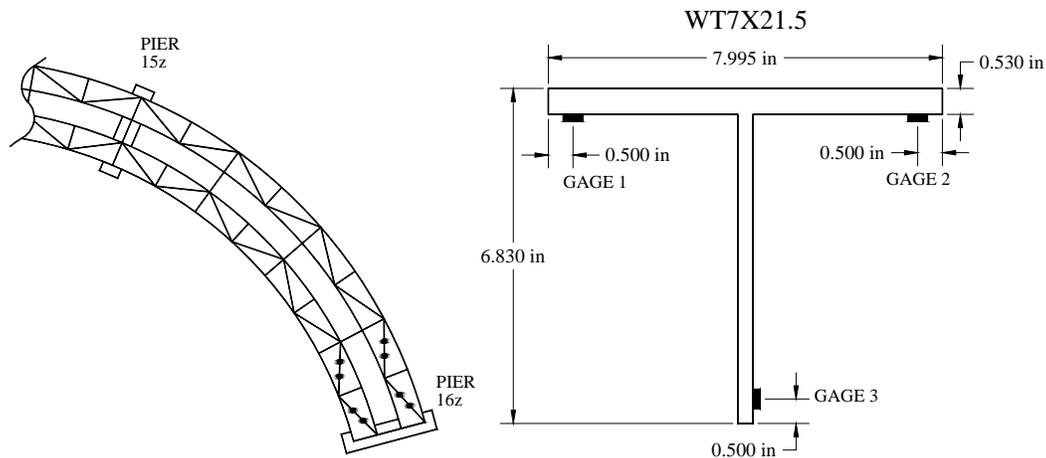
Figure 2.26 Instrumented 16z Top Laterals
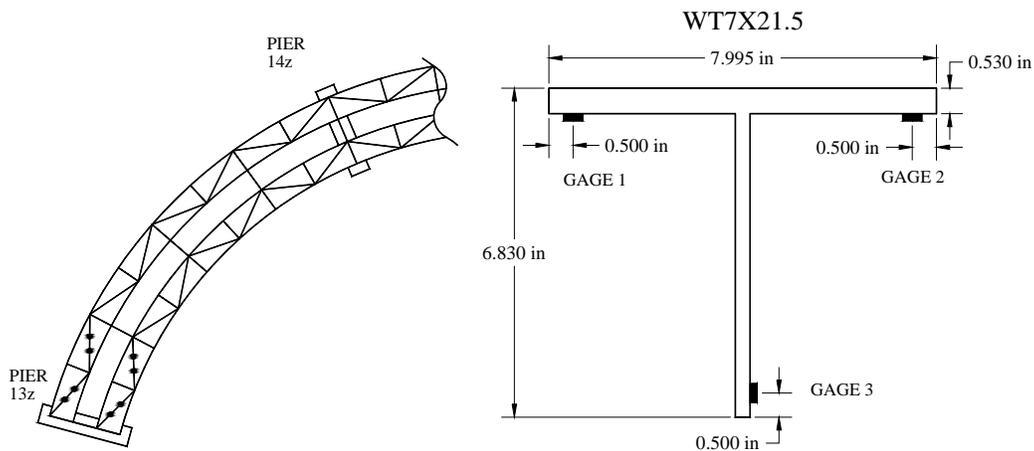
Figure 2.27 Instrumented 13z Top Laterals

2.8.2 K-Connect

As shown in Figure 2.13, eight top lateral braces were instrumented on K-Connect. Each of the top laterals was instrumented at two locations along the member to provide a measure of the accuracy of the measurements. The 16 total cross sections each had the standard three-gauge configuration for a WT section that was used for Z-Connect. This configuration requires strain values from three strain gauges in order to be valid. If one of the gauges malfunctions, then the remaining data from the cross section is of no value. Measuring strain at two locations provides a safety net, as it is not likely for both cross sections on one member to be invalid.

Fortunately, on bridge K, every single strain gauge on the top laterals worked properly for the entire time; therefore, there are two valid cross sections on each of the eight top laterals that were instrumented. The strain values at each cross section were used to calculate the axial force in the member.

2.8.3 Y-Connect

A plan view of the instrumentation in the bridge is shown in Figure 2.28. Four top lateral braces at the east end of the bridge (pier 5Y/23K) were instrumented with strain gauges. The data were collected using one data acquisition system. The system was setup in the same manner as Connects Z and K. The system had two multiplexers attached (a total of 30 channels used).

29
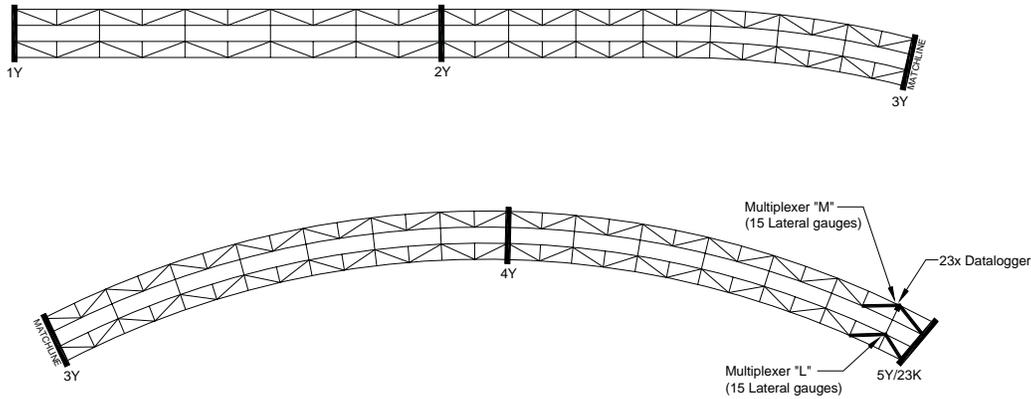
Figure 2.28 Data Acquisition System for Connect Y

Each of the top laterals in the first panel was instrumented at two locations along the member, and each of the top laterals in the second panel was instrumented at three locations along the member. This was done to provide a measure of the accuracy of the measurements. The 10 total cross sections each had the standard three-gauge configuration as in Connects Z and K. As explained previously, this configuration requires strain values from three strain gauges in order to be valid.

On bridge Y, every single strain gauge on the top laterals worked properly for the entire time; therefore, each of the instrumented cross sections is valid. The strain values at each cross section were used to calculate the axial force in the member.

2.9   GIRDER INSTRUMENTATION

Six girder cross sections in K-Connect were instrumented in order to calculate the stress distribution the girder. The locations of these cross sections are shown in Figure 2.13. Strain gauges were affixed to the top and bottom flanges on both sides of the girder. Figure 2.29 shows the typical girder strain gauge arrangement.
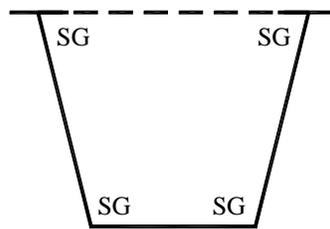
SG = Strain Gauge

Figure 2.29   Typical Girder Strain Gauge Arrangement

2.10   THERMOCOUPLE INSTRUMENTATION

One multiplexer in the data acquisition system at the mid-span of K-Connect was used solely for temperature measurements using thermocouples, wires that can measure temperature directly. Of the 16 channels available in the multiplexer, 12 were used for two separate girder cross sections (six at each cross section), three were used to record the temperature on the instrumented top lateral #19 (one at each end and in the middle), and one was used to take air temperature readings (extending beneath the girder

through a drainage hole at mid-span). The two temperature cross sections were located within the center span of the bridge (see Figure 2.13); the air temperature was measured at mid-span. At the two cross sections, one thermocouple was placed on each top flange, one was placed on each side of the bottom flange plate, one was placed on the underside of the permanent metal deck at the centerline, and one was hung from the metal deck into the center of the girder. Figure 2.30 shows the typical thermocouple arrangement.
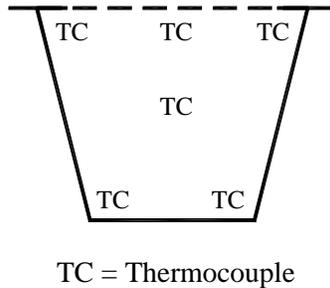
TC = Thermocouple

Figure 2.30 Typical Thermocouple Arrangement

All of the measured temperatures were in degrees Celsius. The temperatures were found not to vary greatly throughout the bridge, except during concrete pours, when the heat generated by the concrete curing occurred where the pours were taking place and was not constant along the bridge.

2.11 SUMMARY

Several lab tests were performed to determine the reliability that could be expected in the field data for the external diaphragms. The diaphragms studied in Z-Connect had only one cross section instrumented per member, leaving no redundancy, while the diaphragms studied in K-Connect had two instrumented cross sections per member. In an ideal truss, the sum of axial forces at a joint can be used to check equilibrium. This could be used as a check of the measured forces, but in the welded diaphragms, equilibrium cannot be reached unless the shears at the cut sections are included in the summation of forces.

The tensile test of a single angle in a test machine showed good correlation between measured and applied loads. However, the tests on the diaphragms did not show nearly the same precision. This is due to several factors, including much lower member stresses and more bending in the angles. For both diaphragm tests, only one out of four members in compression show good correlation between its two cross sections. In general, the tension members show better correlation between cross sections although they do not correlate well with the SAP model. It was found that the axial forces in the SAP model varied, depending on the fixity of each angle at the ends.

The diaphragm data is even less reliable during the crane load test since there were errors due to current loss. Although the data can be corrected with calibration factors, there are small uncertainties in the calibration factors. The measured data in Chapter 3 has been corrected as outlined in Section 2.7. On the average, the diaphragm data for Z-Connect has a confidence level of about 15-20% for the crane load test and of about 15% for the remainder of the field studies. The reliability of this system is not very good and probably could have been improved by fabricating and instrumenting diaphragms that are made of concentrically loaded pipes (Zureick et al., 2000).

CHAPTER 3:
CRANE LOAD TEST

3.1   DESCRIPTION AND PURPOSE

On March 7, 2000, a full-scale load test was performed Z-Connect. TxDOT and Abrams agreed to perform the test by lifting up on a portion of one girder using a crane equipped with a load cell. The test was a significant part of the research for two reasons. It provided a check of the reliability of the data acquisition system before the critical concrete deck pour. Also, the test provided a chance to evaluate the correlation between the finite element model and field measurements with a known point load.   In contrast, the concrete pour is an imprecise, variably distributed load.

There was no type of decking attached to the steel girders at the time of the load test. The crane lifted up on the outer flange of the outer girder near pier 16z as shown in Figure 3.1. The bridge was loaded and unloaded twice at approximately 5 kip increments up to 20 kips. Figure 3.2 shows the crane attachment used to lift the girder.

3.2   TOP LATERAL CRANE LOAD TEST RESULTS

Since the crane lifted only on a single girder, the forces had to be distributed through the external diaphragms from the outer girder to the inner. By examining the forces in the top lateral truss system in both girders, the distribution of load between the girders can be demonstrated. Since two cross sections on each lateral were instrumented (Chapter 2), there was redundancy in the axial force measurements. Figure 3.3 shows a typical graph of the axial forces of two top laterals with time during the crane load test. The forces at both cross sections on a lateral are nearly identical and the plots are on top of each other. This gives considerable confidence in the top lateral measurements.

The force measurements stay nearly constant as the crane is held at the same load. However, the forces in the laterals do not go back to zero once the crane releases the girder. The reason for this is unknown although a similar feature occurs in the outer girder laterals. This may be due to twists in the girders from temperature effects since the entire crane test took approximately one hour. A force change of 5kips can occur within that time since the load test occurred between 10am-11am, a period in the day in which the girder has a high temperature gradient. It was typical that the top laterals would change roughly 10kips in axial force from morning to night due to normal temperature changes.
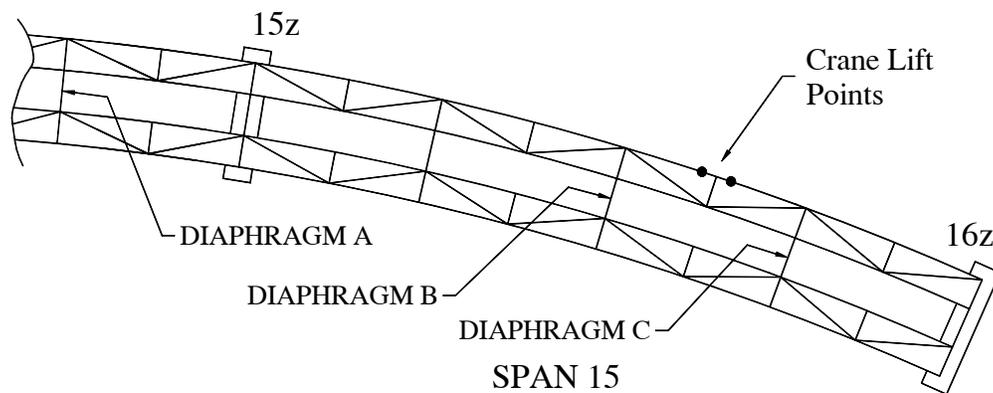
Figure 3.1 Crane Lift Points

Figure 3.2 Crane Attachment
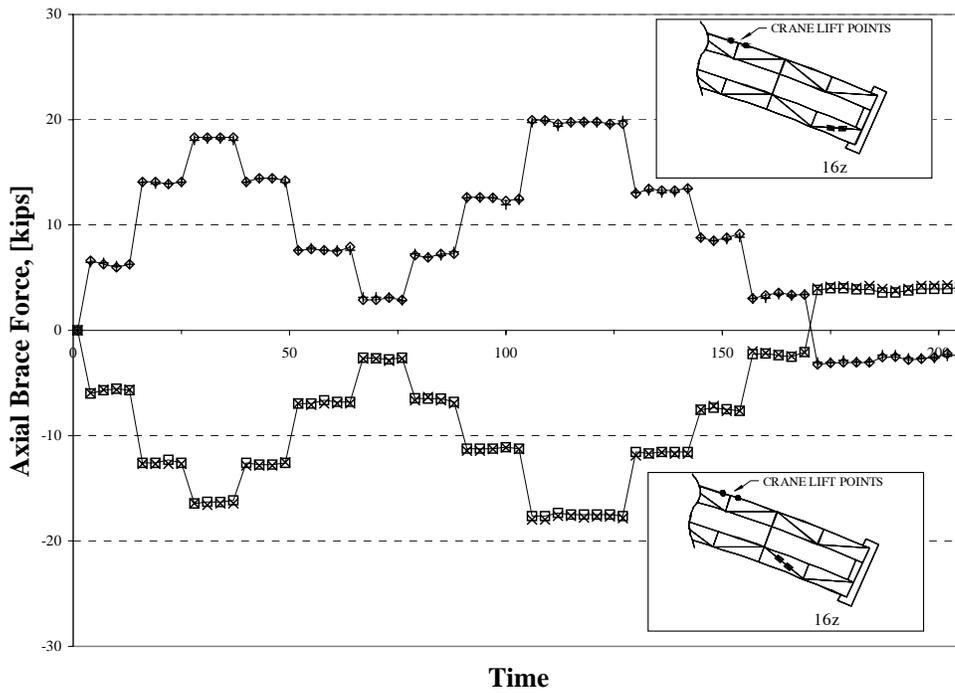
Time

Figure 3.3 Inner Girder Top Laterals – Crane Test Force versus Time

Figure 3.4 through Figure 3.7 show plots of the applied crane load versus the measured axial force for each lateral. The graphs show data as the bridge is loaded and unloaded twice. Ideally, these plots should be linear. The plotted points are the average of the two cross sections for each lateral. A linear trendline is also shown on the graphs as a bold line. This trendline does not pass through the origin of the plot due to the data during unloading. The important aspect of the trendline is the slope since it represents change in force of the lateral with the applied load. This slope was used for further comparisons to the FEM. The correlation coefficient (the proportion of the variance in y attributable to the variance in x) for each trendline was calculated. If the data were perfectly linear, then this value would be equal to 1.0. The lowest coefficient was 0.98, which shows that the trendlines represent the data very well.
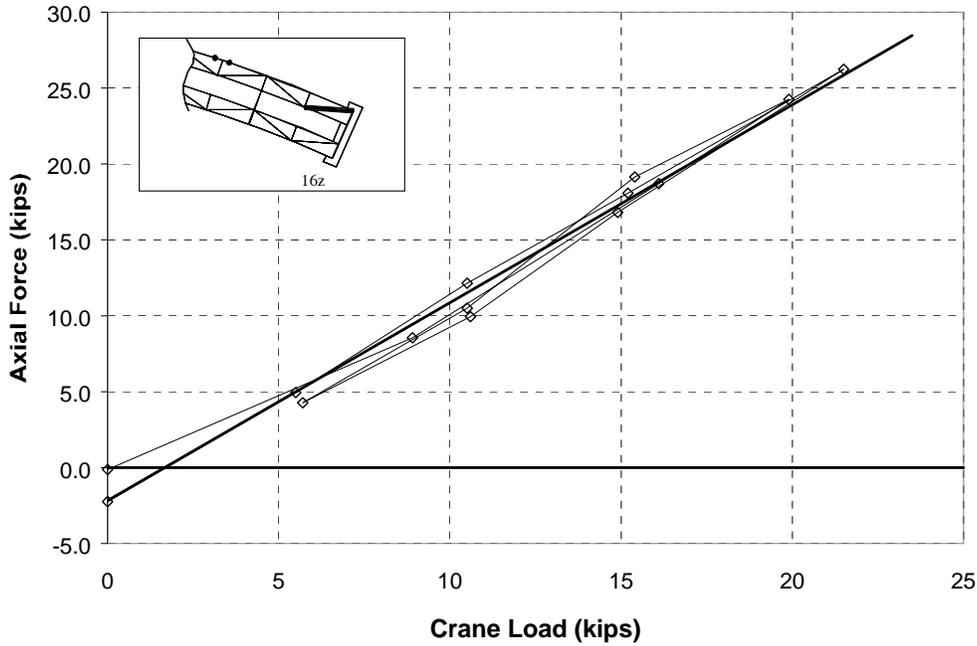
Figure 3.4 Outer First Lateral Force versus Crane Load
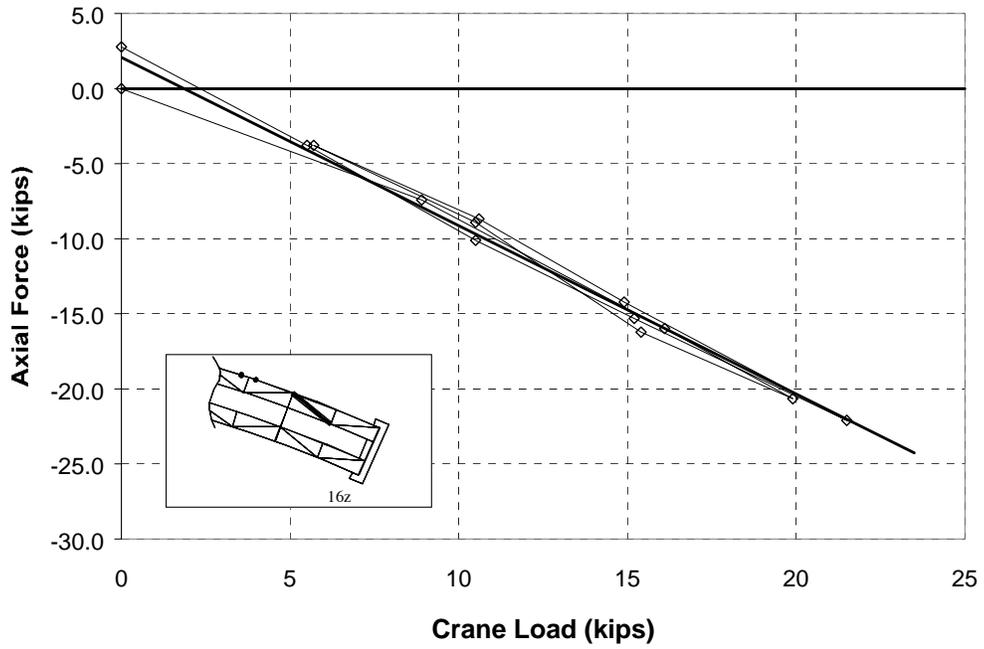
Figure 3.5 Outer Second Lateral Force versus Crane Load
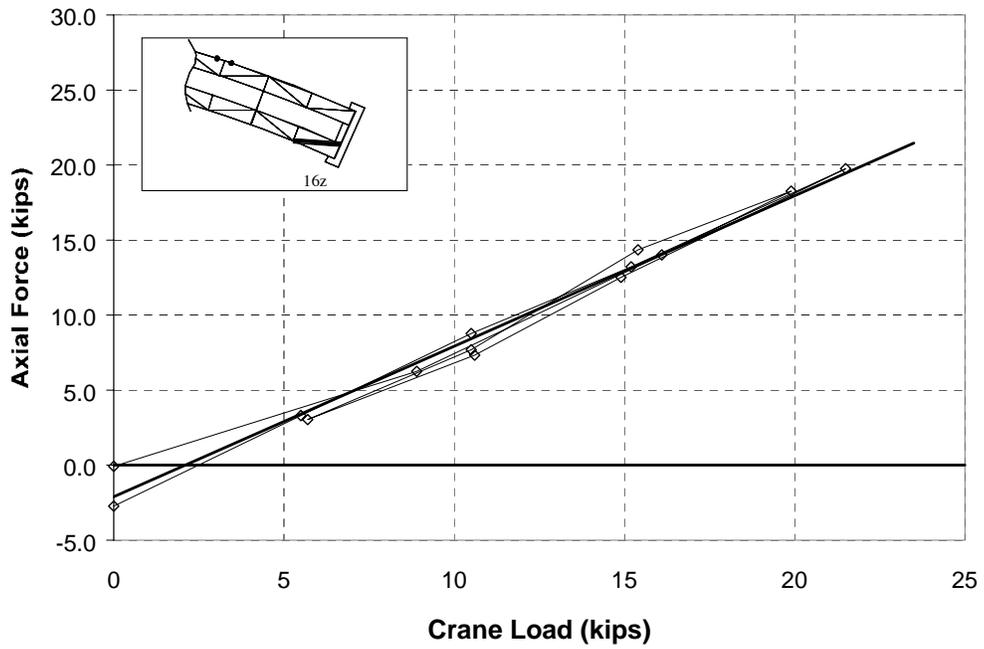
Figure 3.6 Inner First Lateral Force versus Crane Load
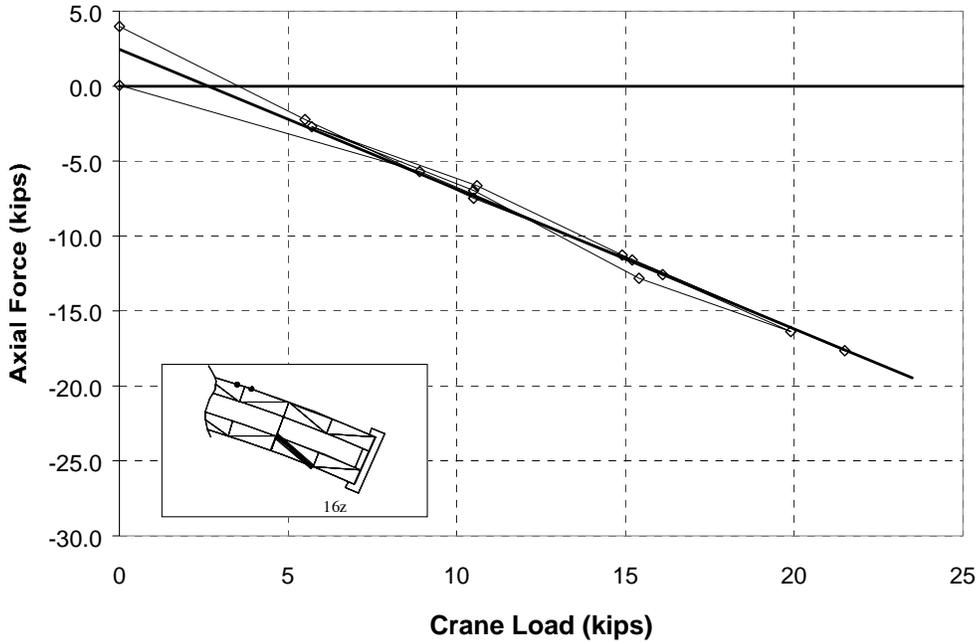
Figure 3.7 Inner Second Lateral Force versus Crane Load

Using the equation $F_{member} = \beta \times Load_{applied}$, where β is the slope of the trendline in Figure 3.4 through Figure 3.7, the measured force in each lateral was compared to the predicted force from the FEM. The results for the measured and predicted top lateral forces for an applied crane load of 10 kips are shown in Figure 3.8. The axial forces predicted for the top laterals in the first panel are greater than in the second panel. This is due to a higher torsion at the ends of the girder. Pulling upwards on the girder creates tension in the first laterals and compression in the second panel laterals due to their orientation.
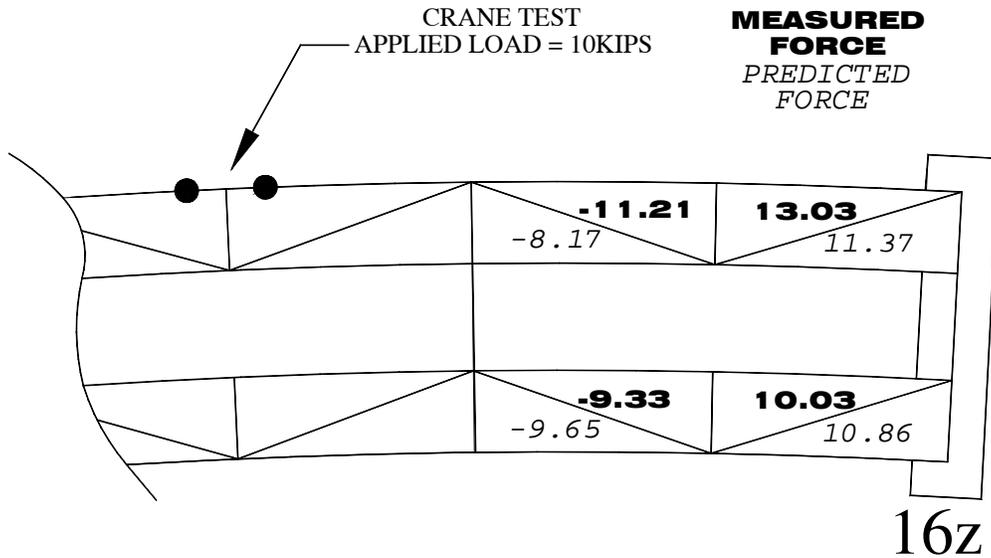
Figure 3.8 Top Lateral Crane Test Results

An interesting effect occurs within the top laterals under this loading. The first outer lateral is predicted to have a higher axial force than the inner lateral, but the second outer lateral is predicted to have less force than the inner. This is probably because there are two components to the resultant axial force: a torsional component and a bending component. Bending creates tension in all of the top laterals as the girders are lifted. Following the moment diagram, the second panel laterals have a higher stress due to bending than the first panel. Also, the load is applied on the outer girder so the eccentricity of the load is much smaller than for the inner girder. Therefore, the axial force in the second panel lateral for the inner girder is primarily due to torsion (compressive) while the second panel lateral for the outer girder has a torsional (compressive) and bending (tensile) component.

The measured results show good correlation with the predicted results, although both outer girder laterals had a higher change in axial force than the inner girder laterals due to the crane load. This means that there was less torsional distribution from the outer girder to the inner than predicted. The discrepancy in the distribution may be due to the reduction in stiffness of the external diaphragms at the connection detail to the box girder. This effect will be examined further in Section 3.3.2.

3.3   EXTERNAL DIAPHRAGM ANALYTICAL MODEL

To understand the behavior of the external diaphragms used on Z-connect, a computer model using SAP was created. The crane load was applied eccentrically on the outer box girder. This load can be converted to an equivalent vertical force and torsion at the centroid of the outer girder (Figure 3.9). The two components were examined separately in the SAP model to determine the expected diaphragm forces from each one.

The diaphragm was modeled as frame elements with ends that have half of the rotational stiffness as the angle member. This approximation was used to account for the one welded leg of each angle at all connections. The ends of one side of the diaphragm were fixed while the other side of the diaphragm was attached to a cross section of a box girder that could translate and rotate (Figure 3.10). The components of the box girder were modeled as rigid elements. Figure 3.10 shows the applied loading condition and schematic of the SAP model of the external diaphragm.

The SAP model represents the forces in the external diaphragms as if all of the vertical load and torsion were distributed from the girder to the diaphragms. The true percentage of vertical load and torsion transmitted to the diaphragm is a function of (among other parameters) the diaphragm stiffness and the stiffness of the girders. If the girders were very stiff compared to the diaphragms, a majority of the load would stay in the outer girder. The measured results in the diaphragm will be compared to the FEM prediction by examining these percentages.
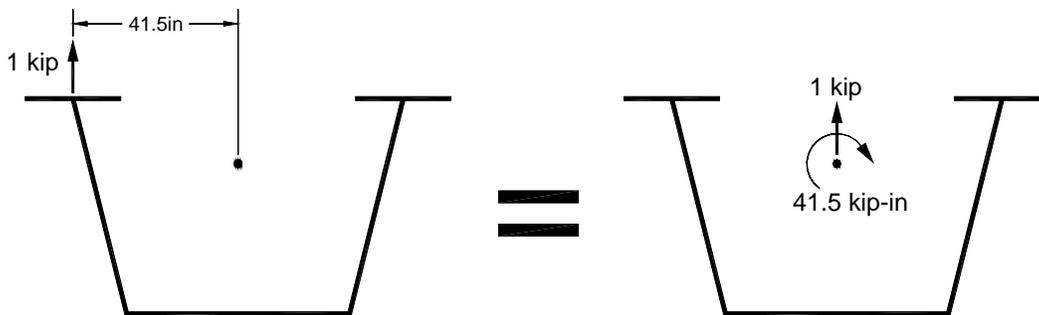
Figure 3.9 Applied Unit Load on External Diaphragm from Box Girder
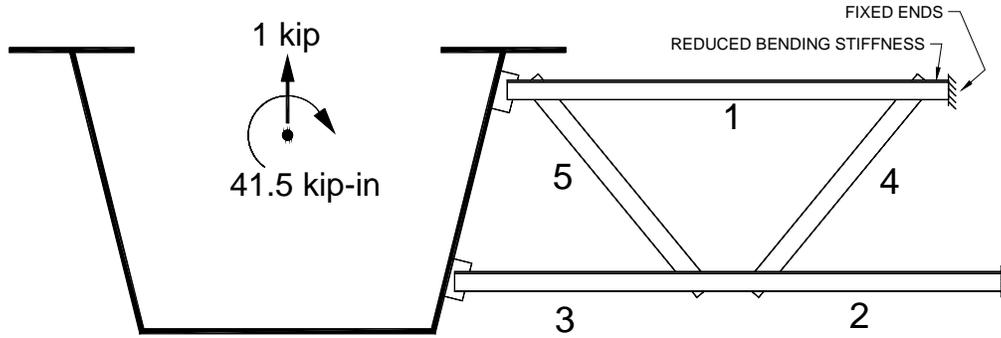
Figure 3.10 Schematic of SAP Model of External Diaphragm

3.3.1   External Diaphragm SAP Model Results

The FEM described in Chapter 1 considered the entire curved girder, while the SAP model was only used to perform a more refined analysis of the external diaphragms. The results for the SAP model are shown in Table 3.1 for the forces due to an applied unit load on the outer flange of the outer girder.

Table 3.1 SAP Results on External Diaphragm

Load	Member 1	Member 2	Member 3	Member 4	Member 5
1 kip Vertical Force at Tub Cent	-2.49	3.80	1.19	-1.69	1.68
41.5 kip-in Torsion at Tub Cent	-1.11	1.11	1.12	0.00	0.00
Total	-3.60	4.91	2.31	-1.69	1.68

When only the vertical force is applied, member 5 goes into tension and member 4 goes into compression. To resist the horizontal thrusts from the diagonals, members 1, 2 and 3 also develop axial forces. For a torsional load on the girder, the diagonals have no change in axial force while the other members must react in equal and opposite direction to form a moment couple. The breakdown of the axial forces into the vertical component and torsional component will be used to compare the measured and predicted results for the external diaphragms.

3.3.2   Analytical Model of Diaphragm Connection Detail

As discussed earlier in Section 3.2, the external diaphragm connection detail to the girder may reduce the stiffness of the diaphragm. The ends of the diaphragms are welded to WT stubs that are bolted to the webs of the girder as shown in Figure 3.11.

To investigate the role the connection detail stiffness played in reducing the stiffness of the diaphragm, a simple model was built using SAP. The model used the least conservative assumptions to determine the greatest possible stiffness of the connection, including the following details:

- Used the longest angle member on the diaphragm (110 in)

- Neglected axial deformation of bolts

- Assumed that the bolts completely fixed the WT stub at the edge of the bolt head

- Assumed that the entire WT stub acts as a single rigid beam element and that all distortions along its width were equal
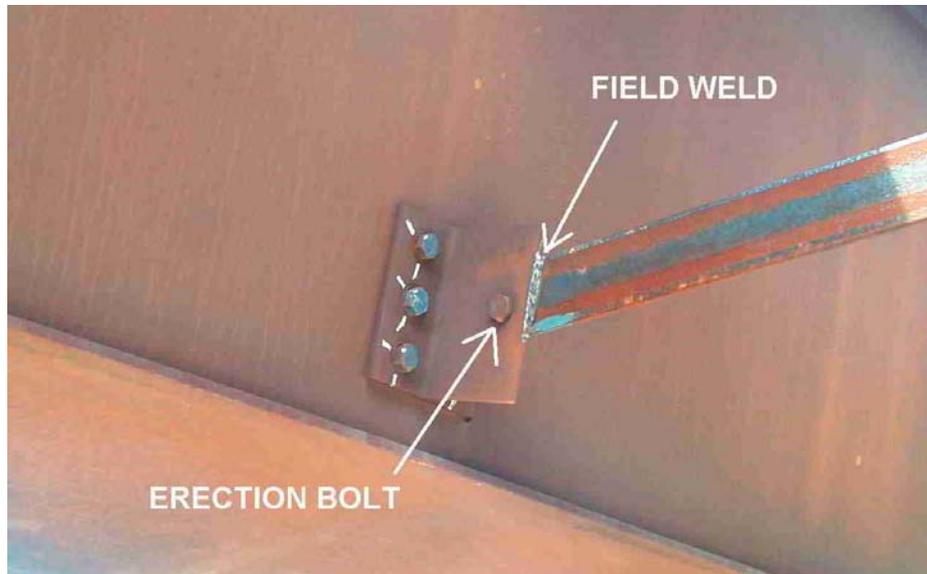
Figure 3.11 External Diaphragm Connection Detail
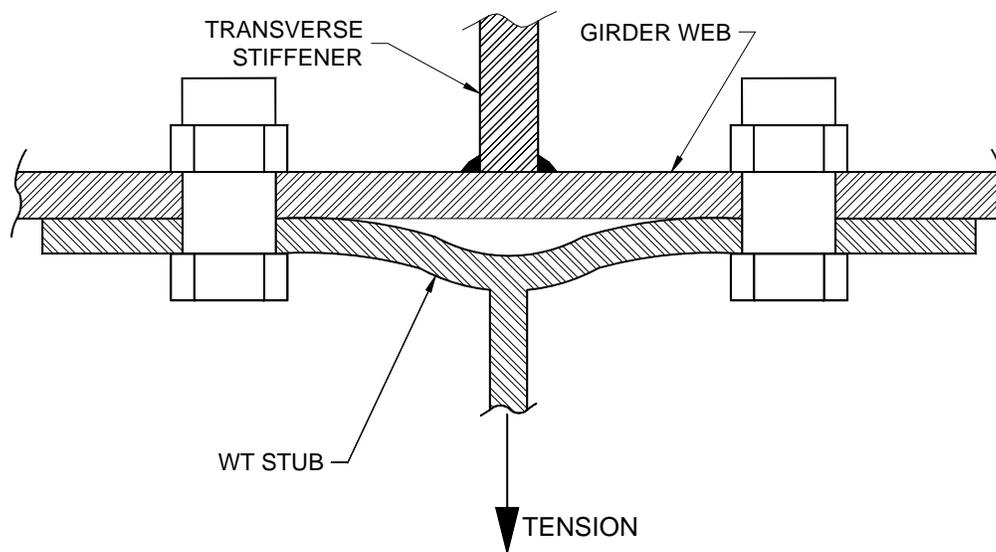
Figure 3.12 Distortion of WT Stub at Diaphragm Connection

The distortion of the WT would only occur when the angle is in tension, as it could pull away from the web. A schematic of this effect is shown in Figure 3.12. With the assumptions stated above in the SAP model, the axial deflection of the longest angle member increases by 50% due to the bending deformation of the WT connecting stub. This is a significant loss of stiffness in the diaphragm when the members connecting to the web are in tension. The stiffness of the connection detail has an even greater effect on the shorter members. This effect was not included in the analysis of the bridge; therefore the FEM may overestimate the predicted distribution from one girder to the other.

3.4 EXTERNAL DIAPHRAGM CRANE LOAD TEST RESULTS

All of the diaphragm data calculations in this section include the calibration factors discussed in Chapter 2. Diaphragm A (Figure 3.1) is on the opposite side of Pier 15z from the applied load and the forces in this diaphragm were very small during the test. Therefore, this section will only focus on the data from the other two external diaphragms, which were very close to the applied load.

The force calculations for the diaphragms were not as reliable as the top lateral data since only one cross section was gaged per member, but there was some repeatability in the test results. Figure 3.13 through Figure 3.16 give an impression of the reliability of the diaphragm data. Two graphs are presented for each diaphragm; each graph represents a load and unload cycle.

Figure 3.13 and Figure 3.14 do not show the results for member 3 on diaphragm B since this member had a bad gage. Similarly, Figure 3.15 and Figure 3.16 are missing the results for member 2 since it also has a bad gage. Since there are only 3 gages per member, if one gage does not function properly, the member's axial force cannot be calculated.

The graphs for each load and unload cycle were compared to determine the repeatability of the data. Similar to the analysis of the top lateral data, a best-fit linear trendline was created for each member and the slope of the trendline was used for the calculation of axial force due to a known crane load. The tabulated results of the slopes for the trendlines in Figure 3.13 through Figure 3.16 are shown in Table 3.2 and Table 3.3. The average slope of the trendline was used for all of the diaphragm force calculations. For example, the average slope for cross section 1 on Diaphragm B is –0.402. This means that the calculated compression in this member is 0.402 times the applied crane load.
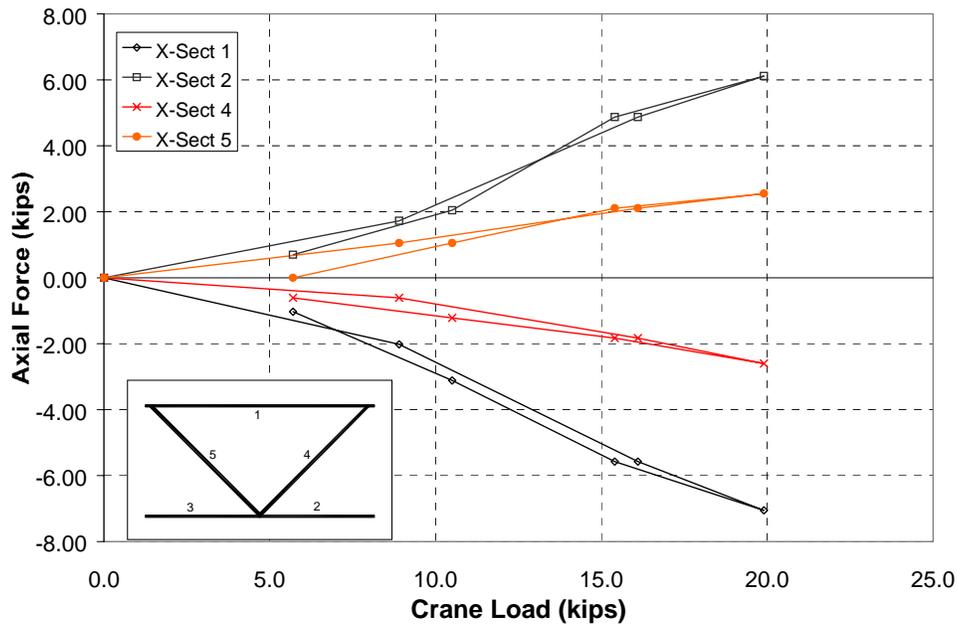
Figure 3.13 Diaphragm B Forces versus Crane Load 1
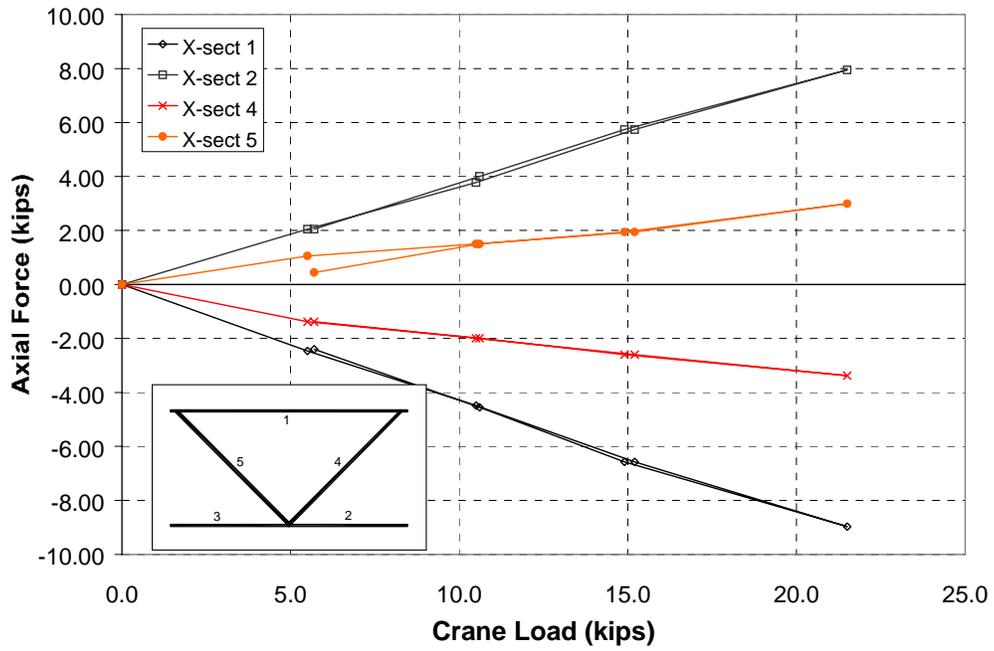
Figure 3.14 Diaphragm B Forces versus Crane Load 2
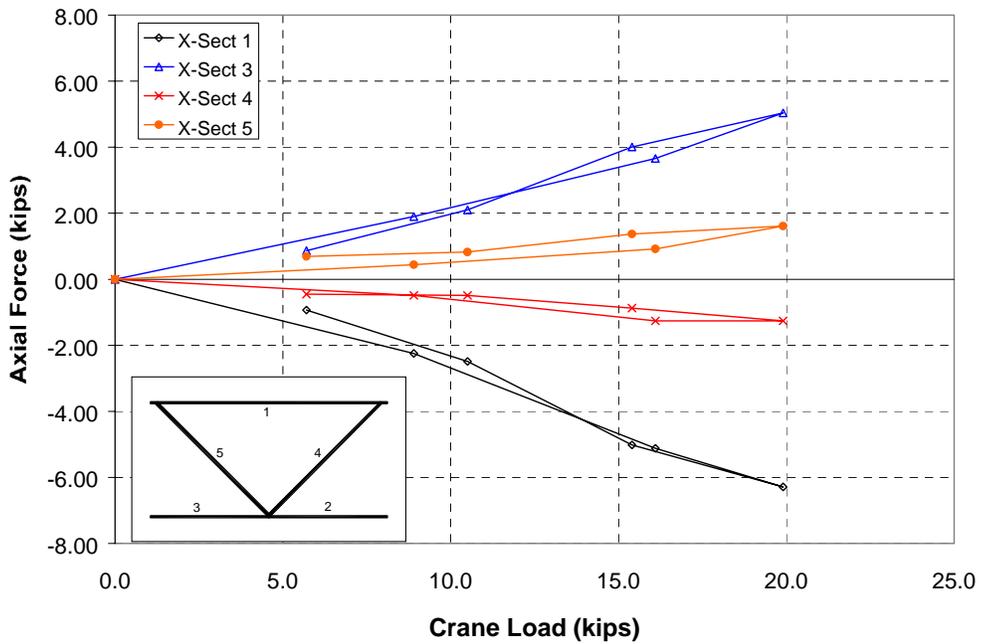
Figure 3.15 Diaphragm C Forces versus Crane Load 1
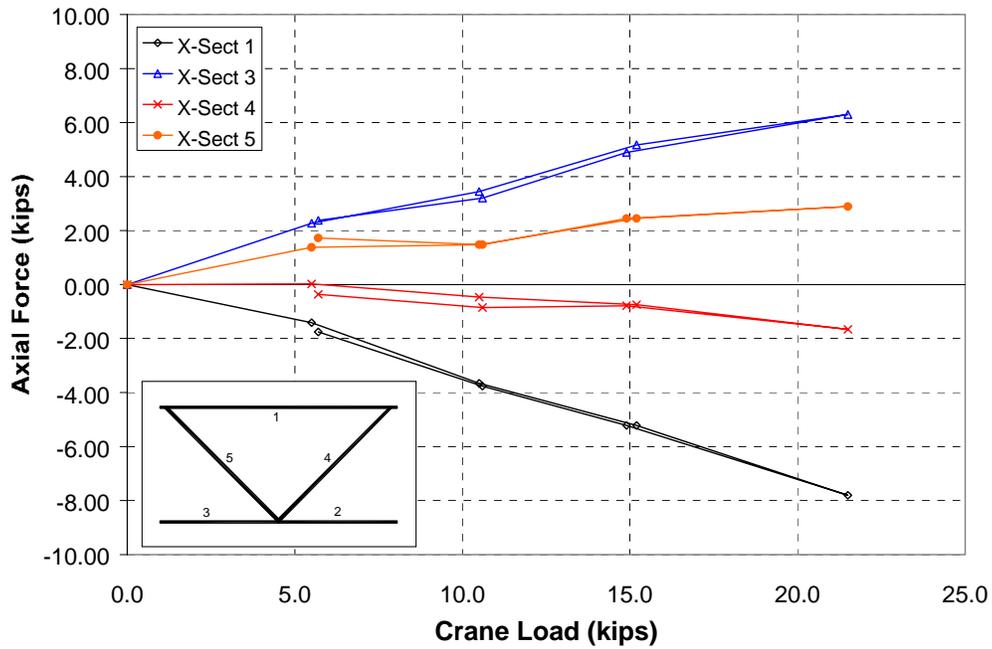
Figure 3.16 Diaphragm C Forces versus Crane Load 2

The percent difference shown in the table is an indicator of the repeatability of the test data. Except for member 5 on Diaphragm C, every member has a repeatable slope of within 15%. Based on the lab tests discussed in Chapter 2, this is the reliability expected for these instrumented members. Some small error is also caused from the accuracy of the crane load cell. Typically, the members with higher stress changes had more repeatable data. Figure 3.17 shows the measured results for the diaphragms during the load test and compares them to the predicted results from the finite element model.

Table 3.2 Diaphragm B Crane Test Results

	Slope of Best Fit Linear Trendline				
	Member 1	Member 2	Member 3	Member 4	Member 5
First Load and Unload	-0.382	0.337	N/A	-0.130	0.146
second Load and Unload	-0.422	0.375	N/A	-0.149	0.136
Average Slope	-0.402	0.356	N/A	-0.139	0.141
% Difference in Slopes	10%	10%	N/A	13%	8%

	Member 1	Member 2	Member 3	Member 4	Member 5
Axial force during 20 kip crane load = Average slope x 20	-8.04	7.12	N/A	-2.78	2.82

43

Table 3.3 Diaphragm C Crane Test Results

	Slope of Best Fit Linear Trendline				
	Member 1	Member 2	Member 3	Member 4	Member 5
First Load and Unload	-0.341	N/A	0.261	-0.065	0.074
second Load and Unload	-0.370	N/A	0.290	-0.074	0.122
Average Slope	-0.355	N/A	0.276	-0.070	0.098
% Difference in Slopes	8%	N/A	10%	12%	40%

	Member 1	Member 2	Member 3	Member 4	Member 5
Axial force during 20 kip crane load = Average slope x 20	-7.10	N/A	5.51	-1.39	1.96
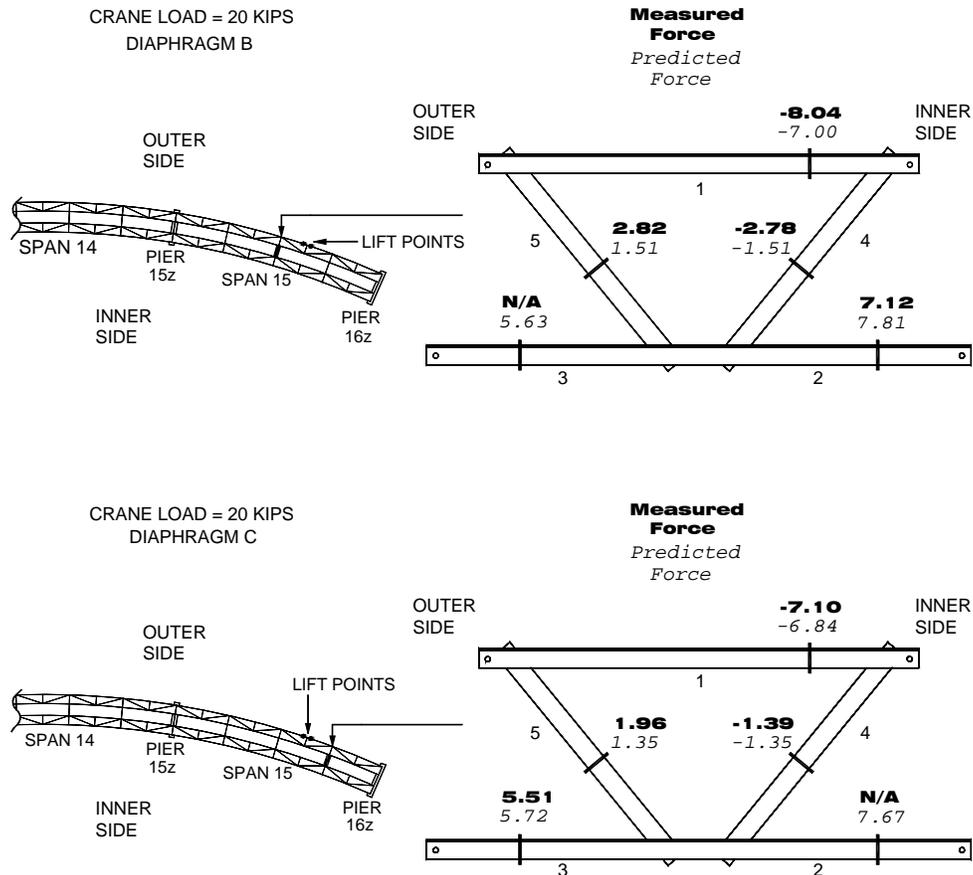
Figure 3.17 Diaphragm Crane Test Results

Considering the expected reliability of the external diaphragm data, the measured axial forces compare fairly well with the predicted forces. In diaphragm B, the measured diagonal forces are almost equal in magnitude, although almost twice than predicted. Since the diagonals do not see axial force from a pure twist of the girder, this diaphragm is probably transferring more vertical force than expected. One discrepancy in the measured results for diaphragm B is that member 1 is higher in magnitude than member 2. As seen in Table 3.1, a pure torsion on the girder would create forces of equal magnitude in these members and a vertical force on the diaphragm would create a higher axial force in member 2. Therefore, the force in member 1 should never be greater than in member 2 for this type of loading. After taking a closer look at this data, it was found that one of the gages on member 1 behaved inconsistently during the load test and went out of range some time later. The force calculation for this member is not as reliable as the others.

Instead of only comparing the measured and FEM predicted forces of each member in a diaphragm, the percentage of girder torsion and vertical load transmitted through the diaphragm was investigated. Figure 3.18 shows a schematic of how the diaphragms were analyzed.
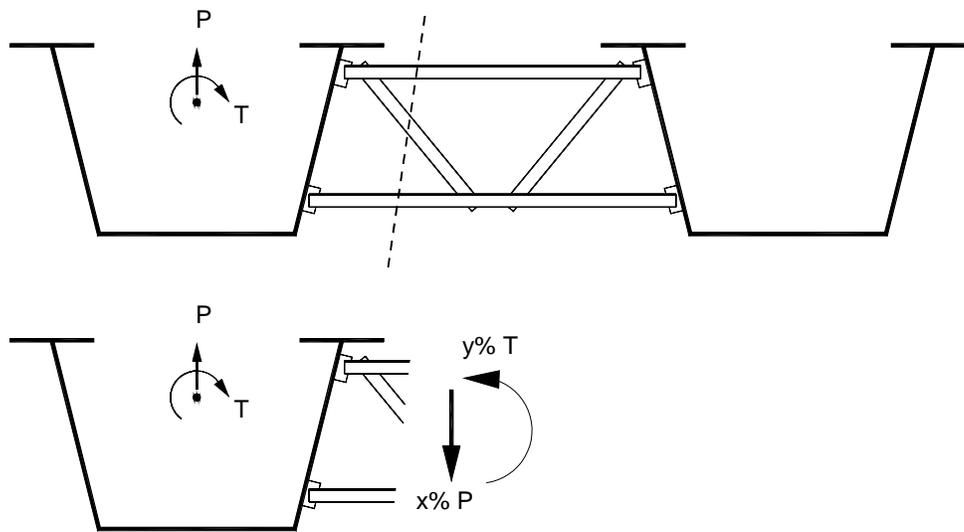
Figure 3.18 Force Breakdown on External Diaphragm

The FEM prediction for the external diaphragm was compared with the SAP model to determine what proportion of the load was distributed to the inner girder. The percentages of torsion and vertical load were adjusted on the SAP model results (Table 3.1) to match the FEM (Table 3.4). This was done by first adjusting the % of vertical load to match the diagonal forces since these members are not affected by torsion. Then, the % of torsion was estimated to match the other member forces with as much correlation as possible.

The best correlation between the models resulted in about 20% distribution of torsion from the crane load and 4% distribution of vertical force at both diaphragms. In other words, as compared to the SAP model in which 100% of the vertical force and torsion have to be transmitted through the diaphragms, the table shows the predicted percentages are forces that are distributed from the outer to inner girder. The SAP diaphragm and FEM diaphragm are modeled somewhat differently; hence there is some slight variance in the force predictions.

The measured results from the crane test were compared to the FEM results using the same technique. The percentages of torsion and force transmitted through the diaphragm in the SAP model were adjusted to correlate with the measured forces. The results are shown in Table 3.5.

Table 3.4 External Diaphragm FEM Results

Percentage of Torsion	Percentage of Vertical Load		Member				
			1	2	3	4	5
		FEM – B	-7.00	7.81	5.63	-1.51	1.51
Percentage of Torsion	**Percentage of Vertical Load**	SAP – B	-6.89	8.06	5.77	-1.51	1.50
21%	4.5%						
		% Difference	2%	3%	2%	0%	1%
		FEM – C	-6.84	7.67	5.72	-1.35	1.35
Percentage of Torsion	**Percentage of Vertical Load**	SAP – C	-6.88	7.82	5.77	-1.35	1.35
22%	4.0%						
		% Difference	1%	2%	1%	0%	0%

Crane Test Results: Load = 20 kips

Table 3.5 External Diaphragm Measured Results

Percentage of Torsion	Percentage of Vertical Load		Member				
			1	2	3	4	5
		Measured – B	-8.04	7.12	-	-2.78	2.82
Percentage of Torsion	**Percentage of Vertical Load**	SAP – B	-4.97	7.14	-	-2.79	2.77
4%	8.3%						
		% Difference	38%	0%	-	0%	2%
		Measured – C	-7.10	-	5.51	-1.39	1.96
Percentage of Torsion	**Percentage of Vertical Load**	SAP – C	-6.83	-	5.77	-1.44	1.43
21%	4.3%						
		% Difference	4%	-	5%	3%	27%

As expected, the measured results did not match the SAP model nearly as well as the FEM. For diaphragm B, the percentages adjusted for correlation between the SAP model and measured results were weighted much more heavily towards members 2, 4, and 5, rather than member 1 since this member's force calculation is questionable. Also, less consideration was given towards fitting the percentages with member 5 on diaphragm C, which did not show good repeatability during the crane test.

Comparing these percentages, diaphragm C compared extremely well with the predicted FEM. Both measured and predicted results show a distribution of torsion of about 20% and a distribution of vertical load of about 4% at this diaphragm. However, diaphragm B did not correlate well with the predicted values. Much higher forces were measured than predicted in the diagonal members; therefore more vertical load was transmitted through the diaphragm. The confidence in these readings is somewhat high since these members showed good repeatable during the test. Also, the compression in one diagonal is equal to the tension in the other. It is unclear whether this diaphragm's measured results are inaccurate or if this is a true phenomenon that is not predicted in the model.

CHAPTER 4:
CONCRETE DECK POURS

4.1 DESCRIPTION

After the steel girders were erected, permanent metal deck forms (PMDF) that span between the top flanges of the girders were installed. Removable deck forms, which cantilevered from the outsides of the girders, provided additional space for the construction workers and the track for the screed (Figure 4.1). Longitudinal and transverse reinforcement were then placed on top of the PMDF and removable forms. Figure 4.2 and Figure 4.3 show before/after pictures of the deck, forms, and reinforcement installation. Figure 4.4 shows the screed used during a typical concrete pour.
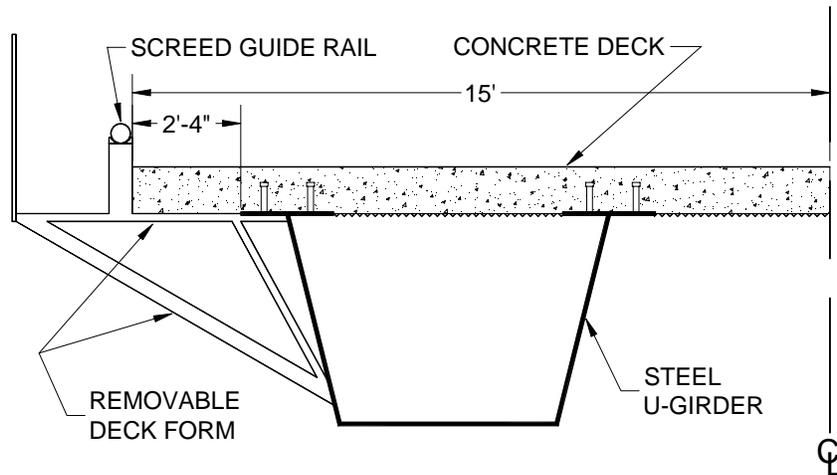
Figure 4.1 Cross Section View of Girder, Forms, and Deck

Figure 4.2 View of Z-Connect from Pier 16Z

Figure 4.3 Deck Forms and Reinforcement Installation

Figure 4.4 Concrete Screed

4.1.1   Z-Connect Concrete Pour Sequence

The designer specified five pours on thesymmetical portion of Z-Connect. As mentioned in Chapter 1, the original lengths of each pour segment were modified based on FEM results. The concrete pour sequence for Z-Connect shown below in Figure 4.5. The arrows in Figure 4.5 indicate the direction the screed moved during each pour segment.
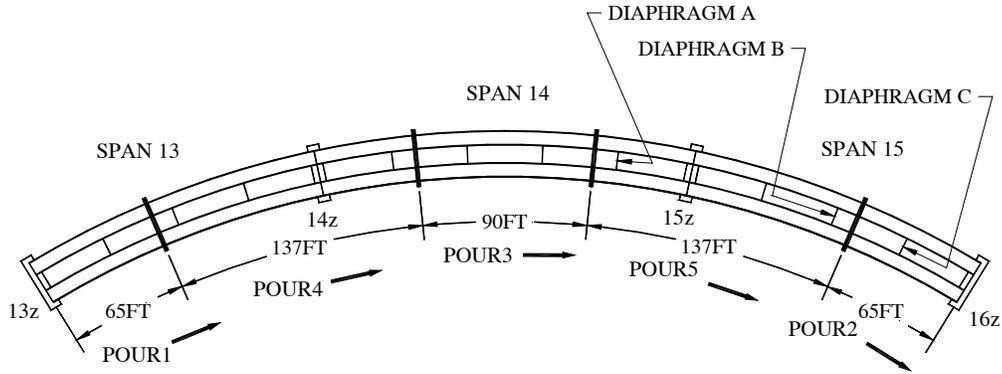
Figure 4.5 Concrete Pour Sequence

The sequence was selected to reduce the stresses in the girders and the top lateral bracing in the end spans. The negative moment regions (over piers 14z and 15z) were poured last to prevent cracking of the concrete deck. Pours 1 through 3 took place on the early morning of September 1, 2000 while segments 4 and 5 were poured a week later on the early morning of September 8. The majority of the pours were performed before the sun came out; therefore stress changes in the bridge due to temperature effects were small for the majority of the concrete pours. The changes in stress due to thermal gradients were considered by comparing the concrete pour data with data from days prior to the pour during similar periods of time.

Figure 4.6 and Figure 4.7 show the times that concrete was poured over certain sections of the bridge. The timing of the pour progress is important because of its effect on early composite action between the new concrete deck and steel girders. This will be discussed further in Section 4.2.1.
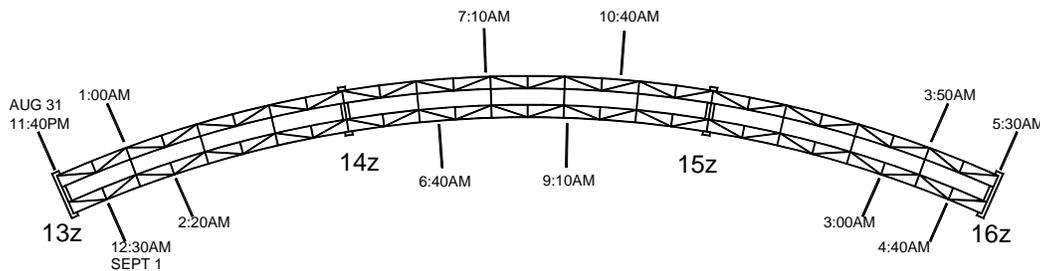
Figure 4.6 Progress of Pours 1, 2 and 3: Aug 31 - Sept 1
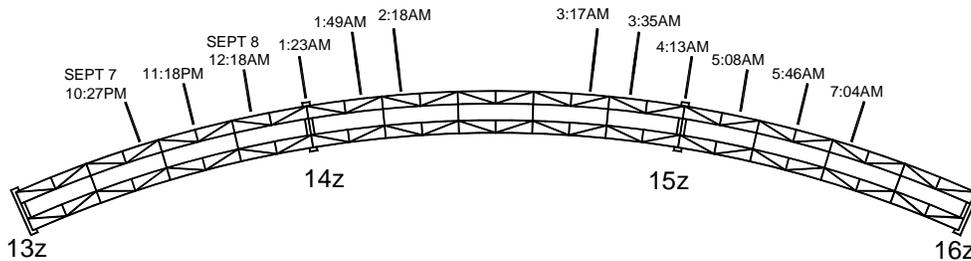
Figure 4.7 Progress of Pours 4 and 5: Sept 7 - Sept 8

The stress changes from the concrete pour discussed in this chapter are due to the weight of the concrete, weight of the screed, and the weight of the construction crew during the pour. Compared to the screed and workers, the weight of the poured concrete is the dominant force acting on the bridge. For example, only 5 ft of poured concrete along the width of the bridge weighs about 15 kips. The weight of the screed is less than 2 kips. The self-weight of the girders, the weight of the PMDF, removable forms, and deck reinforcement are all included in the zero reading for stress and force calculations.

4.1.2 K-Connect Concrete Pour Sequence

The pouring sequence on Bridge K was symmetric, as shown in Figure 4.8. The pours were conducted in one week in March 2001. There were approximately two-and-a-half days in between the first two pours, followed by pours 2 through 5 on consecutive nights. The pour schedule is listed in Figure 4.8. Pour 1 was done in the morning with some cloud cover and temperatures in the mid 60s (°F). The other four pours were done in the overnight hours with some cloud cover and temperatures in the 40s.

4.1.3 Y-Connect Concrete Pour Sequence

The pouring sequence of bridge Y was divided into seven separate sections that were poured on three separate nights in late June 2001. The pouring sequence and schedule can be seen in Figure 4.9. The pours were conducted overnight with clear skies and temperatures in the high 70s and low 80s (°F). Similar to the bridge K concrete pours, no temperature correction was applied to any of the Y pour data.

4.2 TOP LATERAL RESULTS

4.2.1 Z-Connect

Each top lateral WT had two cross sections gaged for redundancy. The majority of force measurements for the two sections of each member was nearly identical during the concrete pour as shown in Figure 4.10 through Figure 4.13. One cross section on the member is indicated by a "☐" and the other by a "✕". Members that do not show both these symbols had a bad gage at one of the cross sections. Fortunately, no member had a bad gage at both cross sections. The graphs shown are for pours 1 and 2, although similar results were found during every pour segment. When applicable, the two axial forces for each member were averaged for each time increment.

4.2.2 Early Composite Action

The measured top laterals were located under regions where the concrete was first poured; it was evident from the data that the concrete was beginning to harden before completion of the pouring sequence. The top laterals are located very close to the compression flange of the steel girder; hence they are far from the neutral axis of the non-composite section and very close to the neutral axis of the composite section (Figure 4.14). This means that the changes in stress due to bending in the members should be much higher before the section is composite. Also, the hardened concrete completes a closed box section that reduces the forces in the laterals due to torsion.
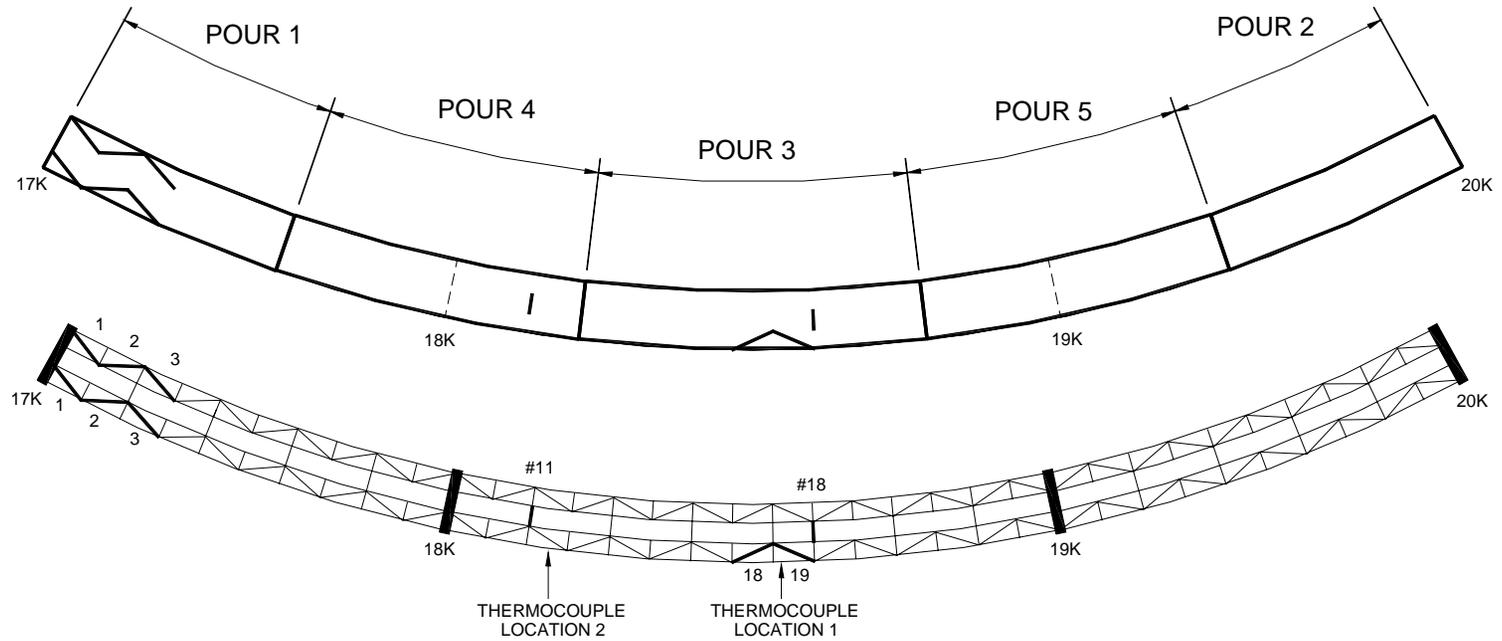
	START		END		DURATION
POUR 1	3/13/01	8:39 A.M.	3/13/01	11:10 A.M.	2 hr 31 min
POUR 2	3/16/01	12:27 A.M.	3/16/01	2:05 A.M.	1 hr 38 min
POUR 3	3/17/01	12:00 A.M.	3/17/01	3:20 A.M.	3 hr 20 min
POUR 4	3/17/01	10:30 P.M.	3/18/01	12:30 A.M.	2 hr 0 min
POUR 5	3/18/01	1:06 A.M.	3/18/01	2:54 A.M.	1 hr 48 min

ALL POURS GO TOWARDS 20K

Figure 4.8 Concrete Pour Sequence for K-Connect

POUR 2

POUR 6

POUR 7

POUR 3

POUR 4

POUR 5

4Y

3Y

POUR 1

2Y

5Y/23K

1Y

4Y

3Y

2 1

2Y

2 1

5Y/23K

1Y

	START		END		DURATION
POUR 1	6/27/01	9:31 P.M.	6/28/01	2:46 A.M.	5 hr 15 min
POUR 2	6/28/01	4:35 A.M.	6/28/01	6:41 A.M.	2 hr 6 min
POUR 3	6/28/01	9:20 P.M.	6/28/01	11:12 P.M.	1 hr 52 min
POUR 4	6/29/01	12:38 A.M.	6/29/01	2:55 A.M.	2 hr 17 min
POUR 5	6/29/01	9:14 P.M.	6/29/01	10:52 P.M.	1 hr 38 min
POUR 6	6/29/01	11:35 P.M.	6/30/01	1:48 P.M.	2 hr 13 min
POUR 7	6/30/01	2:32 A.M.	6/30/01	3:56 A.M.	1 hr 24 min

ALL POURS GO TOWARDS 5Y/23K

Figure 4.9 Concrete Pour Sequence for Y-Connect
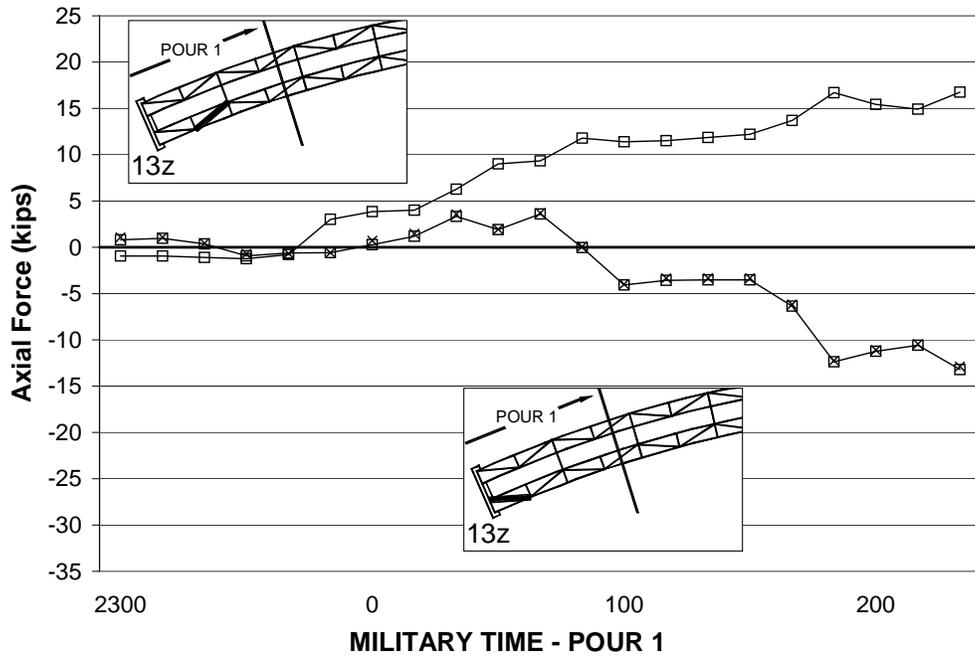
Figure 4.10 13Z Inner Top Lateral Forces during Pour 1
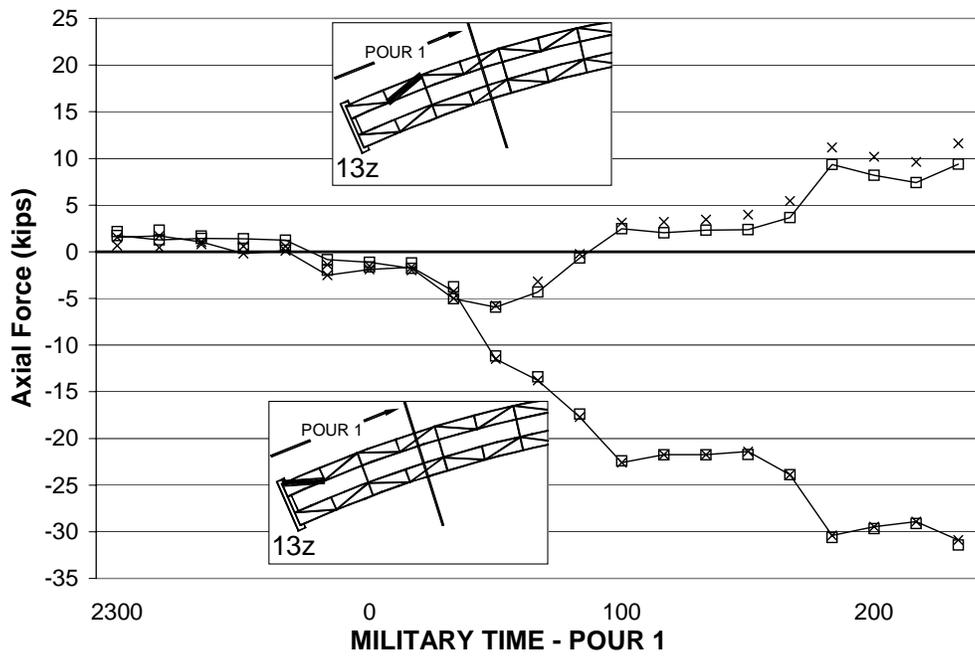
Figure 4.11 13Z Outer Top Lateral Forces during Pour 1
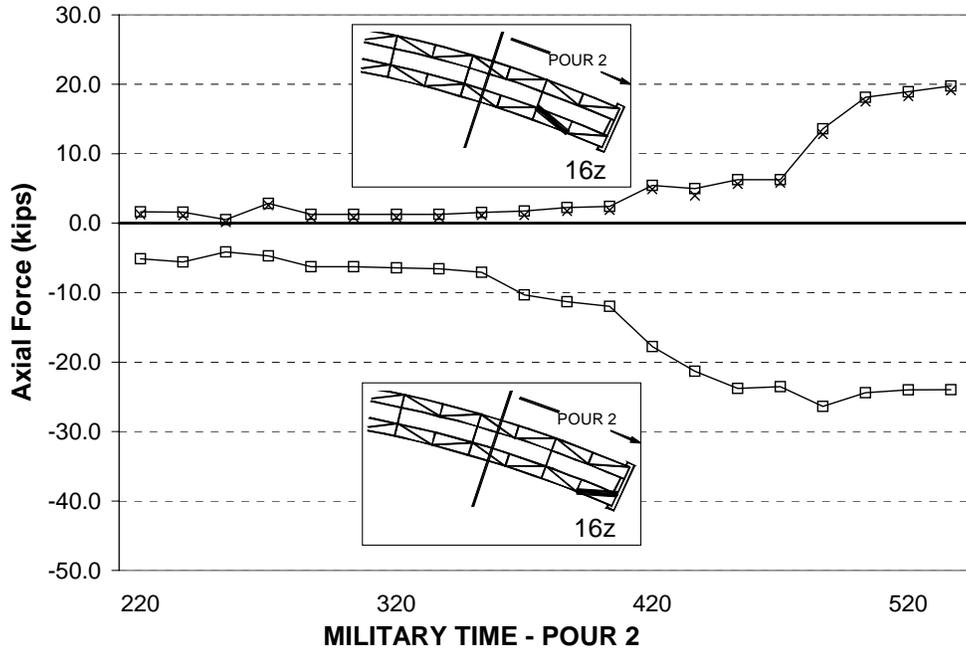
Figure 4.12 16Z Inner Top Lateral Forces during Pour 2
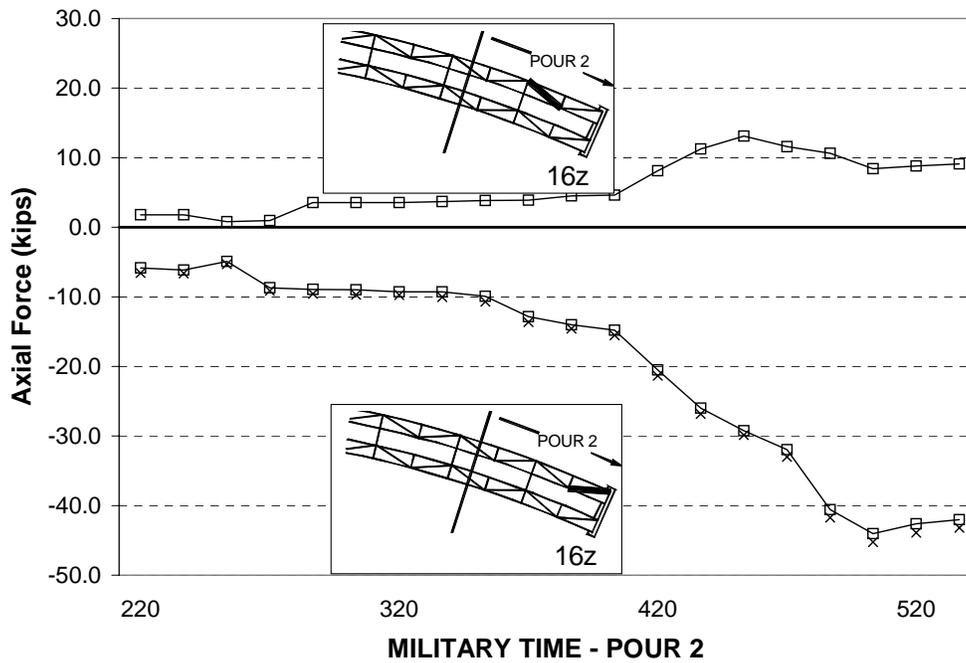
Figure 4.13 16Z Outer Top Lateral Forces during Pour 2
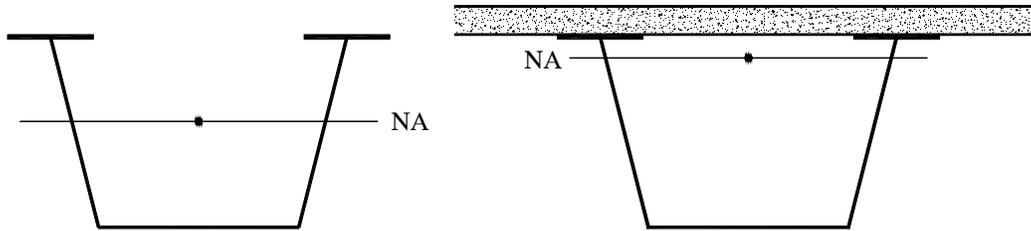
Figure 4.14 Approximate Neutral Axis Locations on Box Girders

The three-span bridge and the pour configuration are symmetrical. Therefore, when the middle span is poured (Pour 3 - Figure 4.15), the change in stress in the top laterals near pier 13z should be identical to the change in the top laterals near pier 16z. This is true assuming that all of the concrete from the first two pours has zero stiffness and does not contribute structurally. The concrete pour over the first two 13z laterals was at the earliest part of Pour 1 and the concrete pour over the first two 16z laterals was during the last part of Pour 2. Therefore, the concrete was setting for a much longer time over the 13z laterals than over the 16z laterals before the third pour. Table 4.1 shows the times for curing over these members during Pour 3.

Table 4.1 Curing Times During Pour 3

Pier	Lateral	Elapsed Time (hrs:min)			
		Pour 3 (0 ft.)	Pour 3 (30 ft.)	Pour 3 (60 ft.)	Pour 3 (90 ft.)
13z	1	6:10	6:40	8:40	10:10
	2	5:40	6:10	8:10	9:40
16z	1	1:10	1:40	3:40	5:10
	2	2:00	2:30	4:30	6:00

The concrete that was poured over the first top lateral at pier 13z was in place and had more than 6 hours to cure before the start of Pour 3. The same section at pier 16z was only in place for about one hour before starting Pour 3.

The axial forces in the eight instrumented top laterals during Pours 1-3 are shown in Figure 4.7 through Figure 4.8. On each of the graphs, section "A" shows the change in axial force in the lateral due to the concrete pour over that lateral. Section "B" shows the change in axial force due to the concrete pour on the opposite side of the bridge. Section "C" shows the change in axial force due to Pour 3. The graphs are arranged in this orientation to show the effect of the curing on the top lateral forces. Ideally, both columns of each section in the graph should be identical if there was no effect from the curing.

Section "A" of each graph shows very similar behavior between the 13z and 16z laterals, as expected. These are nearly identical loading cases for the members. Less change in force occurs in the second section of the graph since the load is two spans away from the measured lateral. Section "C" of each graph shows convincingly that composite action from Pour 1 is occurring. The third pour induces a force change of 20-35 kips in all of the 16z laterals. The 13z laterals, however, have barely any change in force during this pour. This is because the concrete is already hardening over this region carrying the load rather than the lateral. Although the concrete may not be near its full strength, it has increased significantly in stiffness during this time. If the concrete did not contribute to carrying load, then the force change in the 13z laterals would be equal to the 16z laterals.
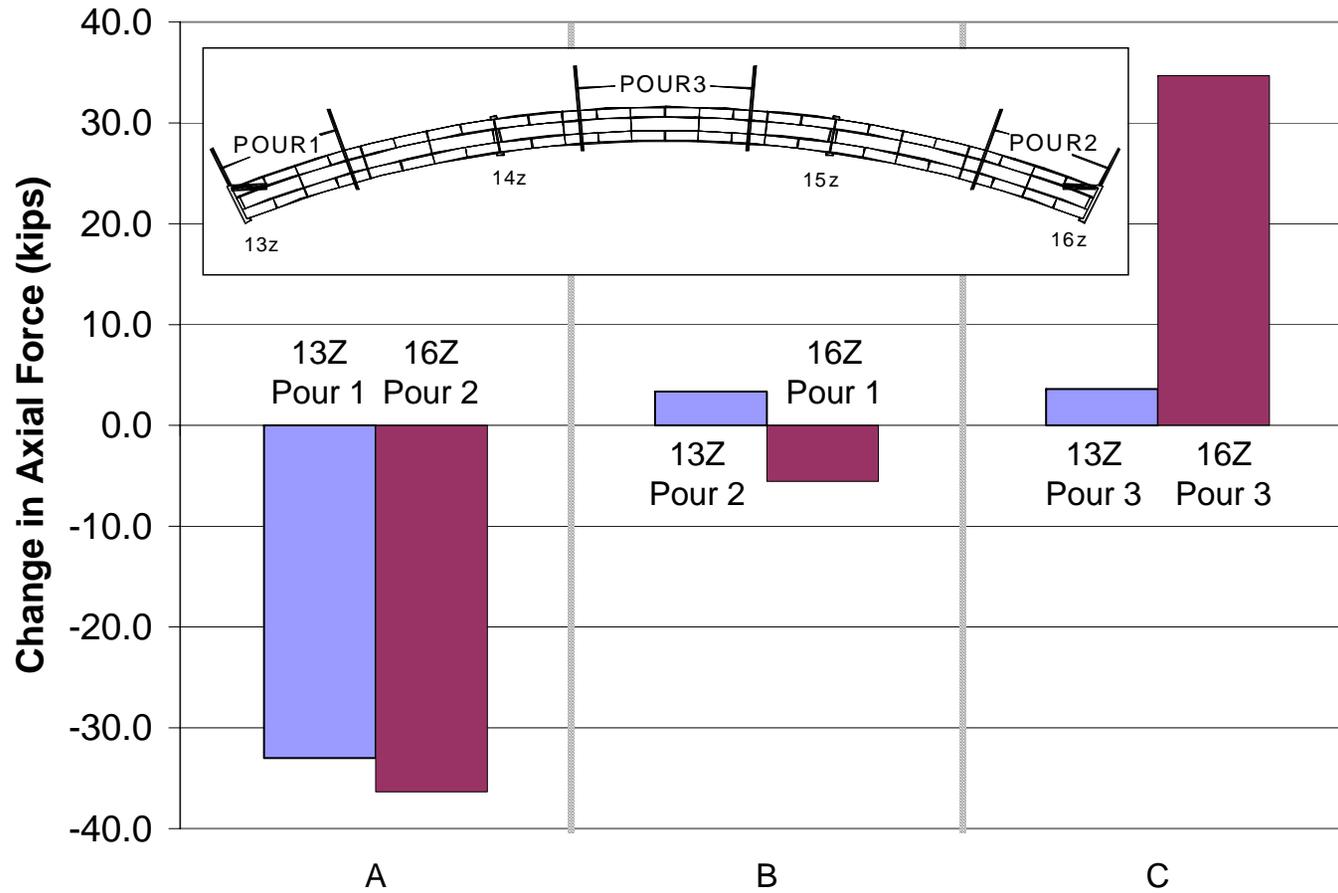
Figure 4.15 Outer First Top Laterals - Change in Axial Force due to Pours 1-3
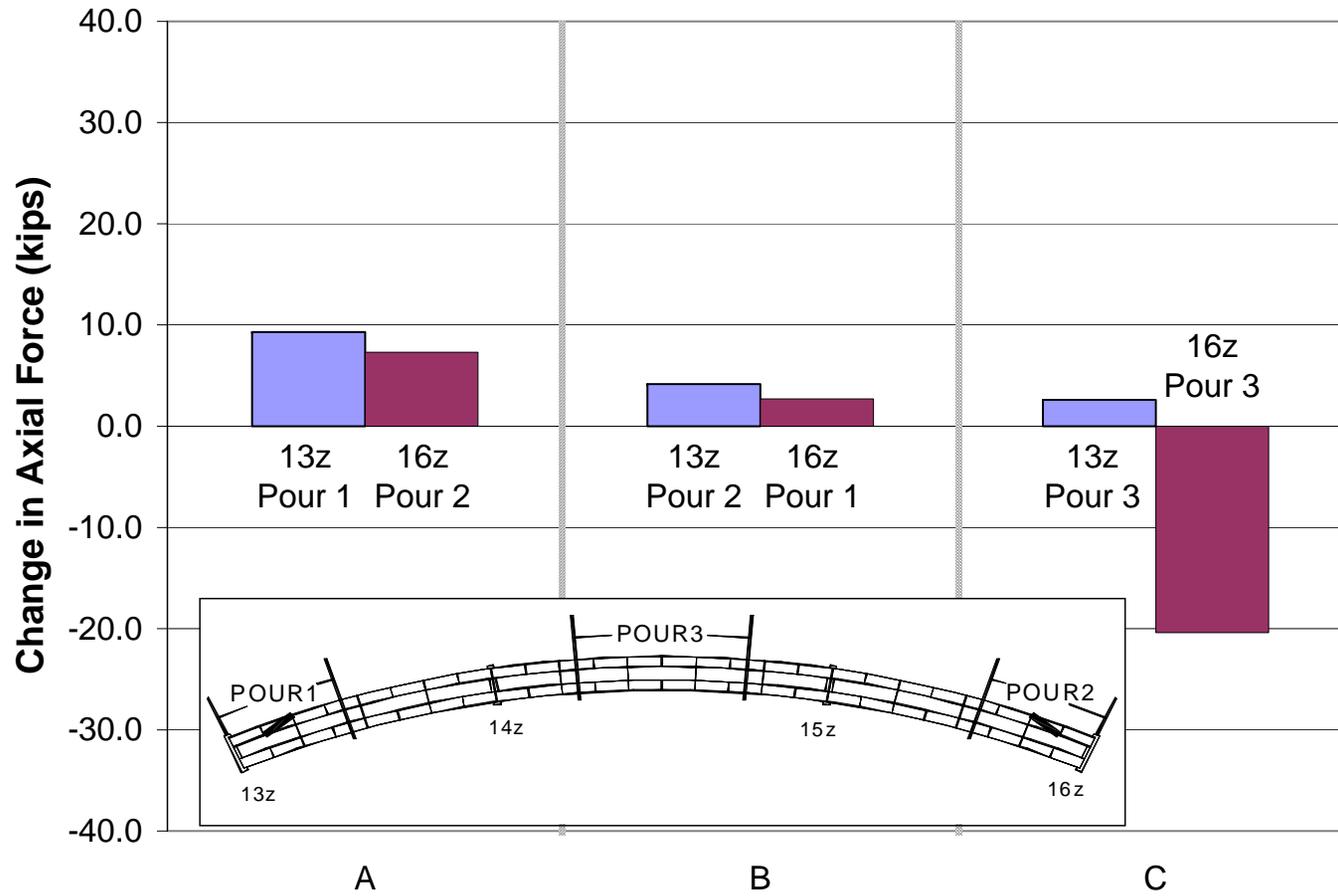
Figure 4.16 Outer Second Top Laterals – Change in Axial Force due to Pours 1-3
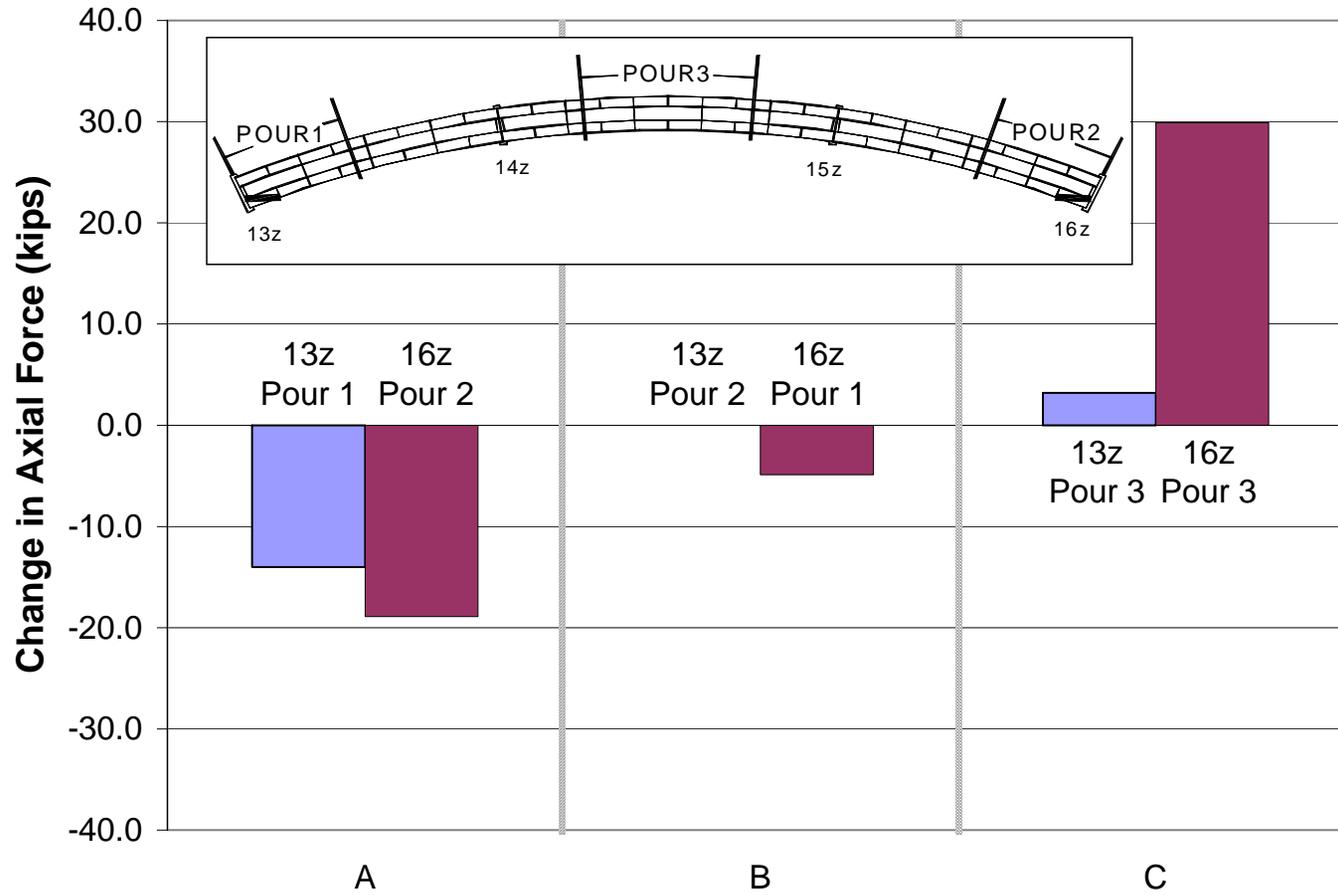
Figure 4.17 Inner First Top Laterals – Change in Axial Force due to Pours 1-3
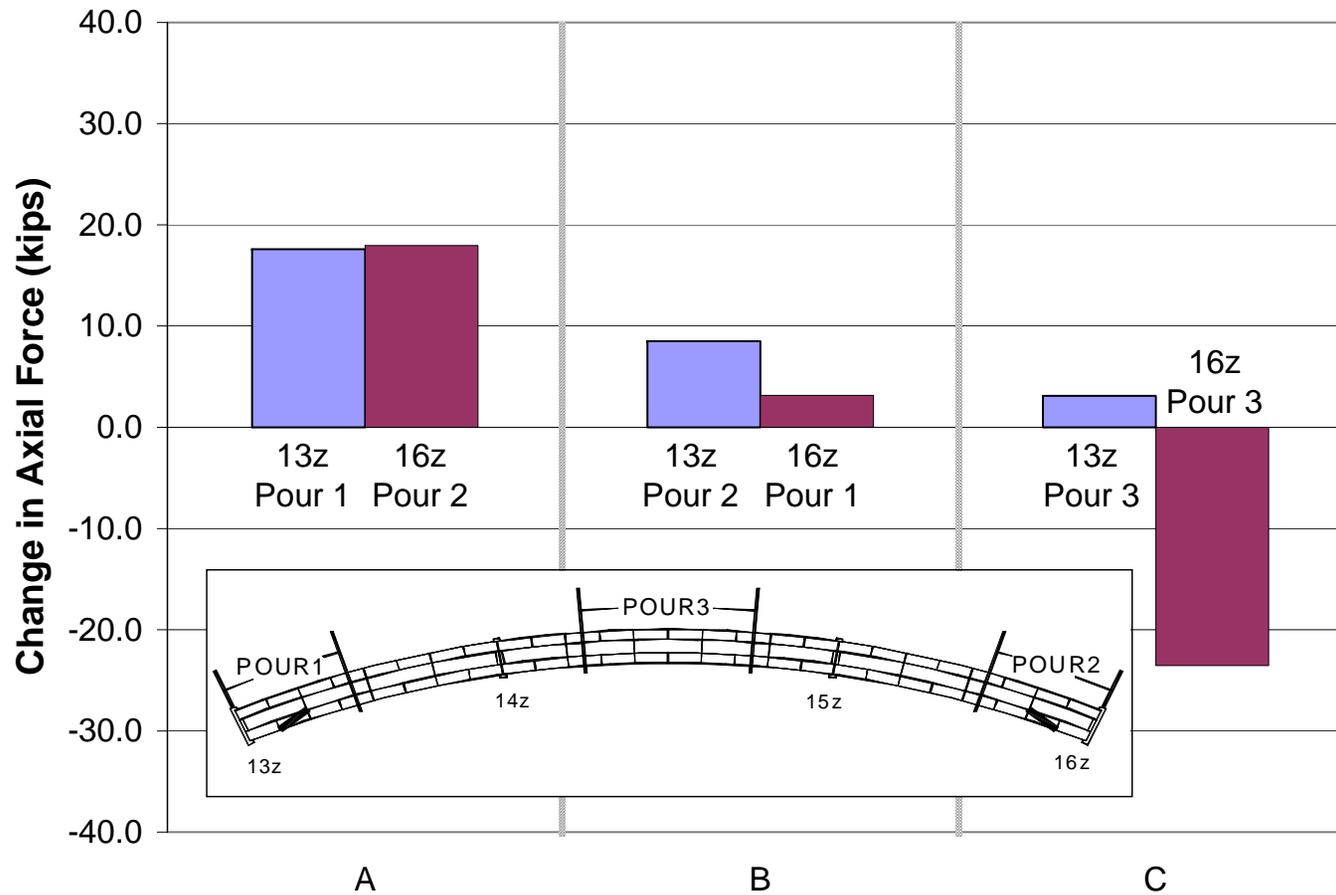
Figure 4.18 Inner Second Top Laterals – Change in Axial Force due to Pours 1-3

4.2.3   K-Connect

During each of the concrete pours, the data acquisition system collected strain gauge readings every 10 minutes. The data were either downloaded using a laptop to directly connect to the datalogger or via modem.

The calculated values of axial forces in the instrumented top laterals were used to determine the measured change in axial force caused by each pour individually. This measured force is simply an absolute change in axial force or stress; the values at the time immediately before the start time of each pour were subtracted from the values at the time immediately after the end time of each pour.

For example, pour 1 began at 12:27 A.M. and ended at 2:05 A.M. The axial force and stress starting values were taken at 12:20 A.M., and the ending values were taken at 2:10 A.M. In all cases, the data showed very little change before the start time and after the stop time, so it was acceptable to use the value calculated only at one point.

The measured changes were compared with the values determined by Topkaya using the bridge finite element model (FEM). These results are presented in Table 4.2. For each instrumented location, there is a bar chart comparing the measured values and the values predicted using the FEM.

A sample bar chart is presented in Figure 4.19. The measured change due to pour 1 matches up well with the predicted change; however, for the remaining pours, the measured change is lower and in some cases, significantly lower, than the predicted change. This is most likely due to composite action between the concrete deck and the steel girders. The finite element analysis (FEA) assumed that the load was carried by the non-composite steel girder.

Figures 4.20 through 4.24 are presented in order to show how the bar chart in Figure 4.19 was developed. Figure 4.20 shows a time history of the axial force in the member. The time scale is so large that only the start times of each pour can be shown. The time axis shows data for two weeks, and the pours only last a few hours; therefore, it is not possible to see both the start and stop times of each pour at this scale.

In addition to the average axial force of the member, the air temperature at the bridge site is also plotted in Figure 4.20. It can be seen that the bridge reacts to the temperature on a 24-hour cycle; however, upon looking at Figures 4.21 through 4.24, which show each of the pours on a smaller time scale, it becomes evident that temperature is not a factor during the pours; the change in force caused the temperature during the pours is negligible compared to the effect of the load of the wet concrete. The same is true for all instrumented cross sections during all pours on the bridge. Therefore, there was no temperature correction made to any of the pour data.

Table 4.2 Top Lateral Forces During Deck Casting, K-Connect

Panel 1	Outer Girder		Inner Girder	
	Field (kips)	**ABAQUS (kips)**	**Field**	**ABAQUS**
Change due to Pour 1	53.8	57.2	34.0	48.4
Change due to Pour 2	2.8	7.5	2.5	7.3
Change due to Pour 3	3.6	-58.1	1.8	-56.3
Change due to Pour 4	-0.3	9.1	-0.3	8.5
Change due to Pour 5	-0.2	-1.2	-0.2	-1.1
Total Change	59.8	14.6	37.7	6.7

Panel 2	Outer Girder		Inner Girder	
	Field (kips)	**ABAQUS (kips)**	**Field**	**ABAQUS**
Change due to Pour 1	-54.7	-66.0	-55.7	-64.8
Change due to Pour 2	2.6	-8.1	2.4	-7.8
Change due to Pour 3	5.2	62.8	3.7	60.2
Change due to Pour 4	-0.4	-10.4	-0.4	-9.6
Change due to Pour 5	0.0	1.3	0.0	1.2
Total Change	-47.4	-20.4	-50.0	-20.8

Panel 3	Outer Girder		Inner Girder	
	Field (kips)	**ABAQUS (kips)**	**Field**	**ABAQUS**
Change due to Pour 1	16.4	17.4	11.8	15.1
Change due to Pour 2	2.7	4.9	2.4	5.0
Change due to Pour 3	5.0	-37.8	4.0	-38.0
Change due to Pour 4	-0.5	4.2	-0.6	4.1
Change due to Pour 5	-0.1	-0.7	-0.1	-0.7
Total Change	23.5	-12.1	17.5	-14.7

Panel 18	Outer Girder		Inner Girder	
	Field (kips)	**ABAQUS (kips)**	**Field**	**ABAQUS**
Change due to Pour 1	-5.2	-6.1	----	----
Change due to Pour 2	11.8	14.1	----	----
Change due to Pour 3	-21.7	-37.1	----	----
Change due to Pour 4	-2.2	-1.7	----	----
Change due to Pour 5	-0.9	-0.9	----	----
Total Change	-18.2	-31.7	----	----

Panel 19	Outer Girder		Inner Girder	
	Field (kips)	**ABAQUS (kips)**	**Field**	**ABAQUS**
Change due to Pour 1	13.5	18.7	----	----
Change due to Pour 2	1.9	6.1	----	----
Change due to Pour 3	-45.9	-97.9	----	----
Change due to Pour 4	-2.0	-1.1	----	----
Change due to Pour 5	-1.0	-3.0	----	----
Total Change	-33.6	-77.2	----	----
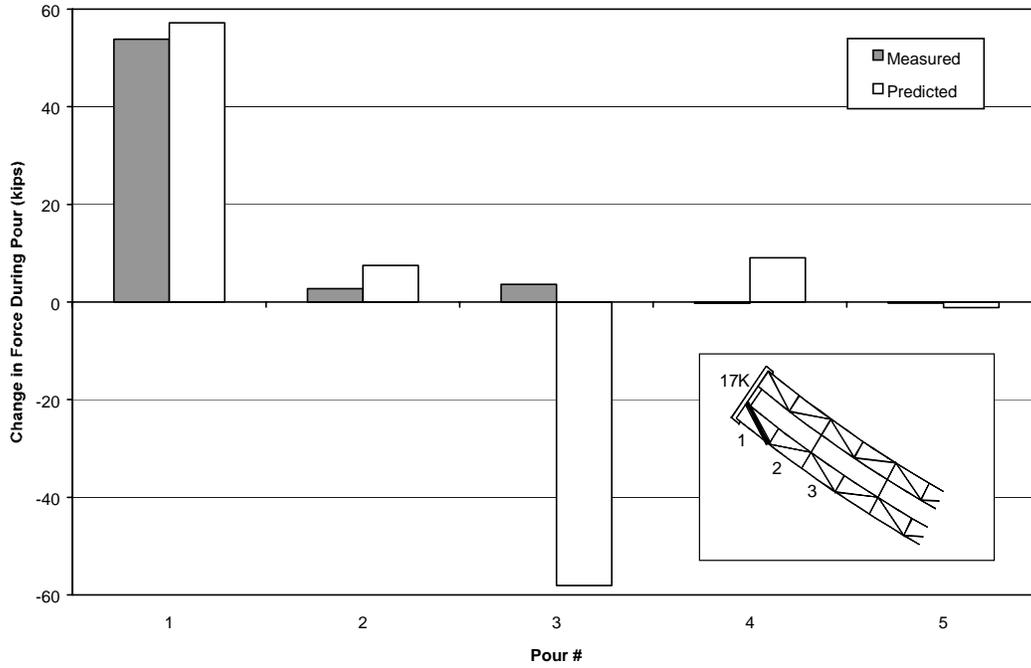
Figure 4.19 Outer Girder Top Lateral 1 Panel from Pier 17K, Comparison
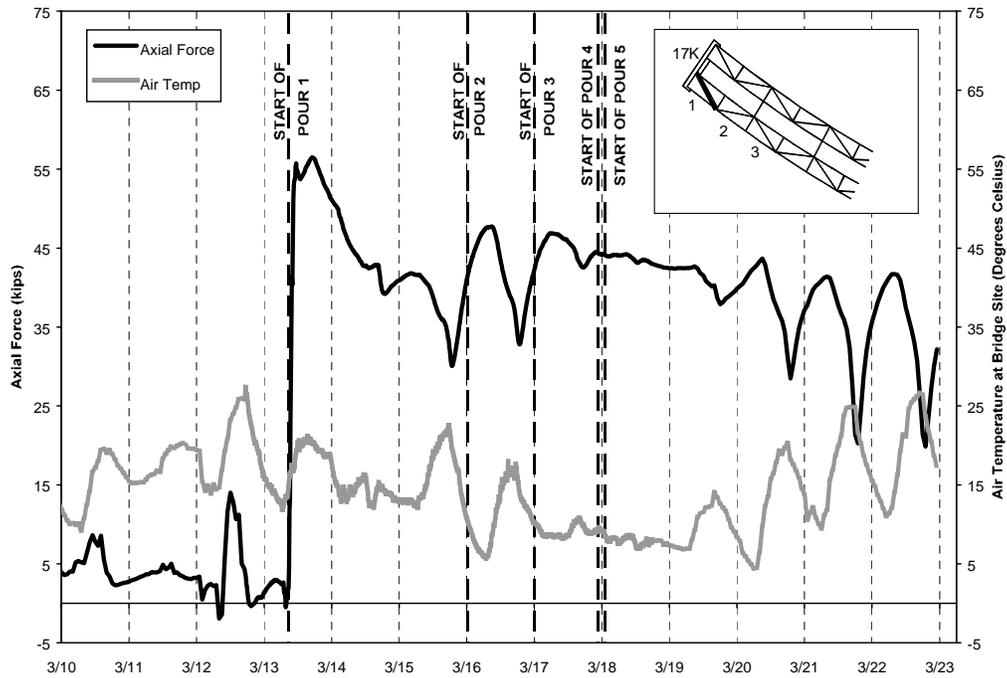
**Figure 4.20 Outer Girder Top Lateral 1 Panel from Pier 17K
during K Pours, Average Axial Force**
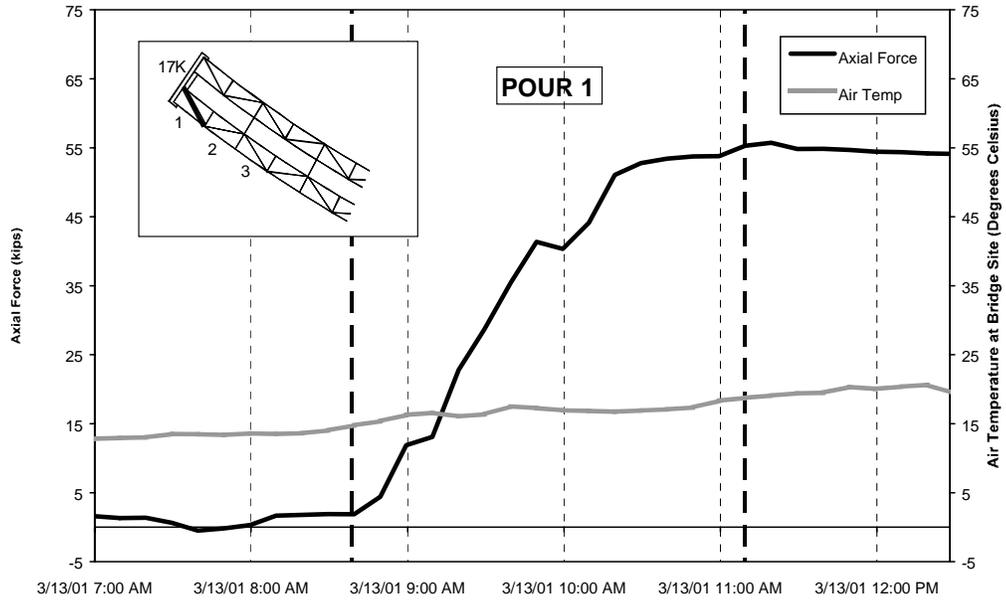
Figure 4.21 Outer Girder Top Lateral 1 Panel from Pier 17K During K Pour 1
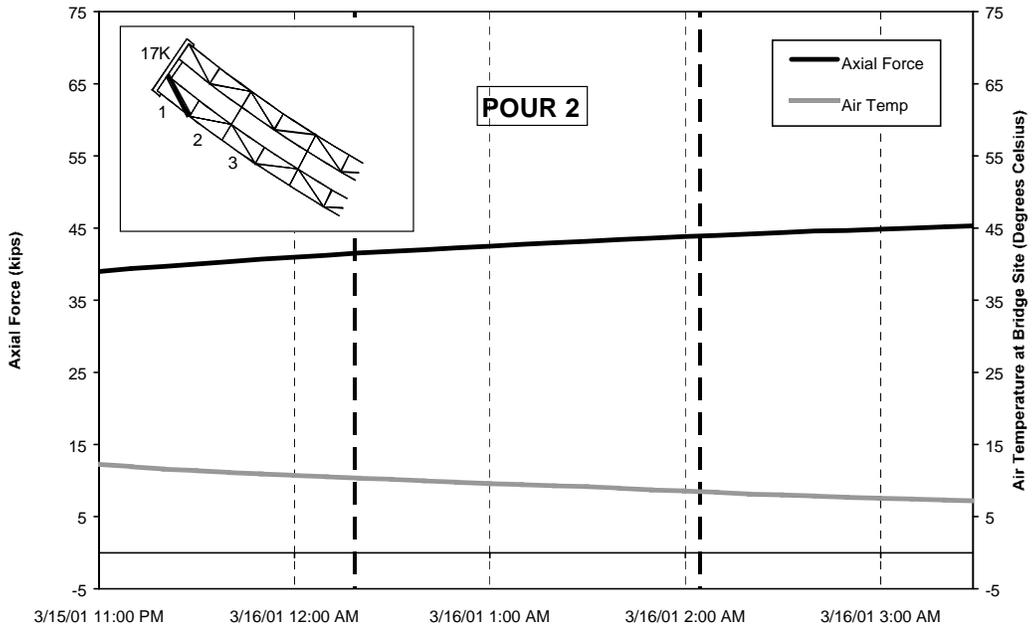
Figure 4.22 Outer Girder Top Lateral 1 Panel from Pier 17K During K Pour 2
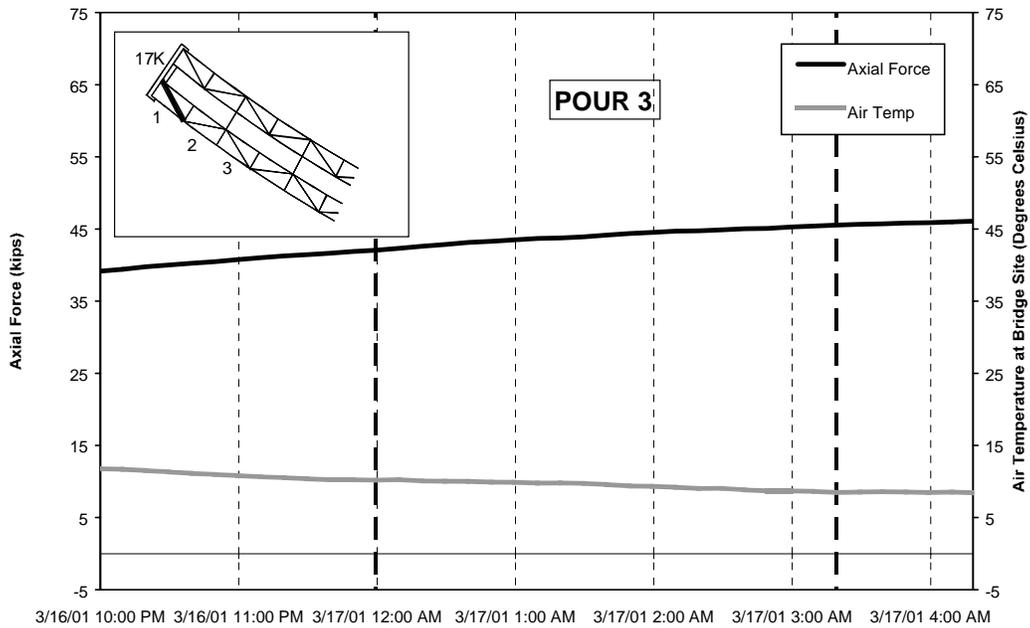
Figure 4.23 Outer Girder Top Lateral 1 Panel from Pier 17K During K Pour 3
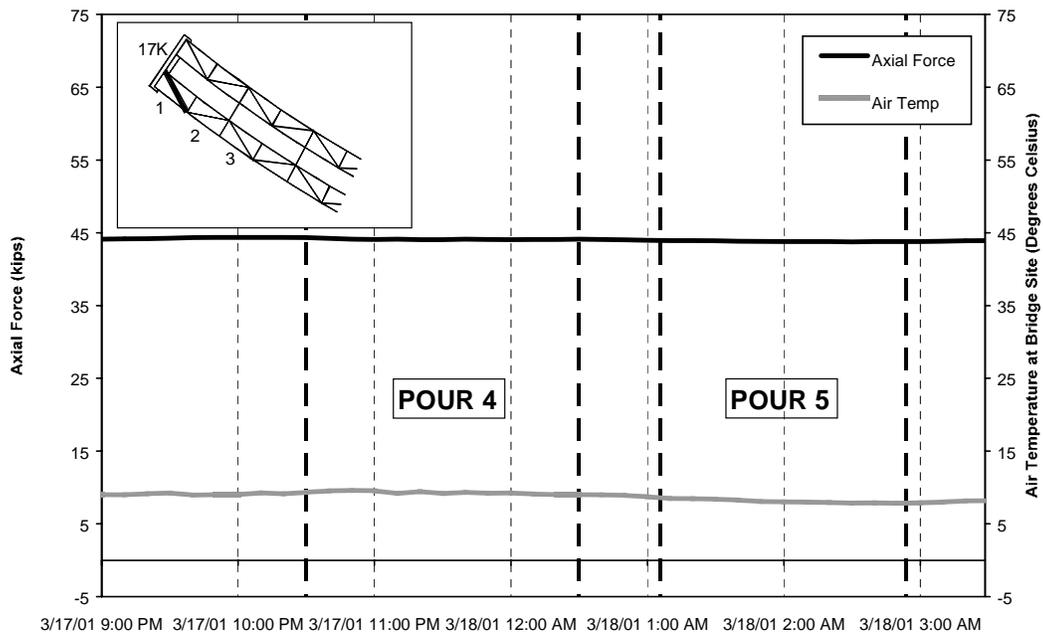
Figure 4.24 Outer Girder Top Lateral 1 Panel from Pier 17K During K Pours 4 & 5

4.2.4   *Y-Connect*

During each of the concrete pours, the data acquisition system collected strain gauge readings every 5 minutes. The data were downloaded using a laptop directly connected to the datalogger. The   calculated

values of axial forces in the instrumented locations were used to determine the measured change in axial force caused by each pour individually. This is the same manner as described for bridge K.

The measured changes were also compared with values determined by Topkaya using the bridge FEM. These results are presented in Table 4.3. For each instrumented lateral, there is a bar chart comparing the measured changes and the changes predicted using the FEM. A sample of the results is presented in Figure 4.25.

Presented along with Figure 4.25 are Figures 4.26, 4.27, and 4.28, which are close-ups of the time history plots of the individual pours on Y-Connect. Figure 4.26 plots the axial force on the first night of pouring (pours 1 and 2); Figure 4.27 plots the axial force on the second night (pours 3 and 4); and Figure 4.28 plots the third night (pours 5, 6, and 7). There is no data for pour 2 and the very beginning of pour 3.

Table 4.3 Top Lateral Forces during Deck Casting, Y-Connect

	Outer Girder		Inner Girder	
Panel 1	**Field (kips)**	**ABAQUS (kips)**	**Field**	**ABAQUS**
Change due to Pour 1	-5.2	-5.0	-5.6	-5.0
Change due to Pour 2	-----	-55.0	-----	-57.0
Change due to Pour 3	79.0	120.0	61.3	123.0
Change due to Pour 4	16.9	16.0	15.6	17.0
Change due to Pour 5	0.6	3.0	0.2	3.0
Change due to Pour 6	-0.9	40.0	-0.1	41.0
Change due to Pour 7	-0.6	-4.0	-0.8	-4.0
Total Change	-----	156.0	-----	160.0

	Outer Girder		Inner Girder	
Panel 2	**Field (kips)**	**ABAQUS (kips)**	**Field**	**ABAQUS**
Change due to Pour 1	10.9	6.0	10.9	6.0
Change due to Pour 2	-----	59.0	-----	61.0
Change due to Pour 3	-69.7	-146.0	-64.2	-141.0
Change due to Pour 4	-11.8	-18.0	-14.5	-18.0
Change due to Pour 5	0.3	-3.0	0.4	-3.0
Change due to Pour 6	-2.7	-44.0	-1.8	-45.0
Change due to Pour 7	-0.6	3.0	-0.9	4.0
Total Change	-----	-188.0	-----	-181.0
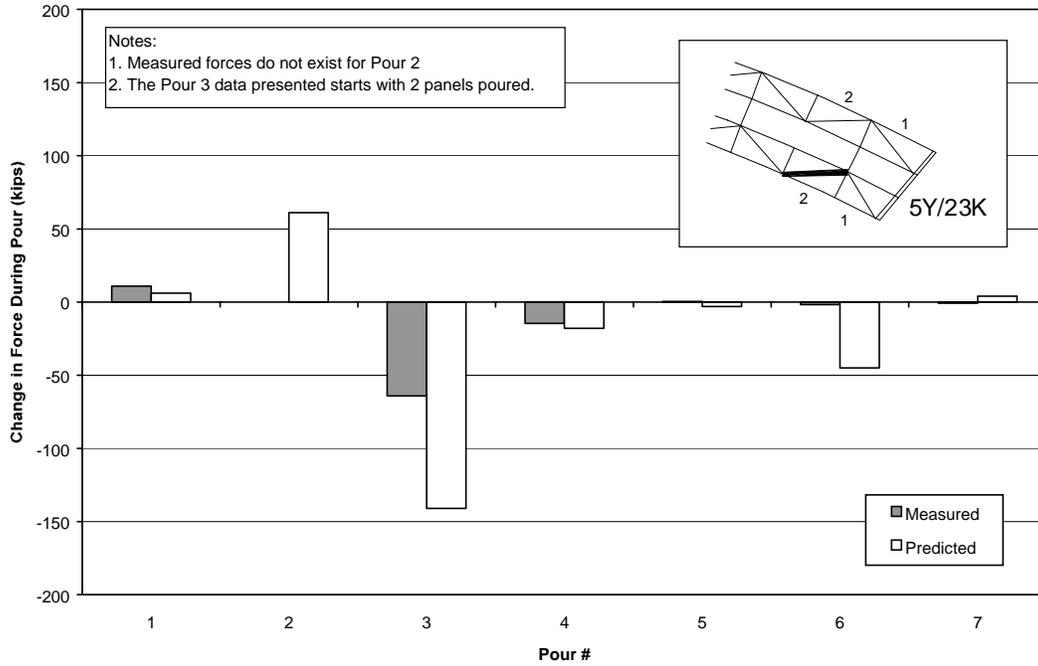
Figure 4.25 Inner Girder Top Lateral 2 Panels from Pier 5Y/23K, Comparison
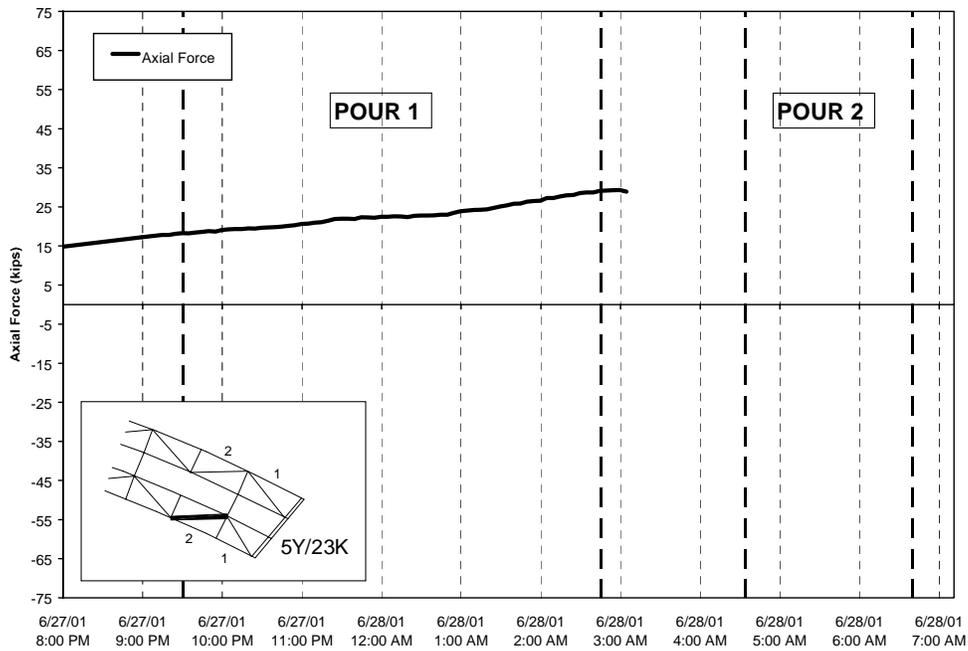
Figure 4.26 Inner Girder Top Lateral 2 Panels from Pier 5Y/23K During Y Pours 1 & 2

66
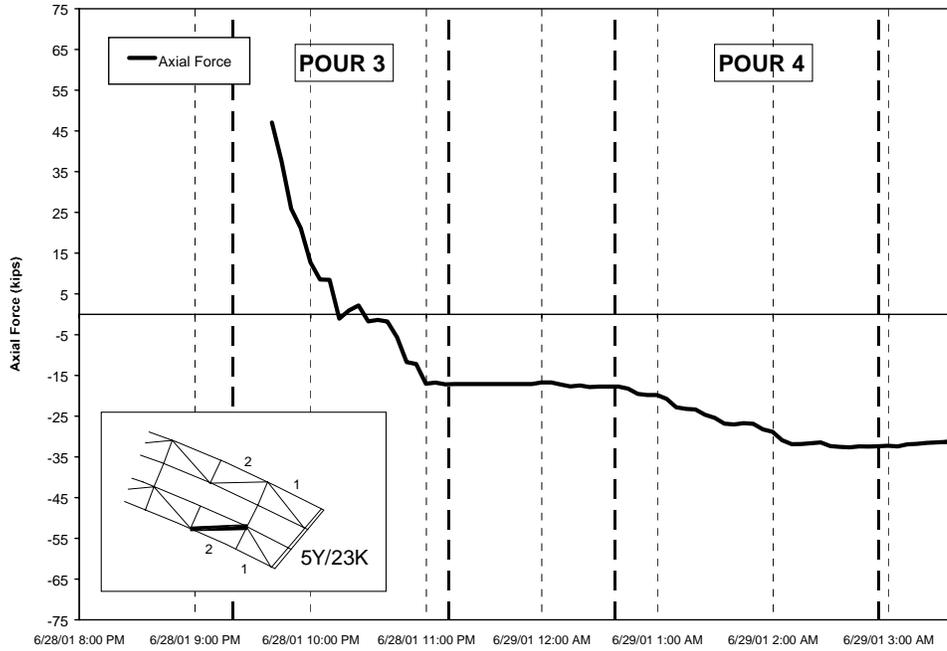
Figure 4.27 Inner Girder Top Lateral 2 Panels from Pier 5Y/23K During Y Pours 3 & 4
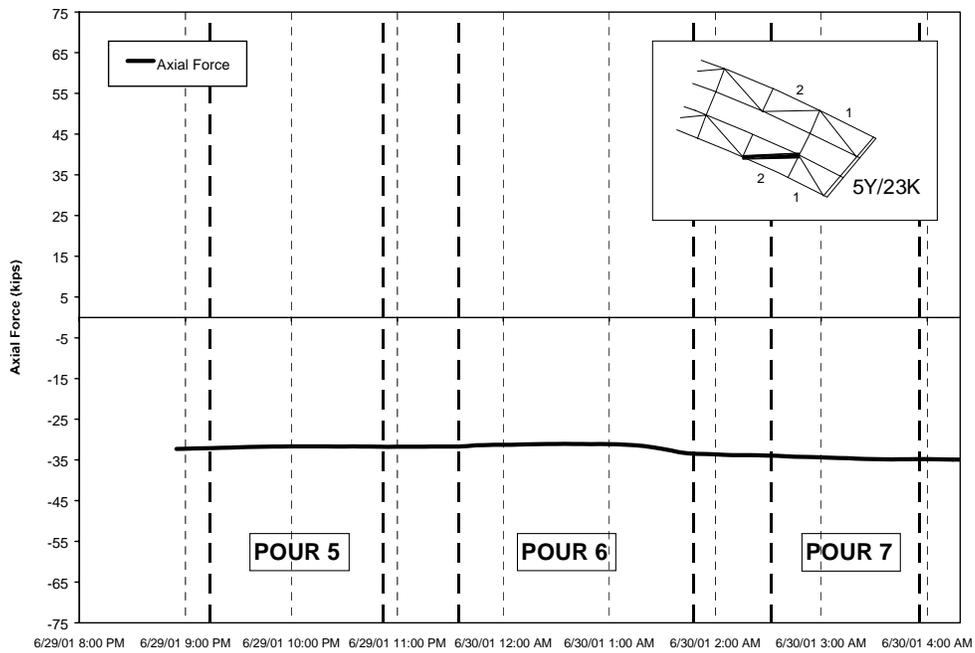
Figure 4.28 Inner Girder Top Lateral 2 Panels from Pier 5Y/23K During Y Pours 5, 6, & 7

4.3 EXTERNAL DIAPHRAGM RESULTS

4.3.1 Z-Connect

4.3.1.1 Temperature Effects on Diaphragms

The majority of the concrete pours took place while the sun was set. Lopez (1999) showed that thermal gradients during this period are small, hence force changes in the bridge should also be small. However, since the stresses developed in the external diaphragms from the concrete pour were not very large, the effect of temperature on the bridge was considered. This was done by examining force measurements of the same members throughout several days prior to the pour.

Figure 4.29 through Figure 4.32 show some typical measurements of force changes in the external diaphragm members during two nights before each pour. Although there is some slight variation in the change of axial force with time, the average force change during a certain time period for a member is nearly the same each day. The change in force due to temperature was examined separately for each pour period. For pours 1 through 3, data was used from days just prior to the pour so the effects of the formwork on thermal gradients would be included. For pours 4 through 5, different history data was used since the bridge was partially composite in some areas and had different thermal characteristics compared to the exposed girders. The temperature plotted in the figures was recorded by the data acquisition system's thermistor, which is located inside the box girder.

Although the majority of temperature data was repeatable from one day to the next, there was some variation of force change as shown in Figure 4.32. This adds some uncertainty to the measurements when differentiating the stresses due to temperature and the stresses due to the concrete weight. However, the majority of the temperature data during the hours of the concrete pour showed good repeatability.
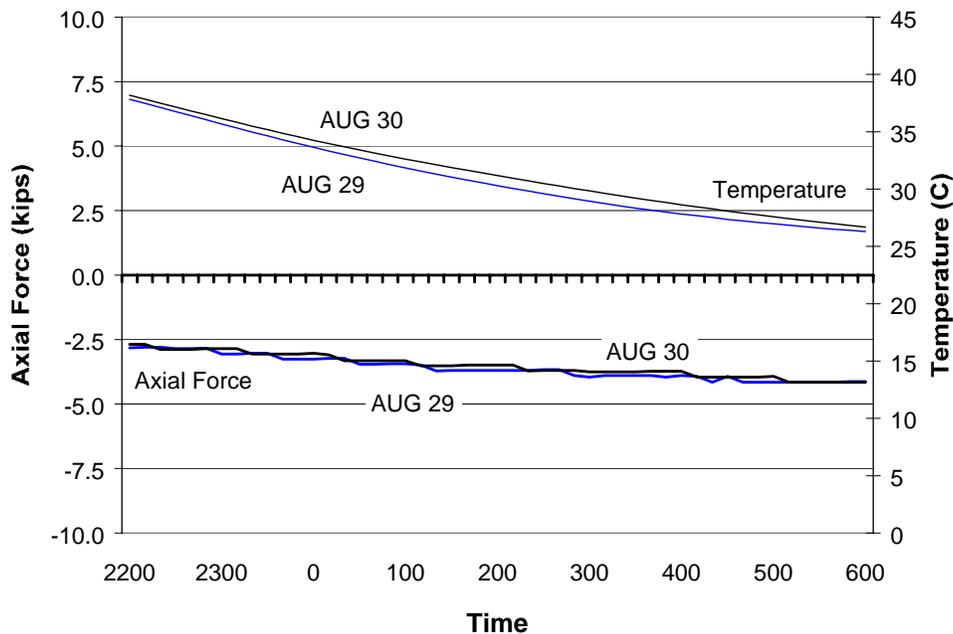
Figure 4.29 Diagonal Temperature Data before Pours 1-3
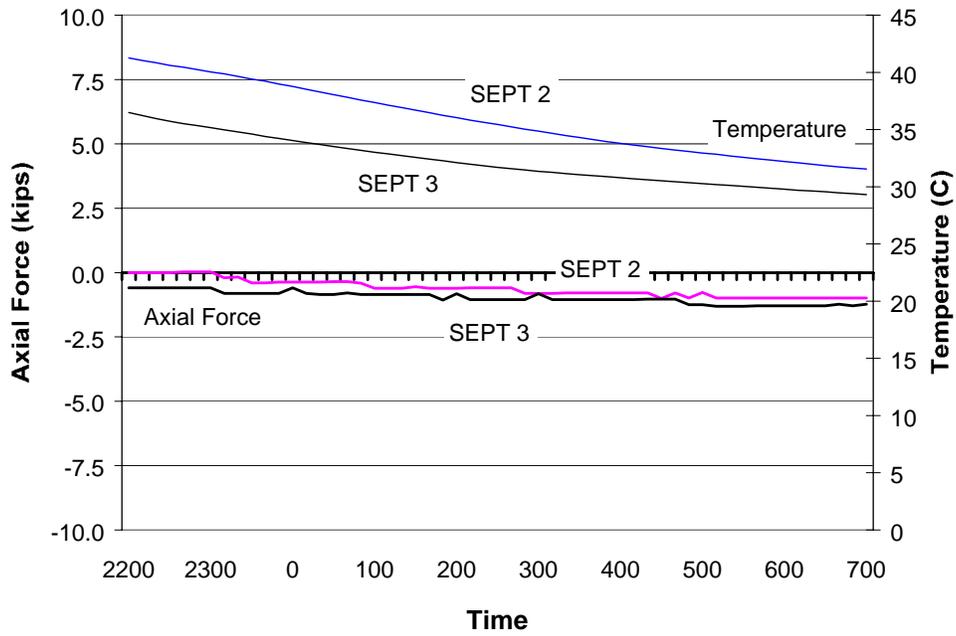
Figure 4.30 Diagonal Temperature Data before Pours 4-5
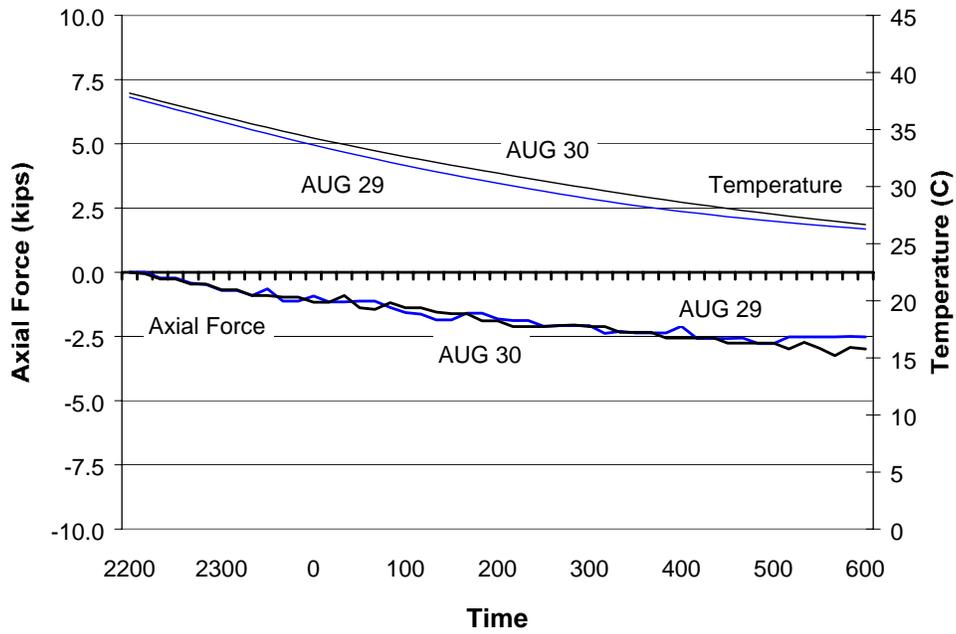
Figure 4.31 Bottom Chord Temperature Data before Pours 1-3

69
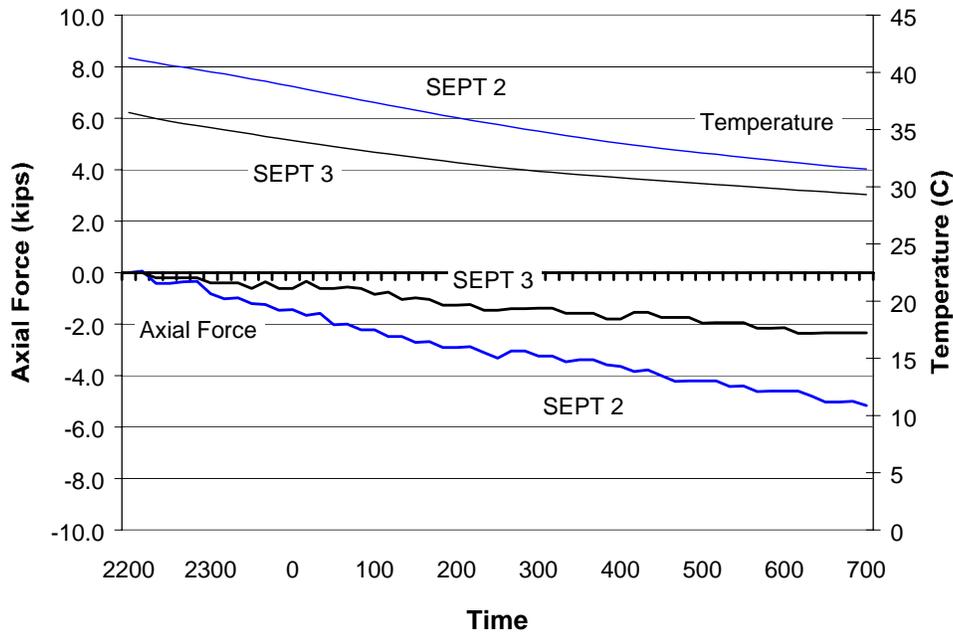
Figure 4.32 Bottom Chord Temperature Data before Pours 4-5

A linear trendline was used as an estimate for the temperature induced stresses in the diaphragms. This estimation is reasonable since the change in stress due to temperature gradients at this time of the day is very gradual. The predicted temperature stresses were subtracted from the original data to determine what stresses were only due to the weight of the concrete. All of the calculated forces in the diaphragms presented in this chapter already include the subtraction of predicted thermal effects.

4.3.1.2 External Diaphragm Analysis

The external torsional, horizontal and vertical loads on the diaphragms were calculated from the internal forces in the members. Since shear and moment are developed in each angle member, the external reactions from the box girders cannot be solved from axial forces alone. However, the instrumentation used on the diaphragms cannot measure the shears in each angle so a SAP model of the frame was used to predict the axial forces due to known torsional, vertical, and horizontal loads. This model includes the shear and moments in the angles; therefore the predicted axial forces can be used to predict the external reactions.

The SAP model used frame elements with reduced rotational stiffness at the ends due to the connection detail (Section 3.3). In the model (Figure 4.33), one side of the diaphragm was rigidly attached to the web of the box girder, which was restrained at its middle by a pin. The other side of the diaphragm was also rigidly attached to a box girder web, except this member was attached to a roller to allow horizontal displacement of one end of the diaphragm. The girder web was modeled as a WT frame section with its stem dimensions equal to the longitudinal web stiffener and the thickness of the flange equal to the web thickness. The width of the flange was approximated as 20 inches. This estimation of web stiffness had very little effect on the axial forces in the diaphragms members.
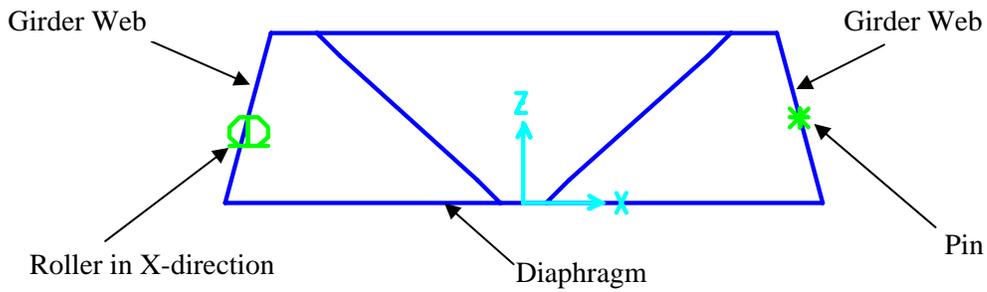
Figure 4.33 SAP Model of External Diaphragm

First, the forces in the diaphragm were determined from a unit torque applied to one side of the diaphragm. The same was done for a unit torque applied to the opposite side of the diaphragm. The forces were also determined for a unit horizontal load. The measured forces in the members for the three applied loading conditions are shown in Figure 4.34. The vertical shear transferred across the diaphragm can be calculated from the applied torsions. Figure 4.35 shows a deflected shape from an applied horizontal force and torsional loads.
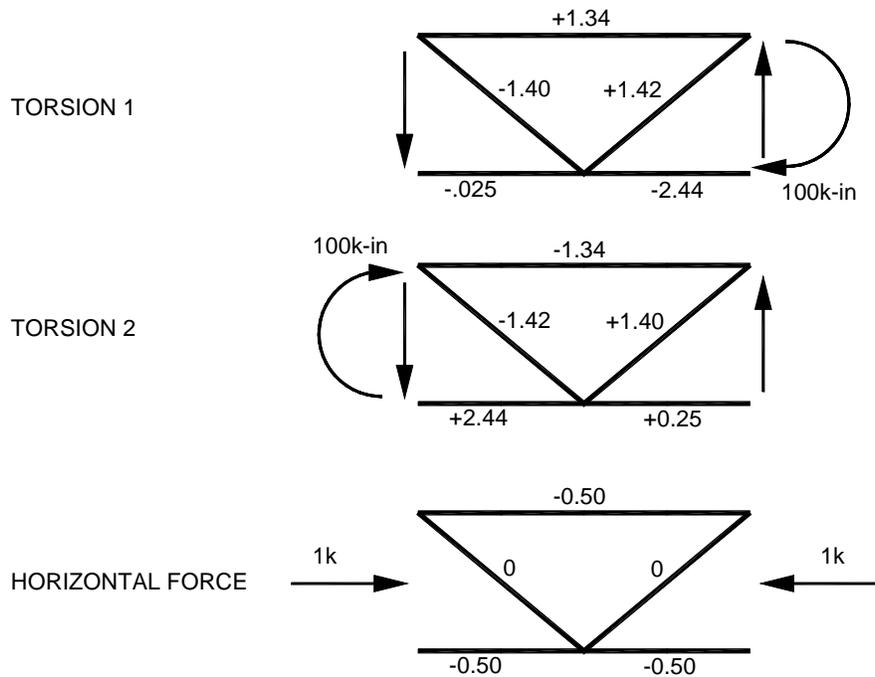
Figure 4.34 Diaphragm Forces from Applied Unit Loads
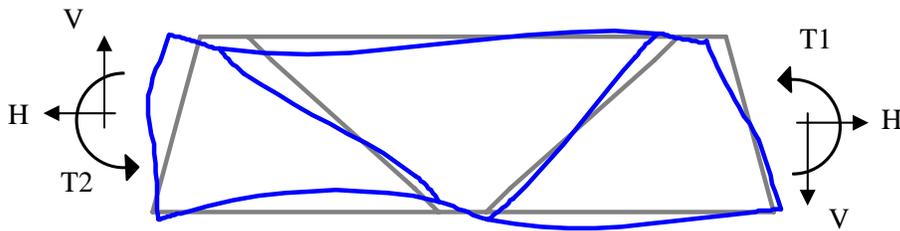
Figure 4.35 SAP Model - Deflected Shape

By taking the internal forces of three diaphragm members, the external reactions acting on the diaphragm can be solved. This is done by superimposing the unit loads in the SAP model until the internal forces for each member are equivalent to the measured or FEM internal forces. The external reactions on the diaphragm (T1, T2, and H) can be solved by using the equation $T1 * M_{T1} + T2 * M_{T2} + H * M_H = F$, where M_i is the member force due to load i and F is the internal force of the angle. Using different member forces, three equations are solved for the three unknown external reactions. The solved torques and forces are applied to the SAP model and all of the member forces are compared with the measured or FEM forces.

There was some variation between the FEM force predictions in the diaphragm members and the SAP force predictions from the solved external reactions. This is due to small differences between the models. The members that were used to solve the external reactions acting on the diaphragm in SAP were equal to the axial forces in the FEM since the reactions were determined from these members. The other two members had some variation between the FEM and SAP model. To prevent the analysis from favoring the forces in some members from FEM more than others, two calculations were done on each diaphragm using different members. The calculated external forces from these procedures were then averaged in order to minimize the variation between the FEM and SAP model. An example of these calculations is shown in Table 4.4.

Table 4.4 External Reactions Calculated from Internal Forces in Diaphragms

				FEM Forces				
				1	2	3	4	5
				(kips)	(kips)	(kips)	(kips)	(kips)
				5.88	-3.82	-5.24	-1.01	0.95
	SAP Loads Calculated from FEM Forces			SAP Forces Caclulated from Loads				
	Torsion 1	Torsion 2	Horizontal	1	2	3	4	5
	(kip-in)	(kip-in)	(kips)	(kips)	(kips)	(kips)	(kips)	(kips)
From FEM 1,2,4	158.6	-233.0	-1.3	5.88	-3.82	-5.45	-1.01	1.09
From FEM 1,3,5	161.6	-226.2	-1.4	5.88	-3.82	-5.24	-0.87	0.95
AVERAGE	160.1	-229.6	-1.3	5.88	-3.82	-5.35	-0.94	1.02
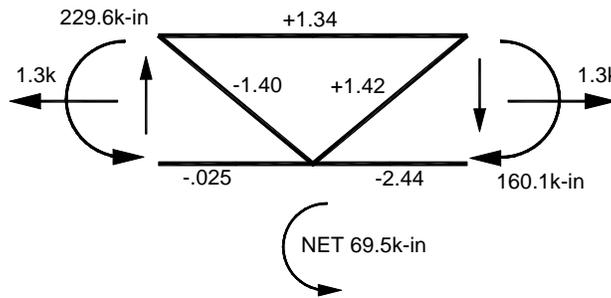
Figure 4.36 External Reactions Calculated in Table 4.2

4.3.1.3 External Diaphragm Results

Details of the FEM analysis are discussed in Section 4.3.2. The FEM member force predictions in the external diaphragms were converted into an equivalent torsion, vertical force, and horizontal force applied to the box girder. These forces were determined from the SAP model and the analysis technique discussed above. The measured forces on the diaphragms were also analyzed using the same method. Unfortunately, the concrete deck was poured nine months after the instrumentation was installed and a considerable amount of degradation occurred over that time. Diaphragm A had only one out of five members giving consistent axial force measurements. Diaphragm B had two out of five reliable force measurements and diaphragm C had four out of five. Therefore, the torques and forces acting on diaphragm C were calculated, but in diaphragms A and B, only the member forces were compared to the FEM. The results for the measured diaphragm forces during the concrete pour are compared to the FEM predicted diaphragm forces in Figure 4.37 through Figure 4.44. These figures show the reactions by the diaphragm on the girders. The forces and torques shown are the changes due only to the individual pour sequence.
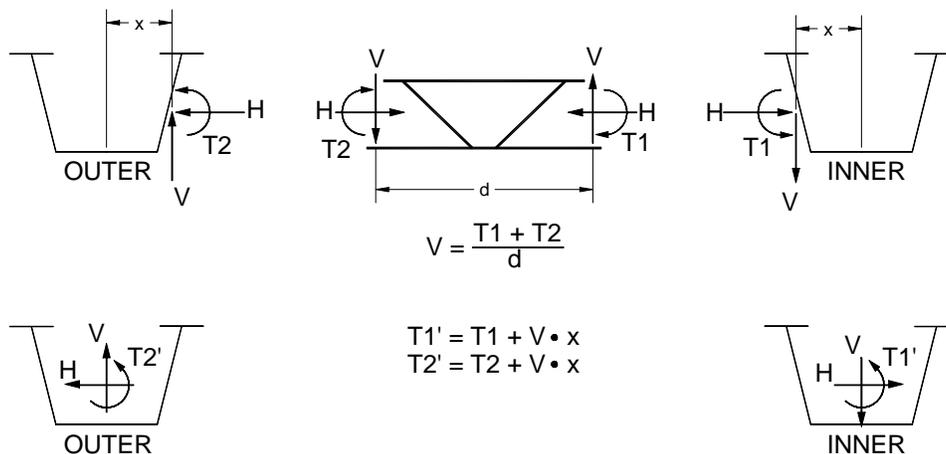
Figure 4.37 Reactions at Box Girder Centroid from External Diaphragms

73

MEASURED | FEM

UNITS: Force = kips   Torque = kip-in

POUR 1

-0.5

n/a   n/a

n/a   n/a

OUTER

INNER

-0.20

0.91   -0.90

-0.18   1.13

0.5
0.3 38

OUTER

0.5
0.3 64

INNER

POUR 2

-1.0

n/a   n/a

n/a   n/a

OUTER

INNER

-2.86

-4.35   4.35

5.58   -0.72

2.6
0.4 343

OUTER

2.6
0.4 145

INNER

POUR 3

5.5

n/a   n/a

n/a   n/a

OUTER

INNER

5.88

0.95   -1.01

-5.24   -3.82

0.6
1.3 250

OUTER

0.6
1.3 140

INNER

POUR 4

0.5

n/a   n/a

n/a   n/a

OUTER

INNER

-0.57

-1.54   1.54

1.70   -0.52

0.9
0 108

OUTER

0.9
0 65

INNER

POUR 5

7.0

n/a   n/a

n/a   n/a

OUTER

INNER

1.84

-4.95   5.08

6.83   -0.41

3.0
5.1 308

OUTER

3.0
5.1 255

INNER

Figure 4.38 Diaphragm A Concrete Pour Results

MEASURED   FEM

UNITS: Force = kips   Torque = kip-in
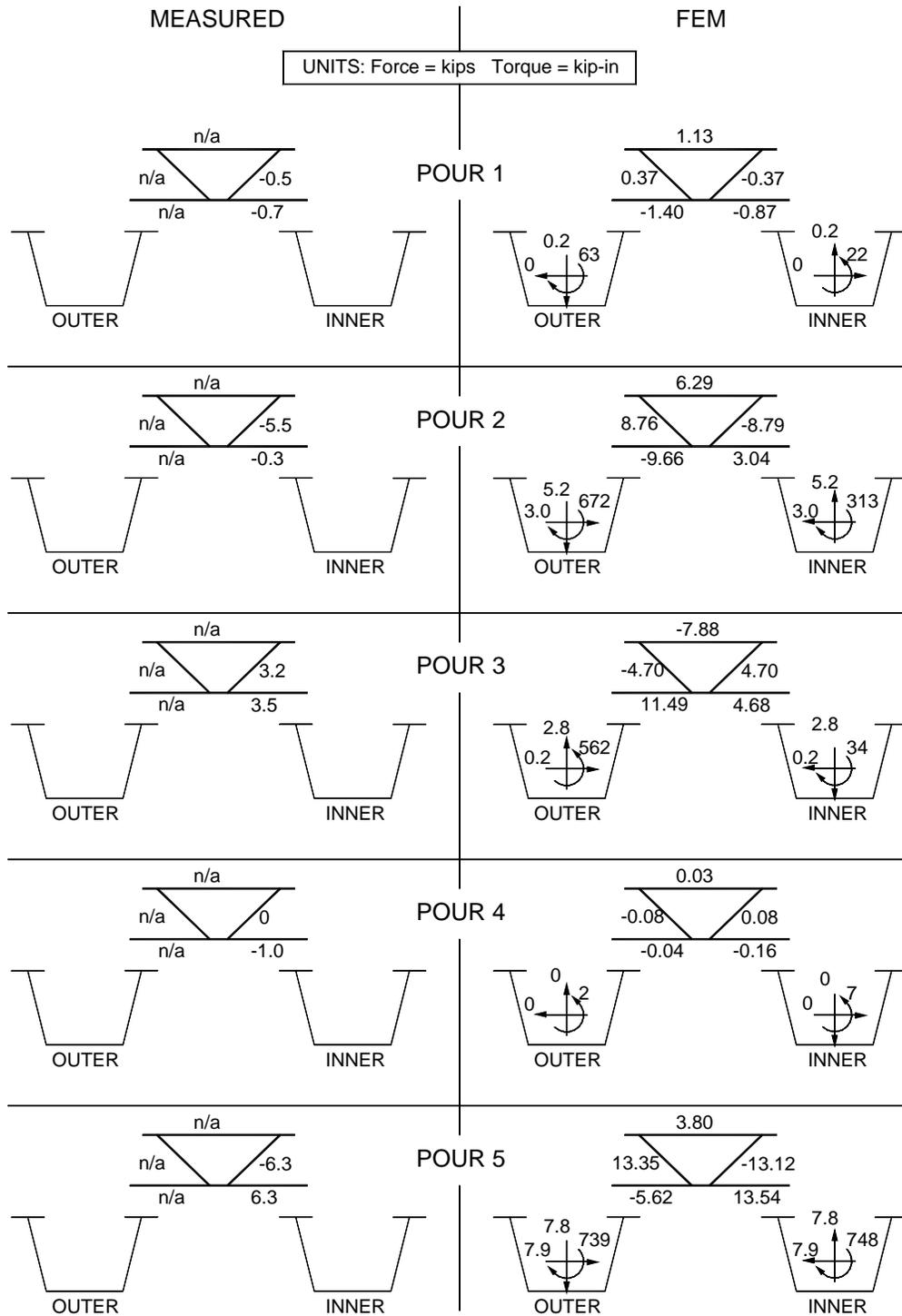
Figure 4.39 Diaphragm B Concrete Pour Results

75
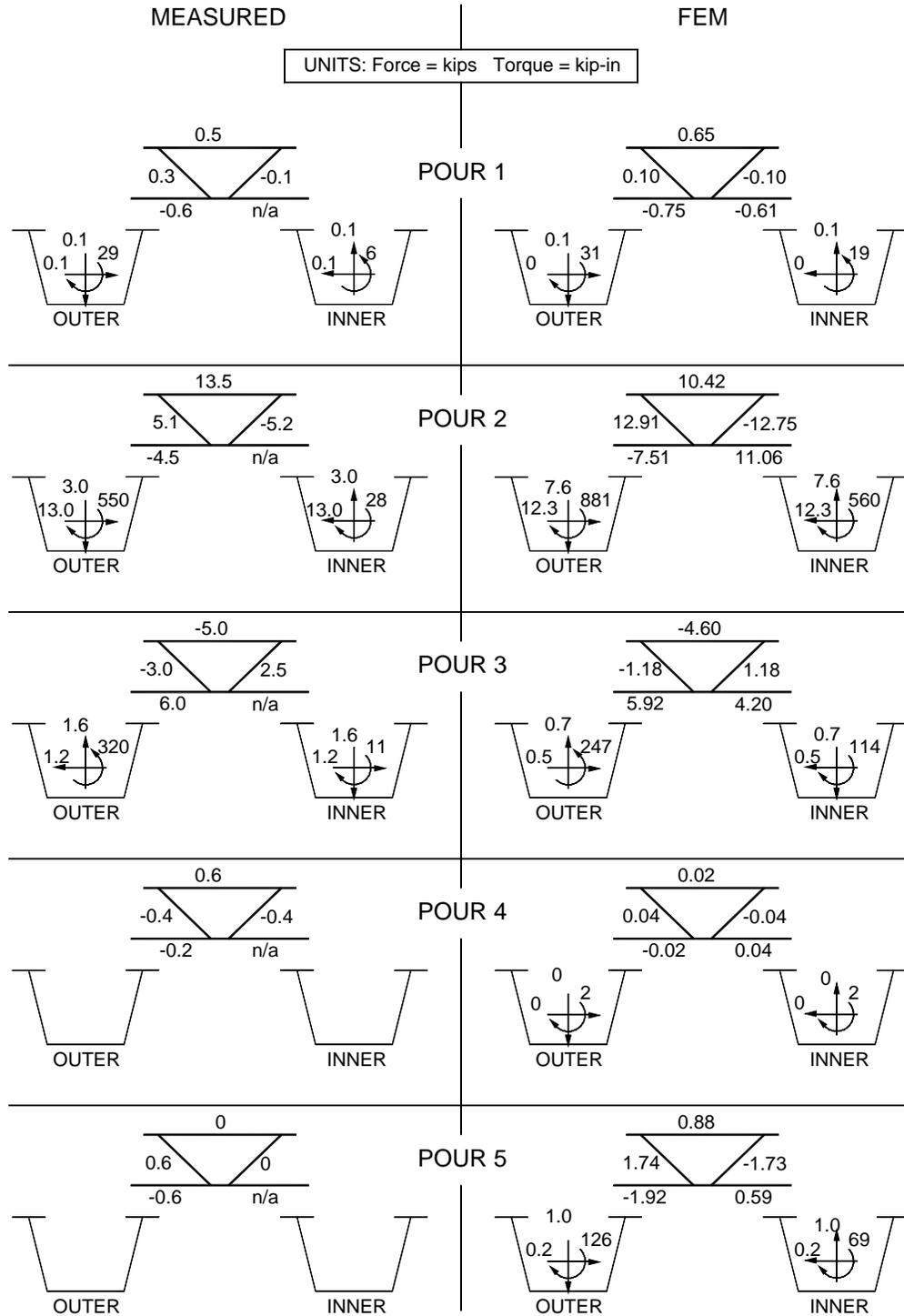
Figure 4.40 Diaphragm C Concrete Pour Results

4.3.2   K-Connect

The calculated values of axial forces in the instrumented diaphragm members were used to determine the measured change in axial force caused by each pour individually.   These measured changes were

compared with the values determined by Topkaya using the bridge finite element model (FEM). These results are presented in Table 4.5. For each instrumented location, there is a bar chart comparing the measured values and the values predicted using the FEM.

Table 4.5 Diaphragm Force during Deck Casting, K-Connect

External #11	Member 1		Member 2		Member 3	
	Field (kips)	ABAQUS (kips)	Field (kips)	ABAQUS (kips)	Field (kips)	ABAQUS (kips)
Change due to Pour 1	3.3	-1.0	0.7	-2.5	0.2	3.9
Change due to Pour 2	-0.2	-0.1	0.0	1.0	-0.3	-0.6
Change due to Pour 3	0.8	2.9	-2.3	-8.4	-0.8	2.2
Change due to Pour 4	8.1	2.8	1.3	-2.4	1.4	4.8
Change due to Pour 5	-1.0	0.0	0.4	-0.3	0.2	0.1
11.0	4.7		0.1		-12.5	

External #11	Member 4		Member 5	
	Field (kips)	ABAQUS (kips)	Field (kips)	ABAQUS (kips)
Change due to Pour 1	0.1	4.6	0.4	-4.6
Change due to Pour 2	-0.8	-1.2	0.4	1.2
Change due to Pour 3	1.9	7.7	-2.1	-7.7
Change due to Pour 4	0.1	5.3	-0.1	-5.3
Change due to Pour 5	-0.3	0.3	0.2	-0.3
Total Change	1.0	16.8	-1.3	-16.8

External #18	Member 1		Member 2		Member 3	
	Field (kips)	ABAQUS (kips)	Field (kips)	ABAQUS (kips)	Field (kips)	ABAQUS (kips)
Change due to Pour 1	2.3	-1.0	-----	-0.3	0.4	1.8
Change due to Pour 2	-1.6	-1.9	-----	-0.1	0.3	2.8
Change due to Pour 3	15.9	11.2	-0.5	12.1	-4.4	-19.8
Change due to Pour 4	-0.2	0.2	-0.2	0.2	-0.2	-0.5
Change due to Pour 5	0.0	0.2	0.6	0.5	0.4	-0.9
16.4	8.7		-----		12.4	

External #18	Member 4		Member 5	
	Field (kips)	ABAQUS (kips)	Field (kips)	ABAQUS (kips)
Change due to Pour 1	-----	1.6	1.3	-1.6
Change due to Pour 2	-----	2.2	-1.2	-2.2
Change due to Pour 3	-6.8	-23.5	8.3	23.5
Change due to Pour 4	0.0	-0.5	0.1	0.5
Change due to Pour 5	-0.2	-1.0	-0.1	1.0
Total Change	-----	-21.2	8.4	21.2

4.4 K-CONNECT GIRDER RESULTS

The calculated values of stress in the instrumented girder locations were used to determine the measured change in stress caused by each pour individually. These measured changes were compared with the values determined by Topkaya using the bridge finite element model (FEM). These results are presented in Table 4.6. For each instrumented location, there is a bar chart comparing the measured values and the values predicted using the FEM.

Table 4.6 Girder Stresses during Deck Casting, K-Connect

Panel 2	Outer Girder Top		Outer Girder Bottom	
	Field (ksi)	ABAQUS (ksi)	Field (ksi)	ABAQUS (ksi)
Change due to Pour 1	-6.2	-6.7	6.3	6.7
Change due to Pour 2	0.0	-0.3	0.2	0.3
Change due to Pour 3	0.4	1.9	-1.7	-2.5
Change due to Pour 4	0.0	-0.6	0.2	0.7
Change due to Pour 5	0.0	0.0	0.0	-0.1
Total Change	-5.8	-5.6	5.0	5.2

Panel 2	Inner Girder Top		Inner Girder Bottom	
	Field (ksi)	ABAQUS (ksi)	Field (ksi)	ABAQUS (ksi)
Change due to Pour 1	-5.7	-6.0	5.2	5.9
Change due to Pour 2	0.1	-0.2	0.1	0.3
Change due to Pour 3	0.4	1.4	-1.6	-2.0
Change due to Pour 4	0.0	-0.5	0.2	0.6
Change due to Pour 5	0.0	0.0	0.0	0.0
Total Change	-5.3	-5.2	4.0	4.8

Panel 3	Outer Girder Top		Outer Girder Bottom	
	Field (ksi)	ABAQUS (ksi)	Field (ksi)	ABAQUS (ksi)
Change due to Pour 1	-9.8	-10.7	9.5	9.7
Change due to Pour 2	0.1	-0.6	0.3	0.6
Change due to Pour 3	0.6	5.1	-2.9	-4.6
Change due to Pour 4	-0.1	-1.3	0.4	1.2
Change due to Pour 5	0.0	0.2	0.0	-0.1
Total Change	-9.2	-7.4	7.3	6.9

Panel 3	Inner Girder Top		Inner Girder Bottom	
	Field (ksi)	ABAQUS (ksi)	Field (ksi)	ABAQUS (ksi)
Change due to Pour 1	-9.0	-9.3	7.6	8.6
Change due to Pour 2	0.1	-0.5	0.3	0.5
Change due to Pour 3	0.6	4.2	-2.6	-3.6
Change due to Pour 4	-0.1	-1.1	0.4	1.0
Change due to Pour 5	0.0	0.1	0.0	-0.1
Total Change	-8.5	-6.7	5.6	6.4

Table 4.6 Girder Stresses during Deck Casting, K-Connect (continued)

Panel 18	Outer Girder Top		Outer Girder Bottom	
	Field (ksi)	ABAQUS (ksi)	Field (ksi)	ABAQUS (ksi)
Change due to Pour 1	-0.7	1.5	-0.6	-1.5
Change due to Pour 2	1.3	1.3	-1.4	-1.3
Change due to Pour 3	-14.9	-13.8	13.5	12.7
Change due to Pour 4	-0.3	-0.3	1.4	0.3
Change due to Pour 5	-0.1	-0.4	0.2	0.4
Total Change	-14.7	-11.6	13.1	10.6

Panel 19	Outer Girder Top		Outer Girder Bottom	
	Field (ksi)	ABAQUS (ksi)	Field (ksi)	ABAQUS (ksi)
Change due to Pour 1	-1.6	0.8	0.1	-1.0
Change due to Pour 2	2.1	1.8	-2.0	-1.8
Change due to Pour 3	-14.2	-12.2	13.6	12.5
Change due to Pour 4	-0.2	-0.3	1.1	0.3
Change due to Pour 5	-0.1	-0.4	0.2	0.4
Total Change	-14.0	-10.2	13.0	10.4

4.5   PERFORMANCE OF DATA ACQUISITION SYSTEMS

4.5.1   K-Connect

4.5.1.1 Axial Force Members

The axial force in the top laterals and diaphragm members should be constant along the length of the member; therefore, the calculated axial force at each of the two cross sections on each member should be the same. In all cases, there was good to very good agreement between the two calculated forces. For this reason, the axial force of the member was taken to be the average of the two cross sections for both the top laterals and diaphragm members.

Figures 4.41 and 4.42 illustrate the range of agreement between cross sections on the various axial force components of the bridge. The calculated force from two locations on each member is plotted versus time for a two-week period encompassing the concrete pours. Figure 4.41 shows what was termed "excellent" agreement between two cross sections, as the two cross sections produced nearly identical values of axial force.   Figure 4.42 shows what was judged as "very good" agreement. All locations for axial force on bridge K had at least "very good" agreement during both the concrete pours and the live load test. The forces at the two locations were averaged to provide the best estimate of the member force.
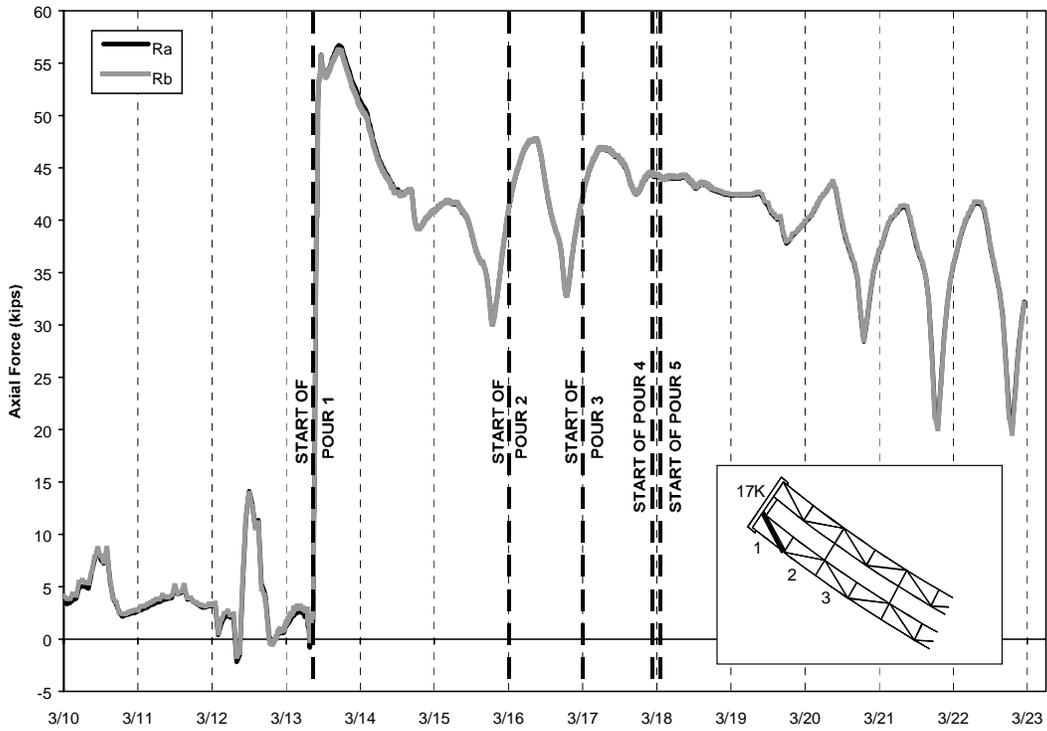
Figure 4.41 Outer Girder Top Lateral 1 Panel from Pier 17K During K Pours, Both Cross Sections
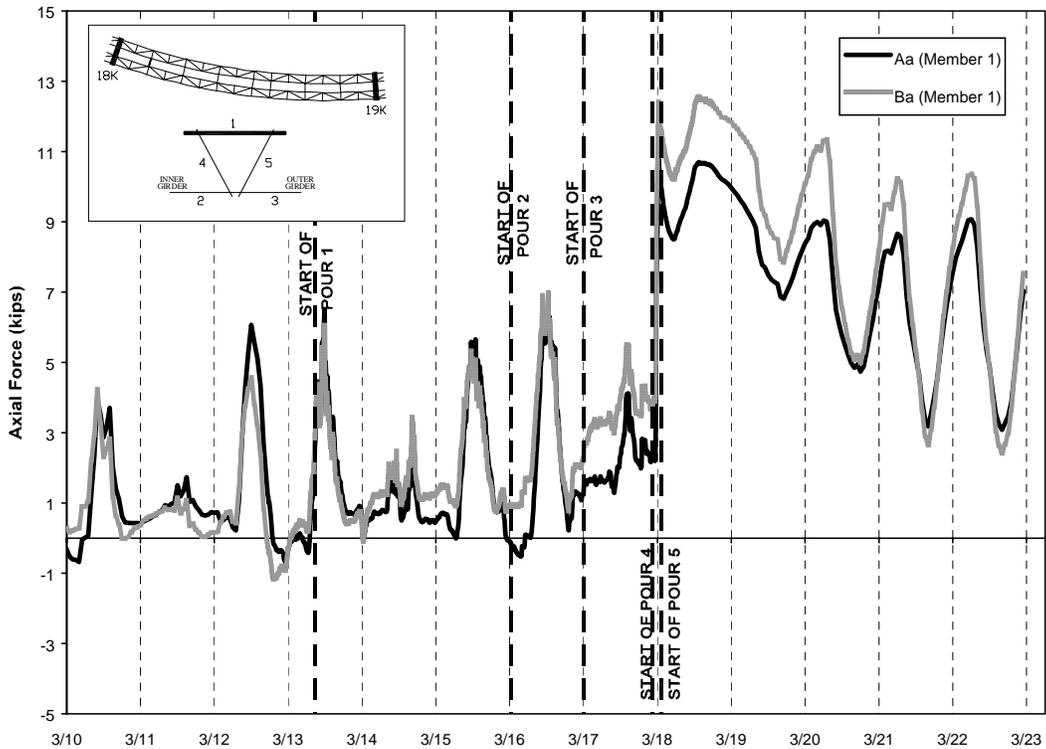
Figure 4.42 External Diaphragm #11-1 during K Pours

4.5.1.2 Girder Strain Readings

Due to the geometry of the steel girder, the stress at any given cross section of the girder should be symmetric about the centerline of the girder. It is expected, therefore, that the two calculated stress values at the top of the girder should be the same and that the two calculated stress values at the bottom of the girder should be the same. In each of the six girder cross sections, it was found that there was good agreement in the calculated stress values for the top and bottom of the girder for both the concrete pours and the live load test. Therefore, the averages of these values were used. Figure 4.43 demonstrates the typical agreement between the two top stress calculations and the two bottom stress calculations. The measured strain values were converted to stress by using an elastic modulus of 29×10^3 ksi.
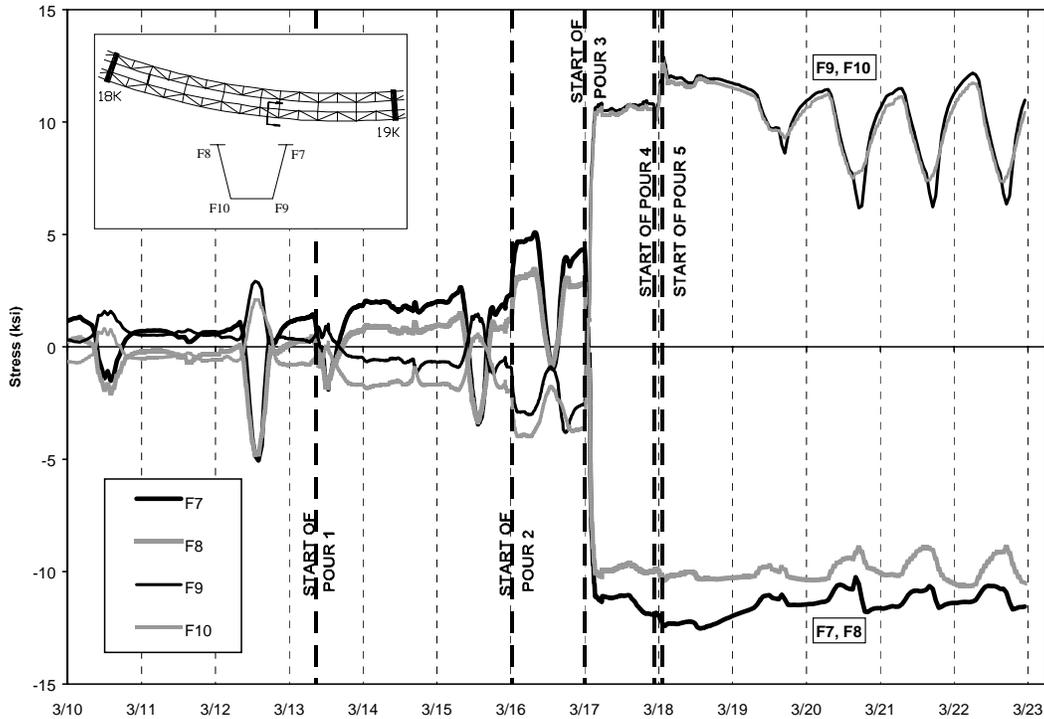
Figure 4.43 Girder Location F during K Pours

4.5.1.3 Malfunctions

There were no problems with any of the instrumented top laterals during either the concrete pours or the live load test. Only one gauge failed among the six girder cross sections. At the cross section with the gauge failure (the first panel from pier 17K in the outer girder), the calculated stress value in the top of the girder was not taken as the average; rather the calculated value from the only properly functioning gauge was used.

Gauge failures occurred on two external diaphragms. The gauges failed at location Bc on Diaphragm #11 (see Figure 2.12) and at locations Cc and Cd on diaphragm #18 (see Figure 2.12). For these members, the axial force was determined using the results from one location. For all other locations, the average of the two gauged locations on each member was used.

4.5.1.4 Discontinuity in Data

Data were collected during the pours for the top laterals, girder gauges, and diaphragm members. Data for locations Ca through Ce on Diaphragm #18 (see Figure 2.12) were not collected for pours 1 and 2 due to a malfunction in the power cable. Once the power cable was replaced, the multiplexer functioned properly except for locations Cc and Cd, as mentioned in the previous subsection.

Because locations Ca and Da were on the same member but the two starting points for the collection of data did not match, it was necessary to adjust all of the data from location Ca so that it would have the same value at its initial reading (which occurred shortly before pour 3) as location Da at that instance. It was assumed that all of the values from location Ca would follow along the same curve after the adjustment because the calculated axial force values at Ca and Da should be the same. As shown in Figure 4.44, this turned out to be the case. It was not necessary to adjust locations Cb and Ce, as those were the only functioning cross sections on their respective members. Also, only the change in force is required from each pour, not the actual force measurements.
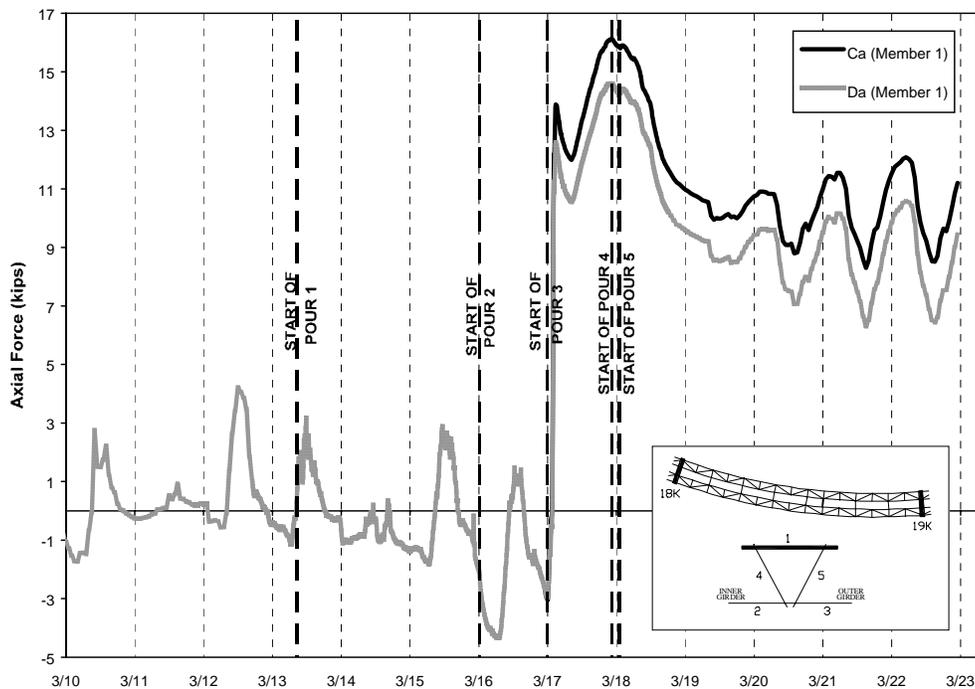
Figure 4.44 External Diaphragm #18-1 During K Pours, Both Cross Sections

4.5.2 *Y-Connect*

As explained previously for bridge K, the calculated axial force at each of the two cross sections on each member should be the same. In all cases, there was what was judged to be "very good" agreement among the calculated values. For this reason, the average of the cross sections was taken to be the axial force of the member for the instrumented top laterals.

Figure 4.45 illustrates the typical agreement among cross sections on the four instrumented top laterals. Following that is Figure 4.46, which plots the average axial force, which was used for comparisons with predicted values. The top lateral shown is from the second panel of the inner girder; there were three gauged cross sections. Displayed in the graphs is the axial force in the said lateral for a week before the first concrete pour up until a few days after the end of the pouring sequence.
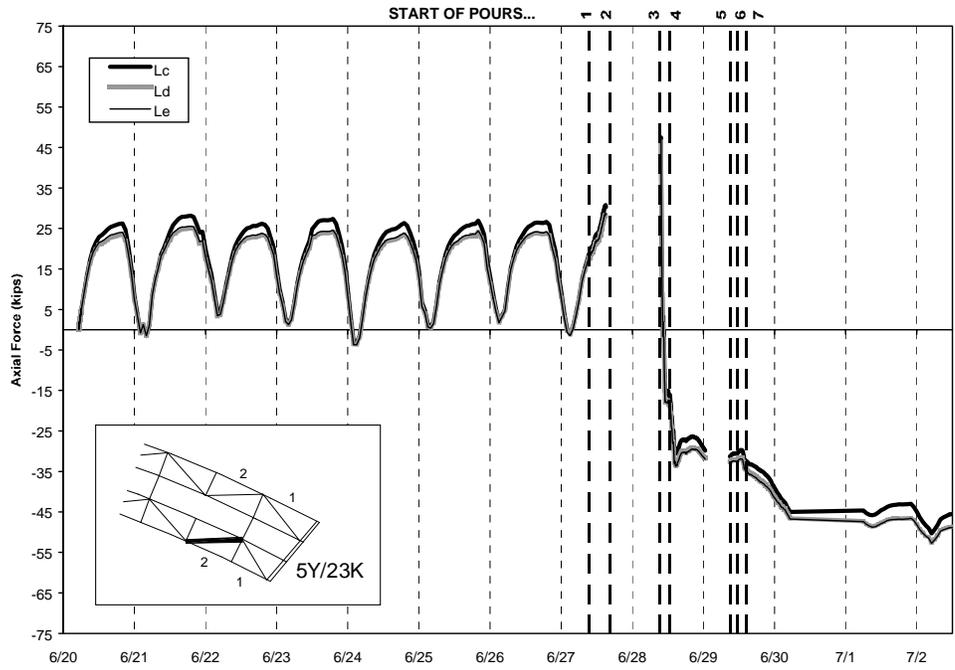
Figure 4.45 Inner Girder Top Lateral 2 Panels from Pier 5Y/23K during Y Pours, All Three Cross Sections
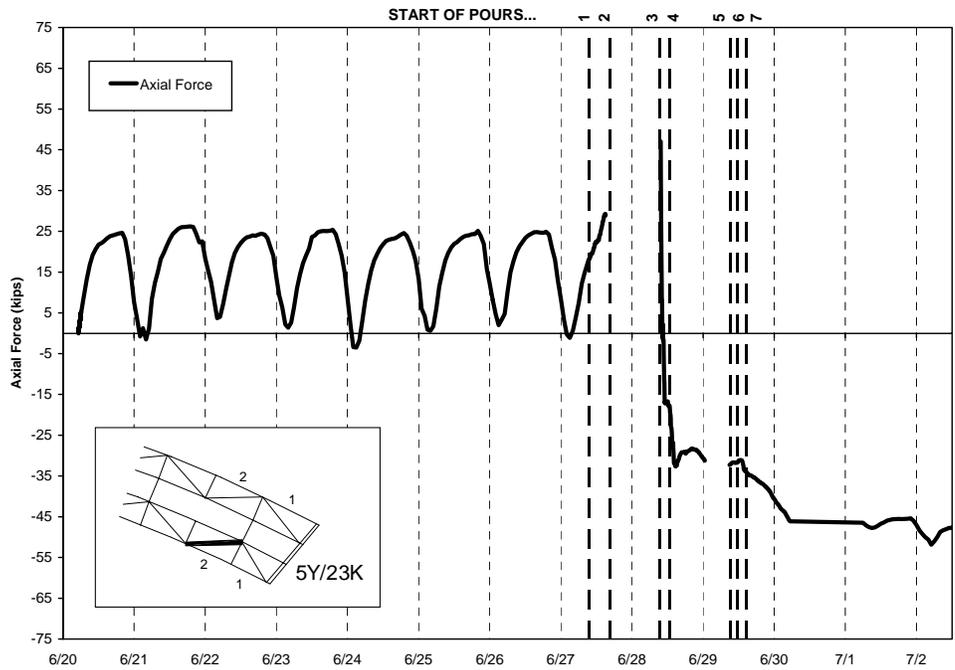
Figure 4.46 Inner Girder Top Lateral 2 Panels from Pier 5Y/23K during Y Pours, Average Axial Force

There were no problems with the operation of any of the instrumentation on the top laterals during the concrete pours; however, there were discontinuities in the field data during the pours. The datalogger had a recurring error that caused the system to malfunction and not record additional data until the system was reset. This malfunction did not affect the performance of the strain gauges; the gauges continued to read properly even when data was not being recorded.

The problem first occurred in between pours 1 and 2; as a result, there is no data for pour 2 or any of the time before pour 3 started. The problem was temporarily fixed 20 minutes after the start of pour 3, and data collection resumed at that point. The problem occurred again after pour 4 but was resolved during the day before the final three pours.

In summary, uninterrupted data exist for the all of the following pours: 1, 4, 5, 6, and 7. No data exists for pour 2; therefore, no comparison could be made with the predicted response. For pour 3, the data begins 20 minutes into the pour. The comparison with the predicted response has taken that into account.

4.6   DISCUSSION OF Z-CONNECT RESULTS

It was apparent from the top lateral data that composite action was occurring between the poured concrete and steel girders within hours of placement of the concrete. This affected the force distribution throughout the girder as other pour segments continued. However, the amount of contribution from the hardening concrete is difficult to model in the FEM since the modulus of elasticity is uncertain and changes with time. Several different cases were modeled to predict the effect of a hardened deck on the external diaphragms, including the following:

	Pour 1	Pour 2	Pour 3	Pour 4	Pour 5
Case 1	Wet				
Case 2	Wet	Wet			
Case 2a	E=1000 ksi	Wet			
Case 3	E=1000 ksi	Wet	Wet		
Case 3a	E=1000 ksi	E=1000 ksi	Wet		
Case 4	E=5000 ksi	E=5000 ksi	E=5000 ksi	Wet	
Case 5	E=5000 ksi	E=5000 ksi	E=5000 ksi	Wet	Wet
Case 5a	E=5000 ksi	E=5000 ksi	E=5000 ksi	E=1000 ksi	Wet

In these cases, "wet" corresponds to zero stiffness. A modulus of elasticity of 1000ksi was estimated as partially hardened. A modulus of elasticity of 5000ksi was used to represent the fully hardened stiffness.

The thickness of the concrete deck in the model was determined from the measurements recorded in the TxDOT logbook during the pour. During pour 2, the FEM forces in diaphragms A, B, and C found to be independent of the stiffness of pour 1 (Case 2 VS Case 2a). Also, the forces in diaphragms B and C during pour 5 were independent of the stiffness of pour 4 (Case 5 VS Case 5a). However, there were differences in all of the diaphragm forces for Case 3 and 3a. This is because the concrete deck from pour 2 is very close to the external diaphragms and significantly changes the force distribution in the girders when hardened. Also, the forces in diaphragm A during pour 5 were dependent on the stiffness of pour 4 (Case 5 VS Case 5a). Based on the measured results in top lateral forces, the FEM models used to predict the diaphragm forces (Figure 4.3 through Figure 4.) were Cases 1, 2a, 3, 4 and 5. In other words, pour 1 was considered partially hardened during pours 2 and 3; pours 1, 2, and 3 were considered hardened during pours 4 and 5.

The measured reactions acting on the girders from external diaphragm A (Figure 4.3) are inconclusive since only one member was giving reliable axial force measurements. The top chord of diaphragm A has some correlation with the FEM during the first 3 pours. This is especially true during pour 3, in which the stresses are higher. There is very little correlation in diaphragm A during pour 4 and 5. This may be due to the estimation of the concrete stiffness in the previously poured segments. During pour 5, the top chord measured a much higher force than the FEM predicted. The measured force change occurred only during the very early portion of pour 5, while the concrete was poured near the diaphragm. Once the screed moved past the pier away from diaphragm A, there were minimal force changes. Strain readings in other members of the diaphragm show the same sudden increase in magnitude during this time interval.

In general, the measured forces in diaphragm B are much lower than predicted with the FEM. During pours 3 and 5, the measured forces in the diagonal and bottom chord are almost equal in magnitude. The FEM predicts a similar behavior in the twisting of the girders as measured, although the magnitudes of the diaphragm reactions are overestimated. This may be due to the reduction in diaphragm stiffness from the connection detail discussed earlier in Section 3.3.2. This detail is not modeled so the ratio of girder to diaphragm stiffness may be greater than predicted.

The external reactions on diaphragm C were calculated from the measured internal forces. During pours 1 and 2, the measured restraining torque was higher in the outer girder than the inner. This is also predicted in the FEM. The measured and predicted results both show that the top of the outer girder twists away from the center of curvature as the diaphragm acts in the opposite direction to restrain it. However, the measured torsions are considerably less than predicted during pour 2. The predicted horizontal reaction from the diaphragm correlates well with the measured reaction during the first two pours.

During pour 3, the measured torsion in the outer girder is somewhat higher than predicted and the measured torsion acting on the inner girder is much smaller than predicted. The measured and predicted torsions on the inner girder are in the opposite direction from the torsions on the outer girder. The top flange of the inner girder is restrained from twisting away from the center of curvature while the top flange of the outer girder wants to twist towards the center of curvature.

The force calculations in the diaphragm members during pours 4 and 5 are smaller than the forces during the other pours since the concrete deck over diaphragm C had time to harden. Torsional and force measurements from the diaphragms were not calculated since the member forces were within expected errors in the measurements. Also, the expected temperature effects during these pours were not as easy to predict since the stiffness of the bridge was slowly increasing with time. This changes the response of the bridge to thermal effects so the background data are not as reliable.

The FEM predicts the same behavioral response in the diaphragms as measured, although it generally overestimates the contribution of the external diaphragms in restraining the girders. Some discrepancy between the predicted and measured results exists from the estimation of concrete deck stiffness. There were considerable changes in the predicted diaphragm forces in the analysis if the concrete deck from previous pour segments was modeled as composite with the steel girders. The maximum axial stress measured in all of the external diaphragm members due to the weight of the concrete was about 3 ksi. In comparison, the top lateral members that were measured had axial stresses up to 7 ksi from the concrete pour.

CHAPTER 5:
TRUCK LOAD TESTS

5.1 DESCRIPTION

5.1.1 Z-Connect

On November 9, 2000, several weeks after the concrete deck was poured, a live load test was performed on the composite box girder bridge by using two trucks. The test was performed before the concrete guardrail was cast in place. To maximize the response out of the instrumented members, the trucks were placed in a back-to-back position (Figure 5.1). The trucks were placed in 20 different positions while about 10 readings on each diaphragm were taken for every position. The positions of the trucks on the bridge are shown in Figure 5.2.

Truck positions correspond to the location of the back of the trucks. The truck positions were marked before the load test so the outer wheel would only be 40 inches from the edge of the concrete deck. The trucks were positioned close to the edge of bridge (Figure 5.3) to create a high torque. This would maximize the response in the external diaphragms. Figure 5.4 shows the truck axles being individually weighed on the bridge using portable TxDOT scales. The truck weights are shown in Table 5.1.

Figure 5.1 Picture of Truck Configuration
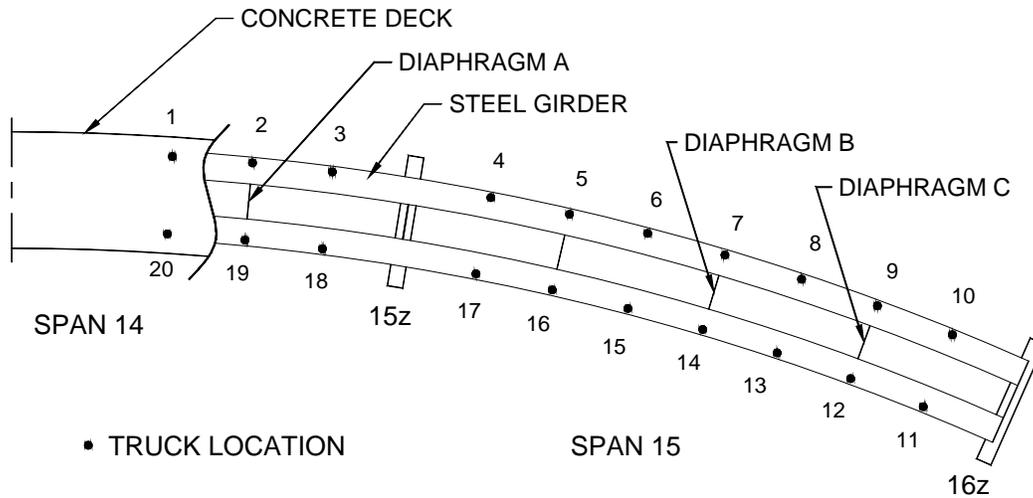
Figure 5.2 Positions of the Two Truck's Center of Gravity

Table 5.1 Wheel Loads (lbs) Measured on Bridge at Position 6

Truck 5474F – Rear Truck during position 1-10; Front Truck during position 11-20

	Front Wheel	**Middle Wheel**	**Back Wheel**
Driver's Side	6050	10150	9850
Passenger's Side	5000	8600	8150

Truck 3337H – Front Truck during position 1-10; Rear Truck during position 11-20

	Front Wheel	**Middle Wheel**	**Back Wheel**
Driver's Side	6050	7000	6850
Passenger's Side	6750	9000	8700

Figure 5.3 Front View of Truck in Position

Figure 5.4 Weighing of Back Axles

The data acquisition system read all of the gages on the bridge once every 30 seconds. The trucks were placed in the 20 positions for about 5 minutes each. The entire load test took about two hours. The temperature effects during the load test were considered when determining the forces generated in the diaphragms due to the trucks.

5.1.2 K-Connect

A similar live load test was conducted on K-Connect on June 7, 2001, from 11:50 A.M. to 3:15 P.M. in order to monitor the response of the instrumented cross sections when two overloaded TxDOT dumptrucks stopped at 30 different locations across the bridge. The 30 locations are illustrated in Figure 5.5. A schematic of the truck geometry is shown in Figure 5.6, and a listing of the truck wheel loads, as measured on site during the load test, is provided in Table 5.2. The two trucks are identified by their license plate numbers: 751-248 and 785-484.
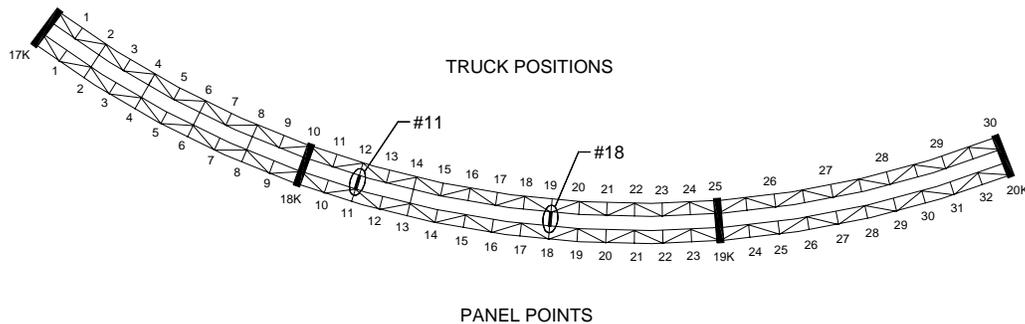
Figure 5.5 Live Load Test Truck Positions for Connect K

From 11:50 A.M. to 1:15 P.M., the trucks moved over the outside girder of the bridge (Truck 785-484 leading), and from 1:30 P.M. to 3:15 P.M., the trucks moved over the inside girder (Truck 751-248 leading). The trucks remained in each position for approximately two minutes in order to collect a good

amount of data for each location. The data acquisition system collected strain gauge and thermocouple readings every 10 seconds, averaging 12 data points per position. The data were either downloaded using a laptop directly connected to the datalogger or via modem.
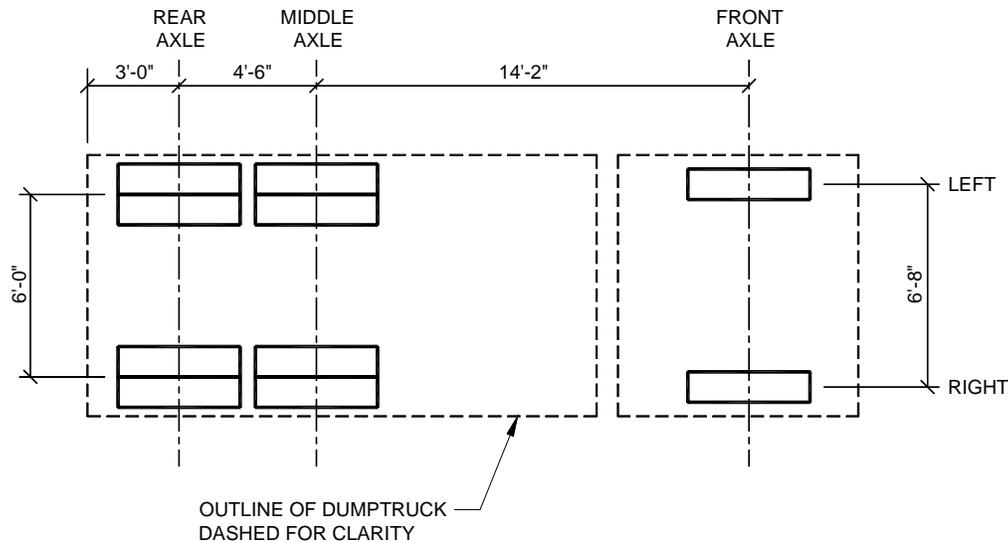
Figure 5.6 Truck Geometry (Top View)

Table 5.2 Dumptruck Wheel Loads (kips)

Truck	Total Wt.	Wheel	Front	Middle	Rear
751-248	43.2	Left	5.75	8.4	7.75
		Right	6.25	7.8	7.25
785-484	45.4	Left	6.95	8.65	7.9
		Right	6.7	8.0	7.2

The two trucks were positioned back-to-back in order to generate the largest possible torsional response on the bridge, as shown in Figure 5.7. The combined axle weights amounted to a concentrated load of 88.5 kips in the center of the two trucks. The trucks remained 40 inches away from the edge of the bridge deck for safety reasons.

In between the concrete pours and the live load test, some of the intermediate external diaphragms were removed from bridge K. Because most of the bridge was directly over the interstate, the diaphragms could only be taken down when the highway was closed down to allow lift access. The contractor had very limited opportunities to close the highway, so the decision was made to remove all of the diaphragms over the highway, with the exception of instrumented diaphragm #18. The diaphragms that were not over the highway, including all of the diaphragms in span 17 and diaphragm #11, were left in place. This was accounted for in the analysis and comparison of predicted and measured values. Figure 5.8 shows a plan view of bridge K with the external diaphragms that remained in place for the live load test.

Figure 5.7 Truck Positioning during K Live Load Test
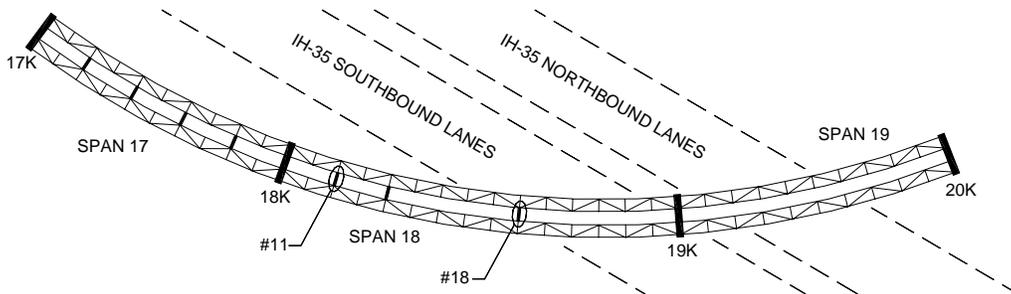
Figure 5.8 External Diaphragms in Place for K Live Load Test

5.2   TEMPERATURE EFFECTS ON DIAPHRAGMS

5.2.1   Z-Connect

Unlike during the concrete pour, there was a considerable change in ambient temperature inside the girder throughout the truck load test. The temperature recorded inside the steel box girder by the datalogger increased about 4 or 5 degrees Celsius during the test. Also, there was a large variation in temperature from one day to the next prior to the load test. Examining the recorded data during the time interval during the test, there was no easily predicted trend in the change of axial force in the diaphragm members. All of these factors made it very difficult to predict the stresses in the diaphragms due to temperature gradients in the bridge. Figure 5.9 and Figure 5.10 show typical plots of the diaphragm data prior to the load test and the change in temperature with time during the load test (November 9).
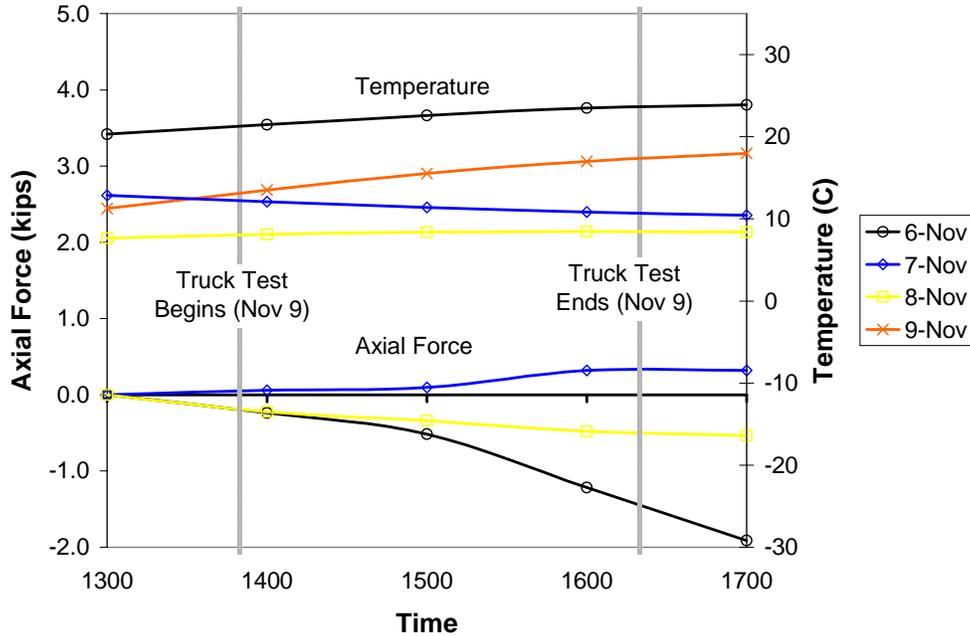
Figure 5.9 Top Chord – Axial Force and Temperature Data
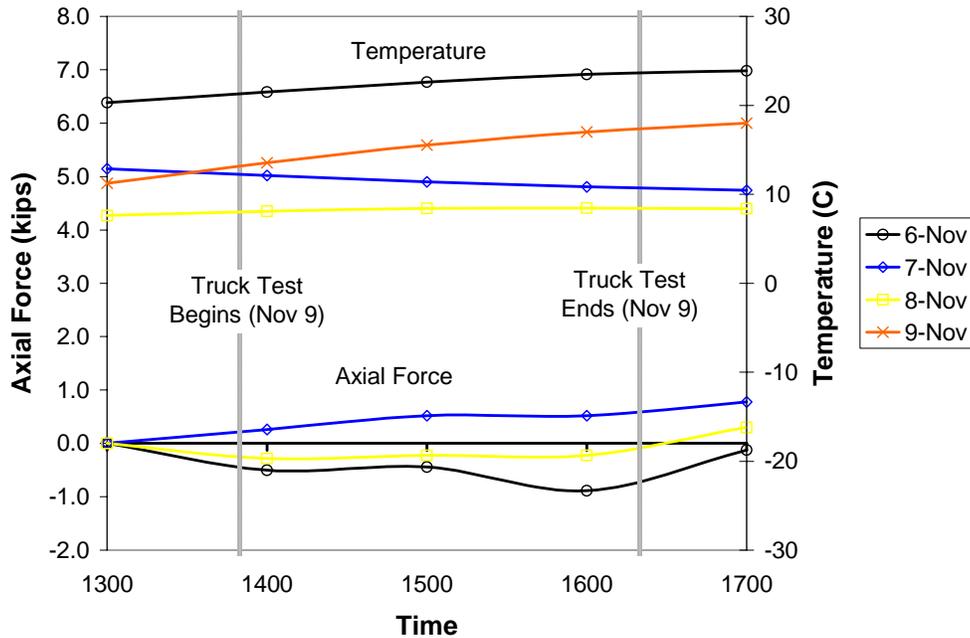
Figure 5.10 Bottom Chord – Axial Force and Temperature Data

The temperature data prior to the load test was too variable to predict the effects on the diaphragms. Instead, the temperature effects were estimated by examining only the diaphragm data during the load test. In a perfectly linear elastic system, the changes in force due to an applied external load are equal and opposite of the changes in force when the load is removed. Therefore the forces in the diaphragm

members should be exactly the same before and after the truck load test, given there were no temperature effects. This also assumes that no yielding in any member of the bridge occurs and that the bearing pads supporting the bridge also act linear elastic. During the load test, the change in axial force due to temperature was estimated as being linear with time for each member. From reviewing the background data, this is probably the most reasonable estimate although not necessarily very accurate.

To avoid this problem in the future, the results could be interpreted much easier if the test were preformed between sunset and sunrise. The thermal gradients during this time are minimal since there is no solar radiation. However, a load test performed during these hours may not be feasible. Another solution to minimize effects would be to perform the test over a shorter duration. In this case, the change in forces due to temperature effects would not be as significant.

5.2.2   K-Connect

Each truck run (outer and inner) was considered as a separate test. Because of temperature effects, the strain values were zeroed before each run when the dumptrucks were off the bridge. The temperature effects prevented the strain values from returning to zero at the end of each test.

The temperature effect was not very significant during the outer truck run, as the cloud cover kept the temperature fairly cool. The air temperature at the bridge site started at approximately 26.5 °C (80 °F) and rose only about 1 °C during the outer run to 27.5 °C (81.5 °F), or about 0.67 °/hr. During the inner run, however, the temperature rose from approximately 27.5 °C (81.5 °F) at the start to 29.5 °C (85 °C) at the end, or about 1°/hr.

The temperatures at location 1 during both live load tests are shown in Figure 5.11. The temperatures at location 2 are very similar and follow the same patterns. Figures 5.12 through 5.14 show the temperatures at location 1 on the inner side, outer side, and inside of the girder, respectively. The increase in rate of change of temperature as the day progressed is evident in the Figures.

At the start of the outer truck run, the sun was directly above the bridge; by the end of the inner run, the sunrays were striking the bridge from the west. As a result, the temperatures were larger on the outer side of the girder than the inner side. The temperatures directly underneath the slab experienced more gradual changes in temperature than the bottom of the girder because of the thermal effect of the composite slab; concrete conducts heat at a much slower rate than steel. Similarly, concrete dissipates heat more slowly than steel, and the slab remains heated for several hours after the sun sets. Additionally, the temperatures at the top of the girder were cooler because the slab shaded the top of the girder from direct sunlight. The temperature inside the girder was nearly identical to the temperature of the underside of the metal deck in the center of the girder until the beginning of the inner truck run, when the sun started heating the outer side of the girder. The heat captured by the steel plate on the outer side of the girder was transferred to the air inside to girder, producing the increase in temperature.

Also, as mentioned previously, the temperatures at each end and in the middle of top lateral #19 were monitored. Those temperatures are shown in Figure 5.15. Similar to Figures 5.12 through 5.14, the temperatures on the lateral are shown in Figure 5.16. As evident in the figures, there is much less variation in the temperature on the instrumented top lateral than in the girder cross section. This is because the top lateral is located a few inches below the slab.
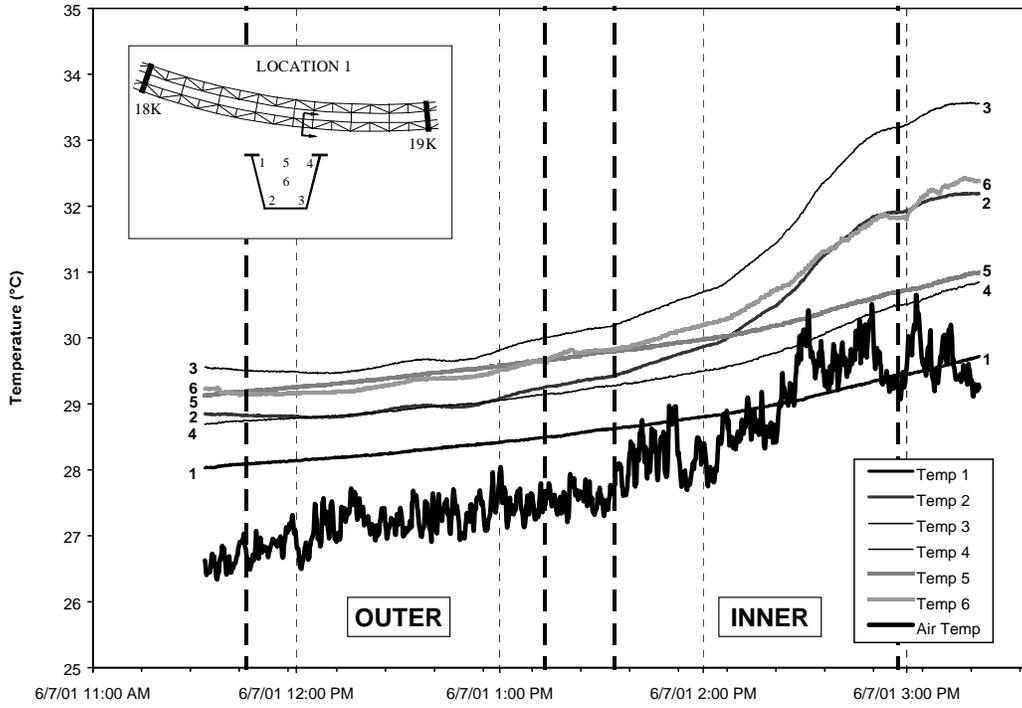
Figure 5.11 Temperatures at Location 1 during Live Load Test
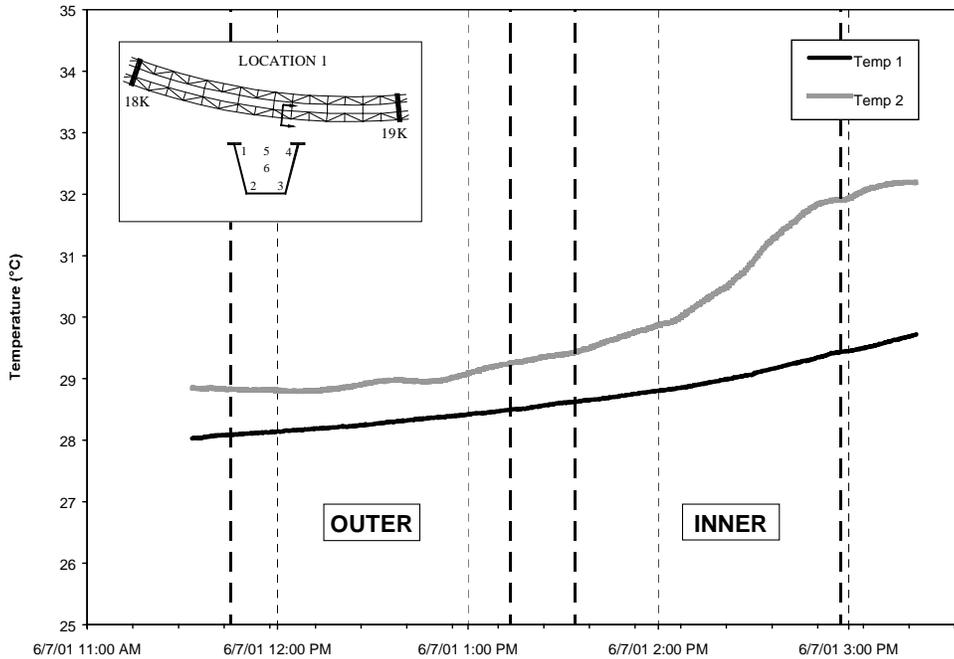
Figure 5.12 Temperatures at Location 1 on Inner Side of Girder during Live Load Test
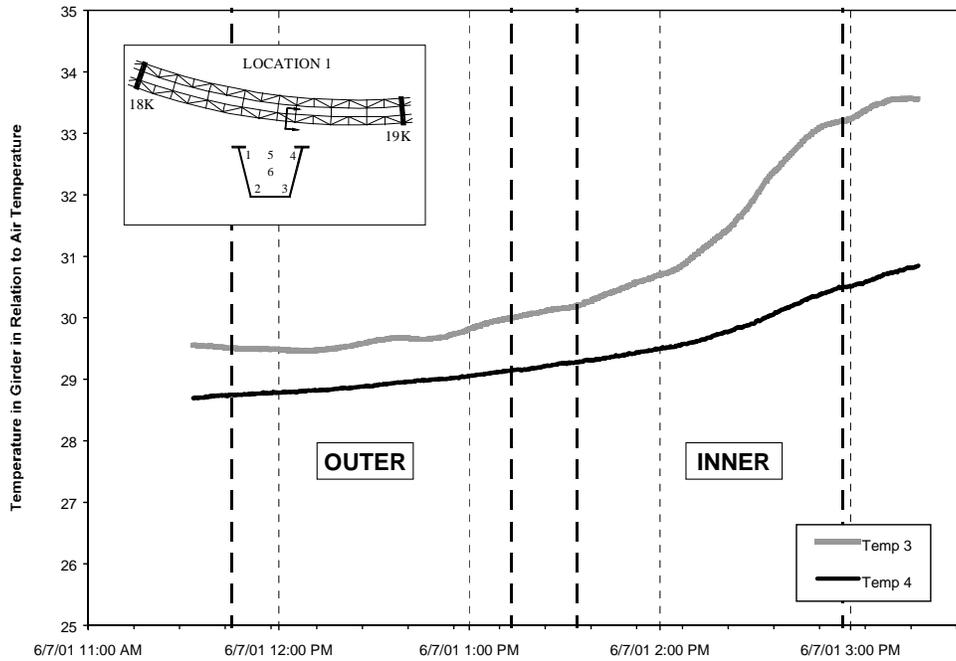
Figure 5.13 Temperatures at Location 1 on Outer Side of Girder during Live Load Test
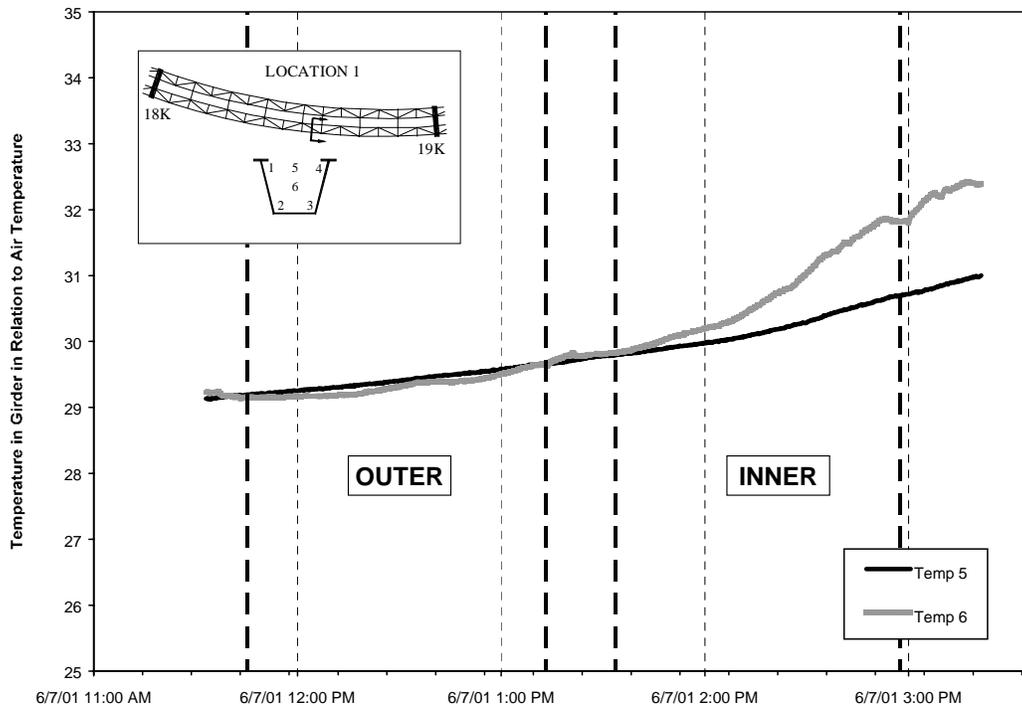
Figure 5.14 Temperatures at Location 1 on Inside of Girder Live Load Test
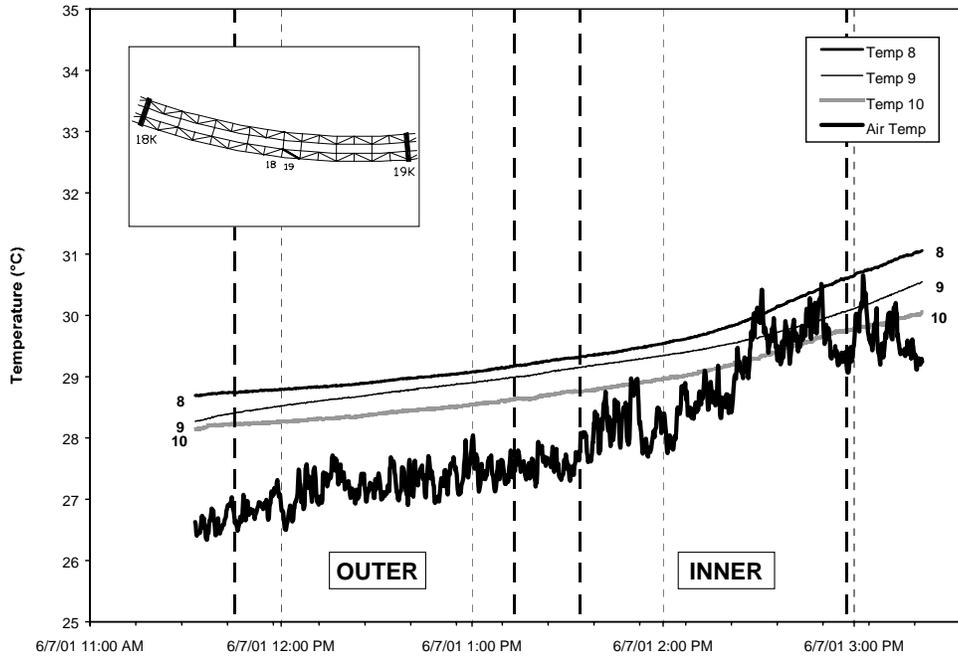
Figure 5.15 Temperatures on Top Lateral at Mid-Span during Live Load Test
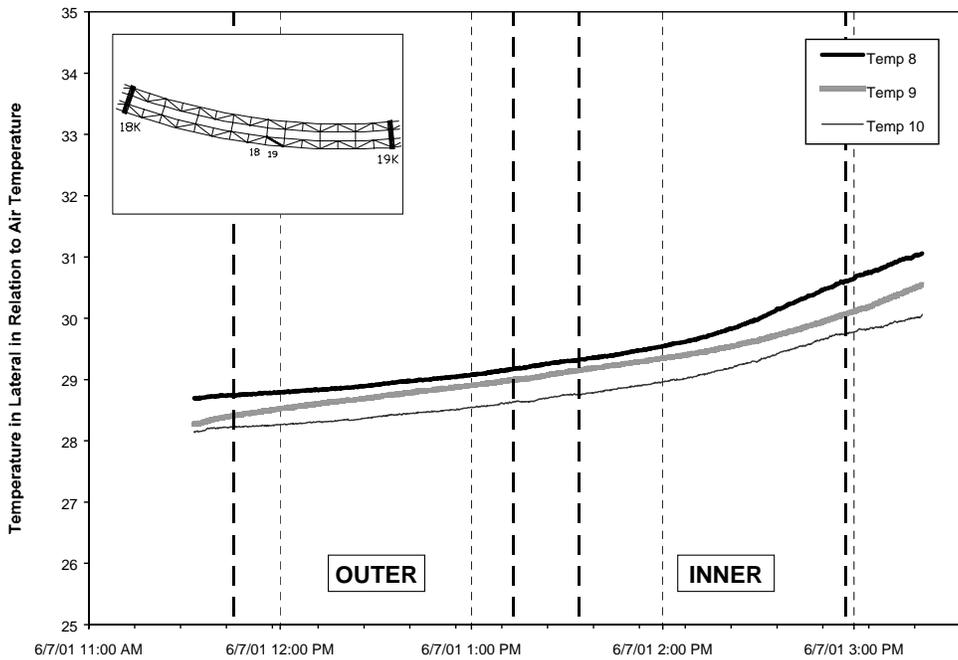
Figure 5.16 Temperatures on Top Lateral at Mid-Span during Live Load Test

All of the instrumented members experienced temperature effects during the outer test. During the inner run, the instrumented top laterals near pier 17K were significantly affected, while the effect was minor in the instrumented top laterals at mid-span. The same is true for the girder cross sections. On the external

diaphragms, only the horizontal members experienced any temperature effect; the diagonals were basically unaffected by the change in temperature. The top horizontal member in each diaphragm felt a minor effect, while there was a very large effect on the bottom horizontal members. The largest temperature effect recorded was in the bottom horizontal members of diaphragm #18. There were approximately 6 kips of axial force in these members at the end of the inner run.

This temperature effect was accounted for by applying a linear temperature correction to all of the data from the live load test, as was performed for the Z-Connect data. The temperature-corrected data at any time during the test run were determined by linear interpolation. For example, the axial force in member #18-2 at the final position of the inner test was -6.2 kips (the duration of the inner test was approximately 1.4 hours). At the middle of test, approximately 0.7 hours into the test, the temperature correction applied was approximately +3.1 kips. A full plot of the axial force in member #18-2 during the inner girder truck run before and after temperature correction is shown in Figure 5.17 as an example.
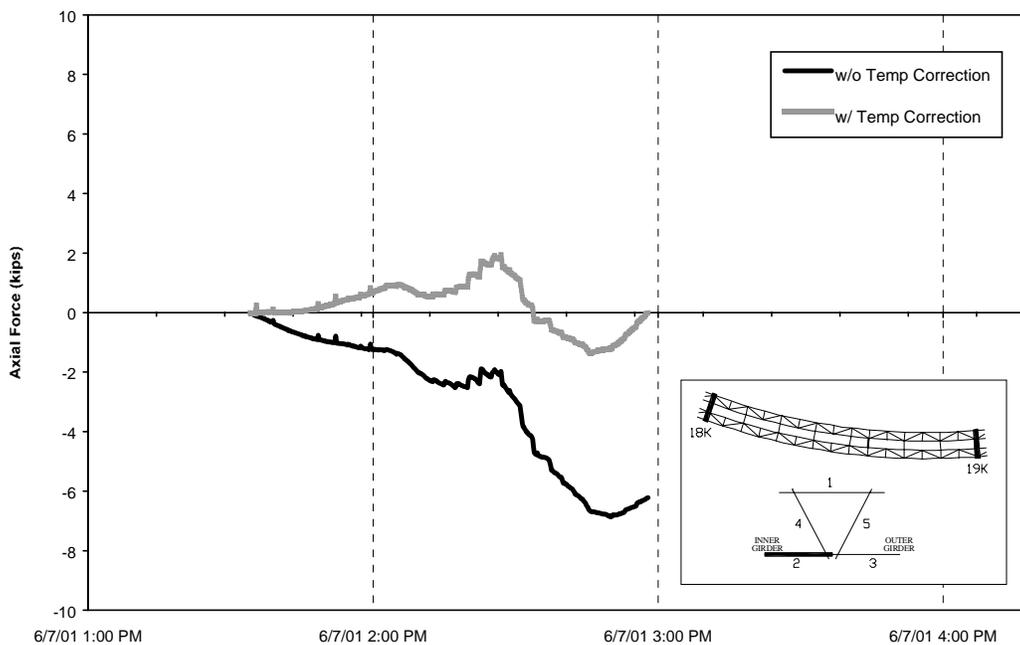
Figure 5.17 Temperature Correction for Diaphragm #18-2
during Live Load Test over Inner Girder

5.3   DIAPHRAGM RESULTS

5.3.1   Z-Connect

5.3.1.1 Experimental Results

The external diaphragm member forces were determined by subtracting a linear estimation of the temperature effects from the measured force calculations. An example of this technique is shown in Figure 5.18 and Figure 5.19 on a member. The first graph is the original measured axial forces in one of the diagonals. A line representing the estimated temperature effect is superimposed over the plot from the origin to the last data point. The difference between the measured force and the line is the estimated axial force due only to the weight of the trucks. The plateaus on the plots are caused from multiple data readings while the trucks are stationary.
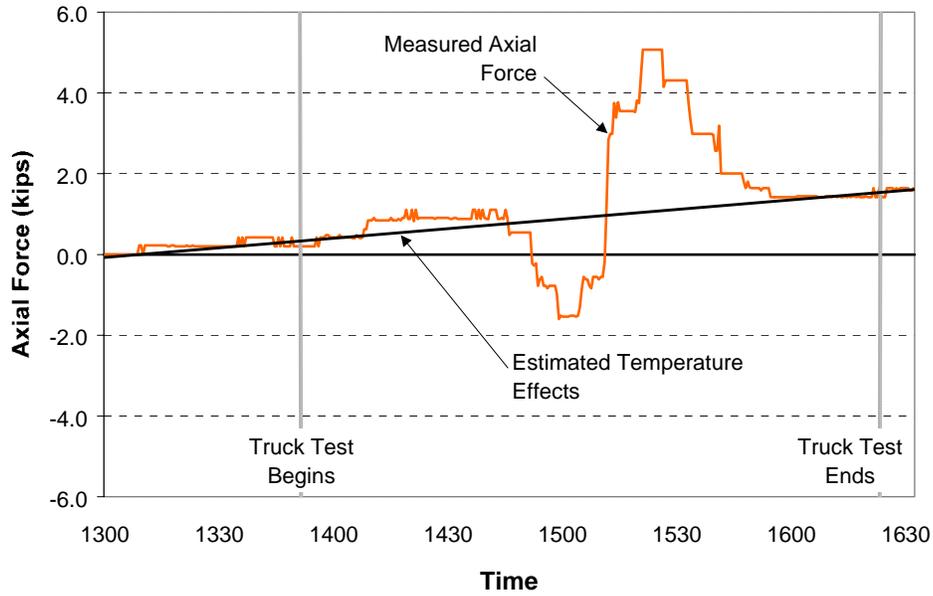
Figure 5.18 Measured Diaphragm Forces – Diagonal
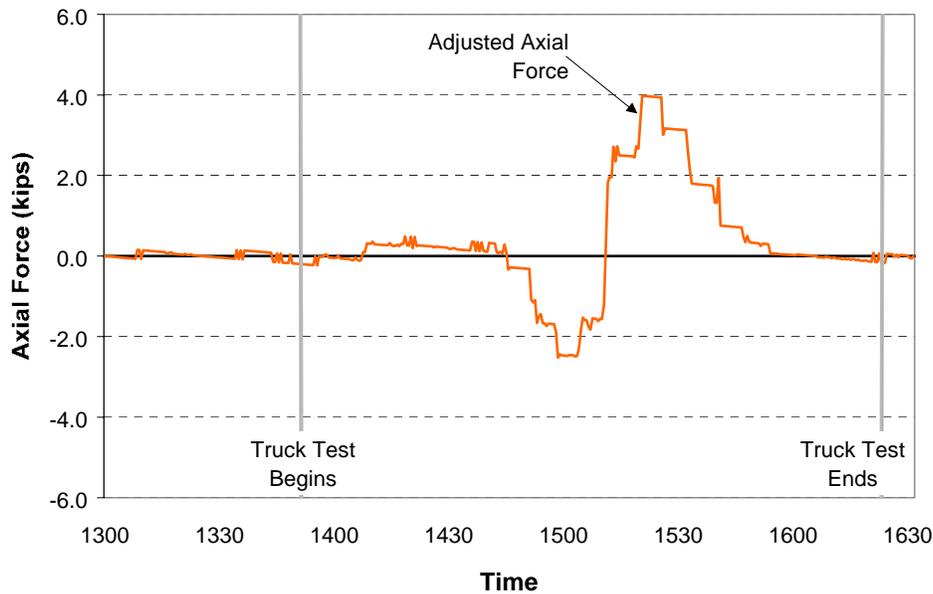
Figure 5.19 Adjusted Diaphragm Forces for Temperature Effects – Diagonal

This method of adjusting the measured forces by subtracting the temperature effects was used for the remainder of the diaphragm force calculations in this section. Figure 5.18 shows a substantial change in force from before and after the load test. In Figure 5.19, the axial force in the member remains fairly constant as the trucks are left in each position. There is a reversal in force at time 1510 (3:10pm) as the trucks are moved from the outer side of the curve (position 10 - Figure 5.21) to the inner side (position 11).

Figure 5.20 and Figure 5.21 show the labeling system for the external diaphragms and their members. Diaphragm A had very little response during the load test. Member A1 had a change in axial force between

0-0.6 kips. This is relatively close to the expected error in the readings. Therefore, only diaphragms B and C will be examined in this section. Half of the members on diaphragms B and C were reading reliable force measurements during the truck load test. Influence lines are shown for these members in Figure 5.22 through Figure 5.24. For each truck position, seven to eight data points are plotted. Ideally the data points at a certain truck position should identical. Therefore, the fewer points shown at a position yields more repeatability. Many of the symbols for the data points overlap on the graphs.
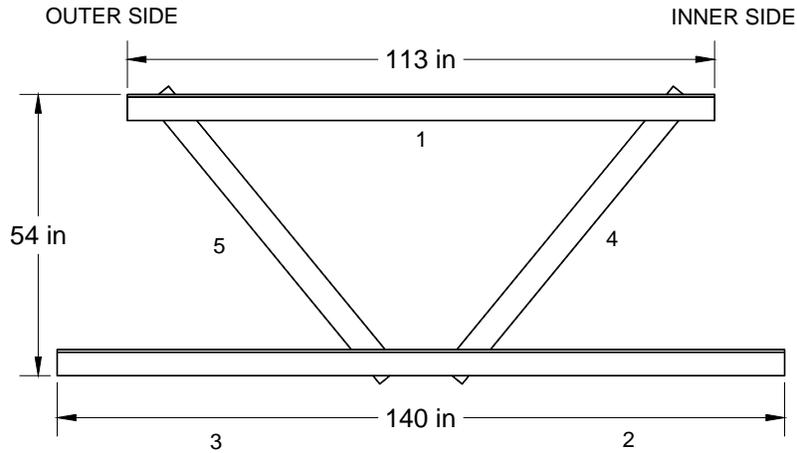
Figure 5.20 External Diaphragm
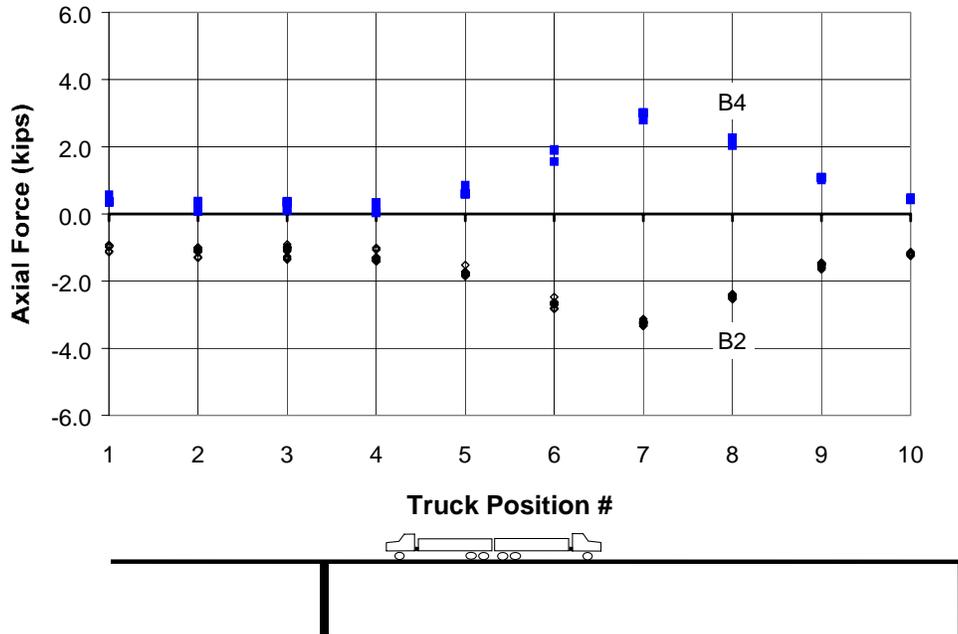
Figure 5.21 Outer Side Influence Line for Diaphragm B
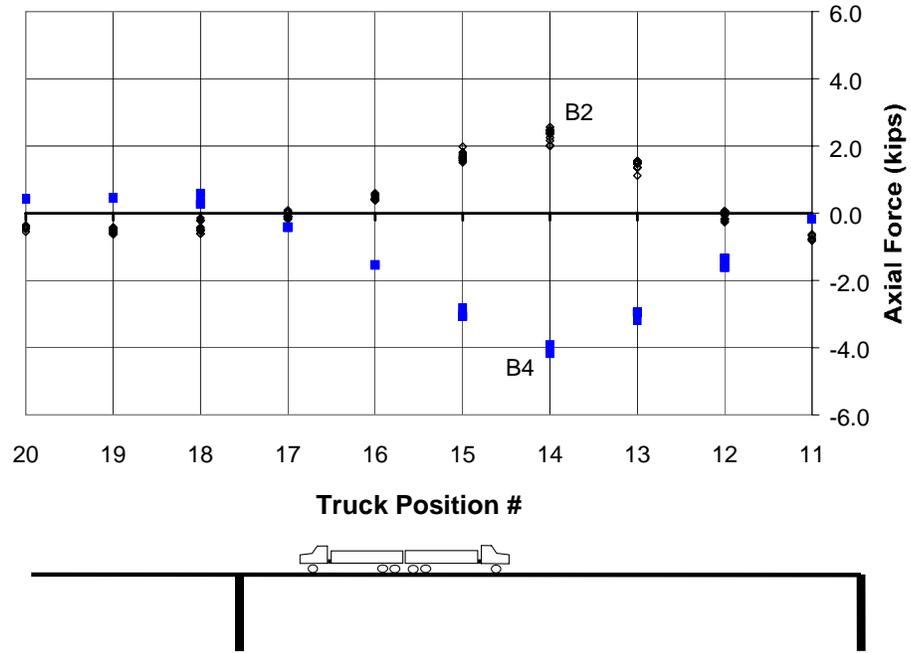
Figure 5.22 Inner Side Influence Line for Diaphragm B
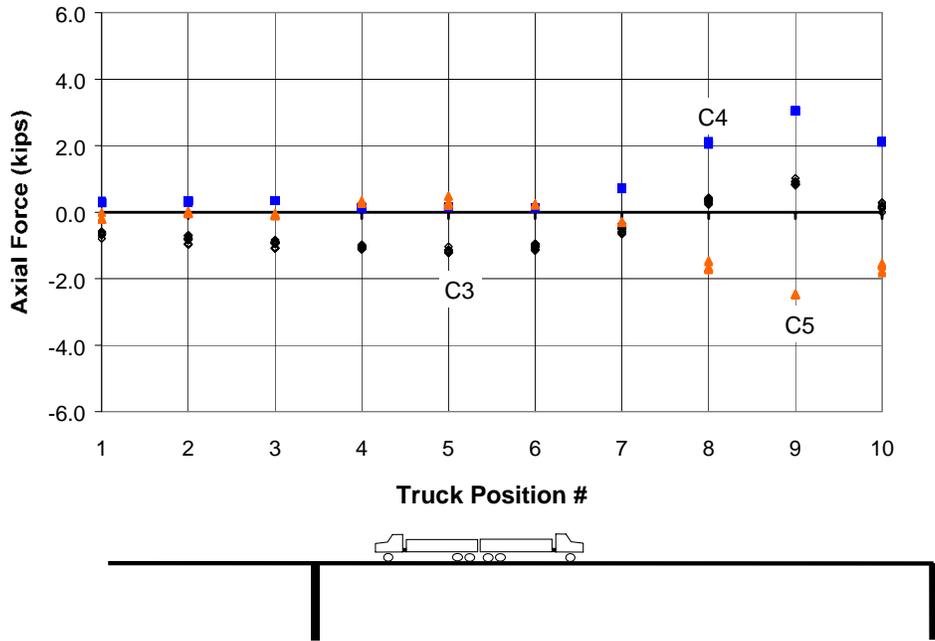
Figure 5.23 Outer Side Influence Line – Diaphragm C
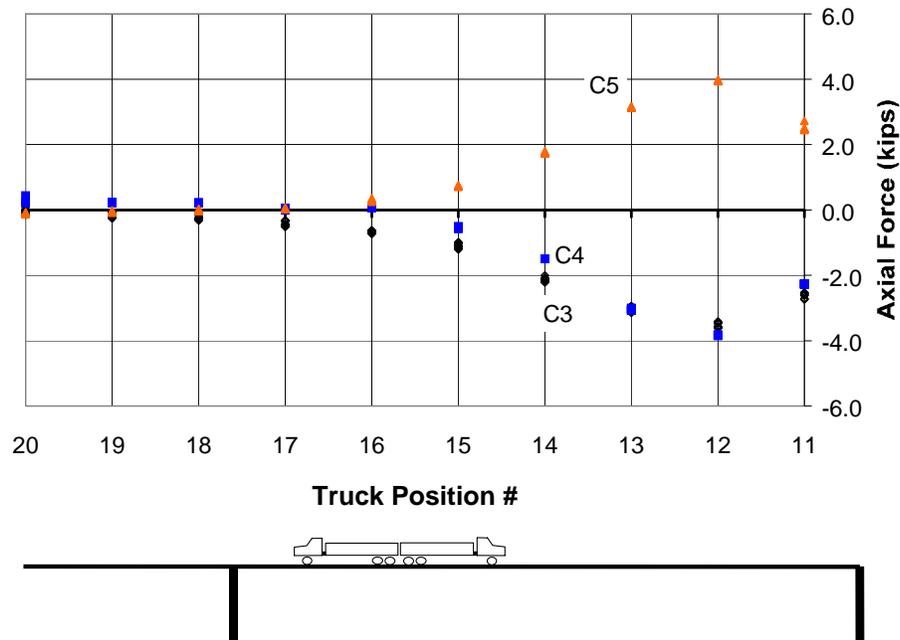
Figure 5.24 Inner Side Influence Line – Diaphragm C

As expected, the greatest magnitudes in diaphragm forces were measured while the trucks were positioned at the external diaphragm. Figure 5.21 and Figure 5.22 show that truck positions 7 and 14 produce the highest forces in diaphragm B. Similarly, Figure 5.23 and Figure 5.24 show the highest forces in diaphragm C occur when the trucks are in positions 9 and 12.

5.3.2   *Predicted Results*

The FEM of the composite girder modeled the concrete slab as having a modulus of elasticity of 4000 ksi. The estimation of concrete stiffness was based on the equation from the current *AASHTO LRFD Bridge Design Specifications,* $E = 57000\sqrt{f'_c}$, where f'_c is the 28-day concrete strength equal to 5000 psi. Analyses were performed using a higher modulus of elasticity of concrete than expected (E=5000 ksi) and it was found that the FEM diaphragm forces were not very sensitive (approximately 3% difference).

The model generally predicted the same type of response out of the diaphragms as measured, although the forces that were predicted were higher. In general, the forces predicted by the model were 2-3 times higher than measured from the load test. Figure 5.25 through Figure 5.28 show the comparison between the predicted and measured axial forces in the diaphragm members. The measured force shown in each figure is the average of the force readings while the trucks remained in a certain position.

In every member, the trends in the measured and predicted forces are the same although the measured forces were considerably less than predicted with the FEM. The highest measured forces from the load test were in the diagonal members while the trucks were positioned over the inner girder. Diaphragm member B4 recorded up to 4.0 kips compression when the trucks were in position 14 and diaphragm member C5 recorded 4.0 kips tension when the trucks were in position 12. In contrast, the FEM predicted 11.2 kips compression in member B4 and 10.9 kips tension in member C5 while the trucks were in these positions.
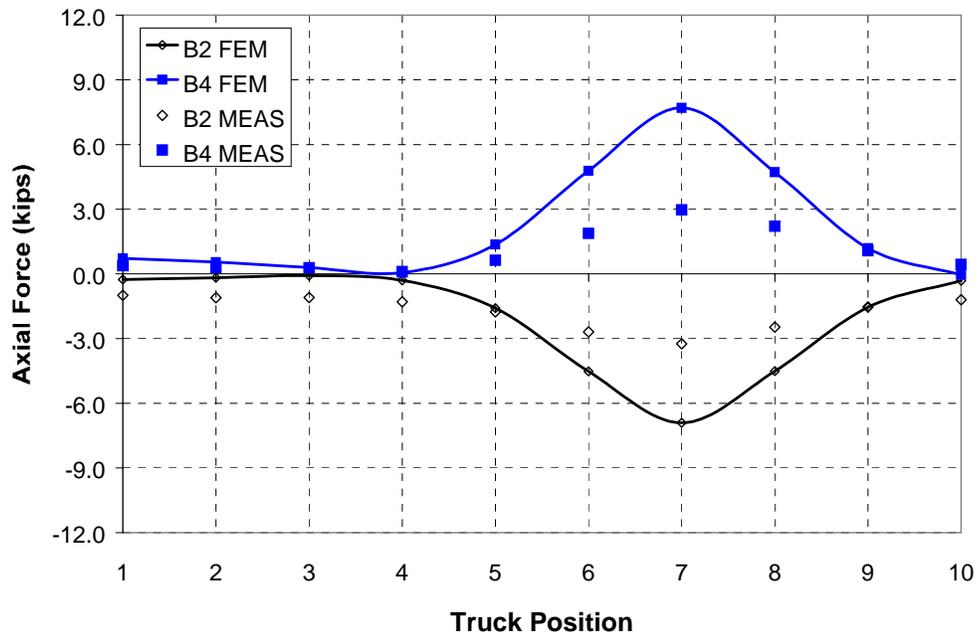
Figure 5.25 Outer Side – Measured and Predicted Forces in Diaphragm B
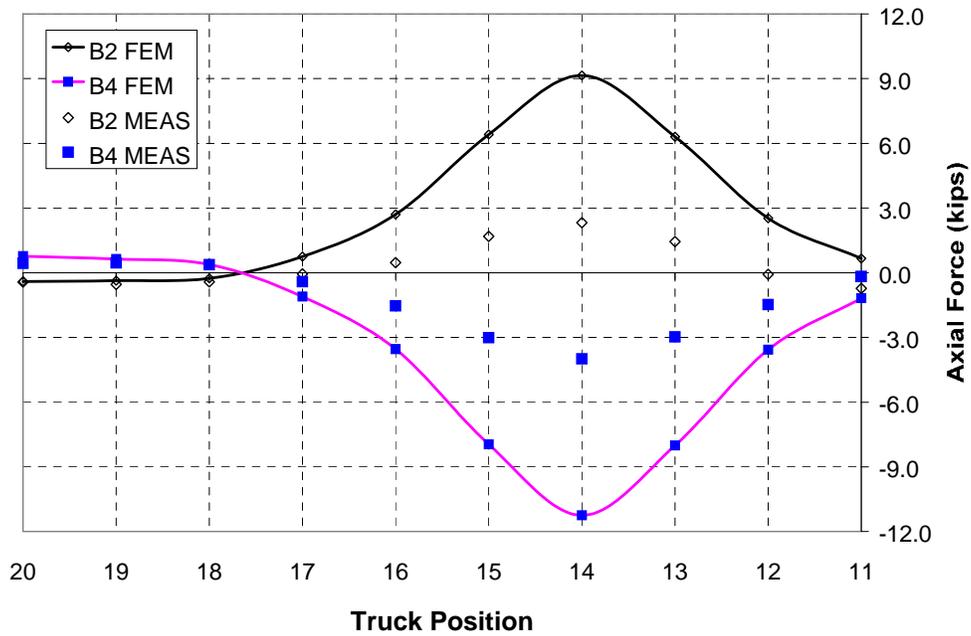
Figure 5.26 Inner Girder – Measured and Predicted Forces in Diaphragm B
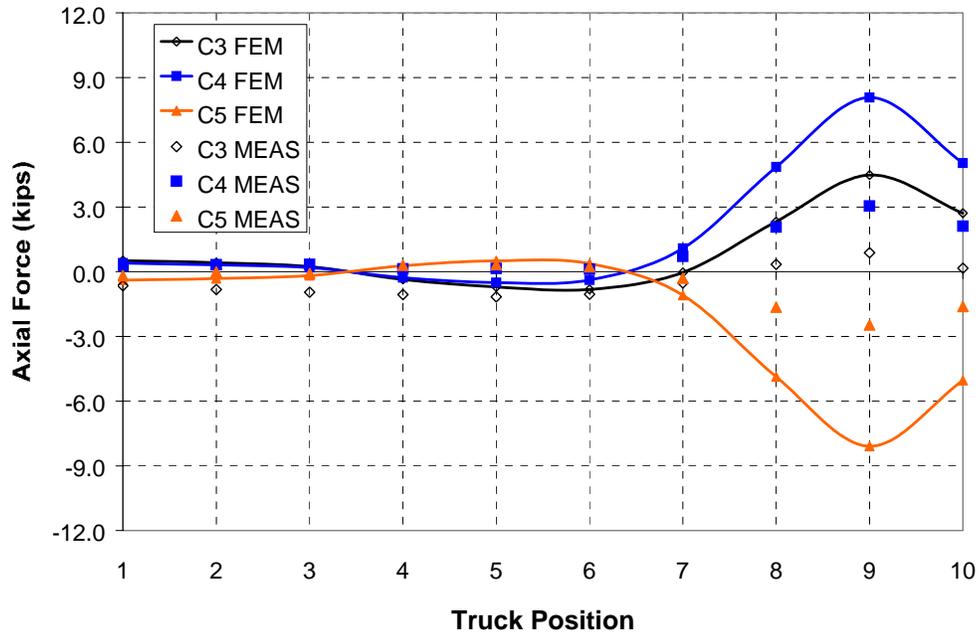
Figure 5.27 Outer Girder – Measured and Predicted Forces in Diaphragm C
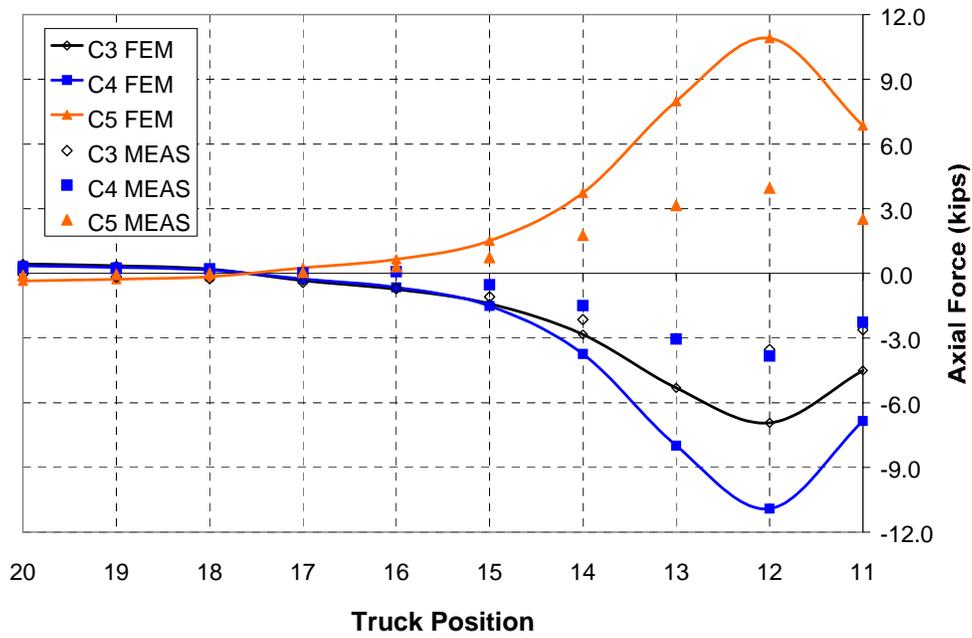
Figure 5.28 Inner Girder – Measured and Predicted Forces in Diaphragm C

5.3.3 K-Connect

The values of axial forces and stresses determined from the strain gauge data in the instrumented locations and cross sections were used to create influence curves of axial force/stress versus truck position. The axial forces and stresses at each position were calculated by averaging all of the values collected at that position. For example, the trucks sat at outer girder position 6 during the live load test from approximately 12:10 P.M. until approximately 12:12 P.M. The axial forces and stresses presented for this position is the average of all readings (one reading each 10 seconds). In all cases, there was little scatter in the readings at each position.

The measured influence curves were compared with influence curves created using predicted values determined by Topkaya using the bridge finite element model (FEM). Samples of the results are shown in Figures 5.29, 5.30, and 5.31. Figure 5.29 shows an example of measured influence curve that matches up very well with the corresponding predicted influence curve. Figure 5.30 shows an instance when the measured influence curve is lower than expected. Shown in Figure 5.31 is a measured influence curve that is larger than the predicted influence curve.

There were three instances when data did not record during the live load test for unknown reasons; however, these instances only lasted one, two, and three minutes, respectively. There was still enough data to calculate the axial force and stress values at all truck positions; therefore, this is not a concern.
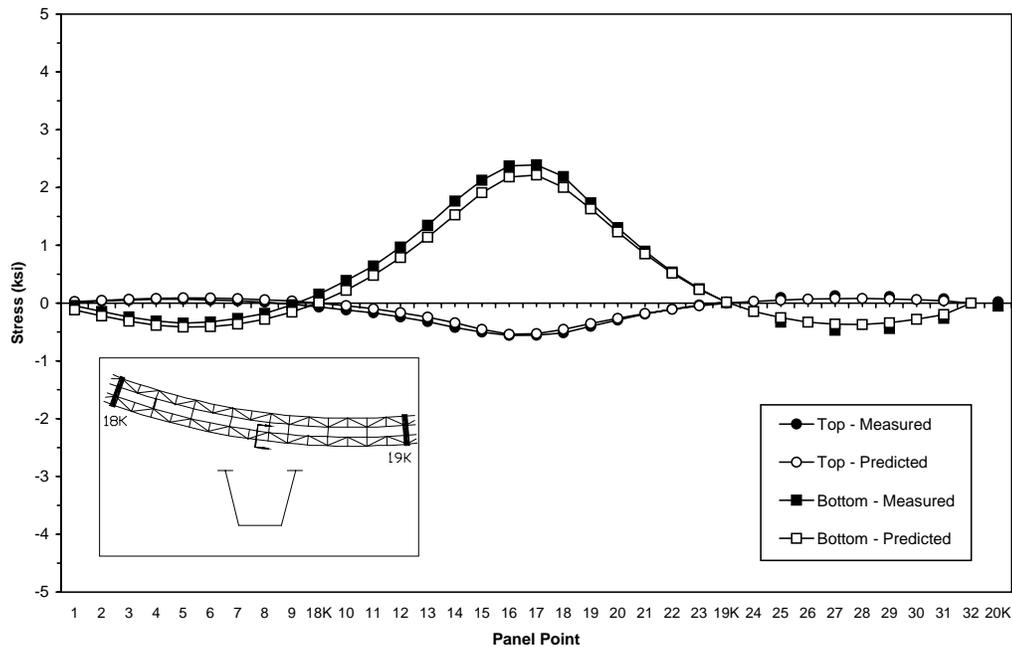
Figure 5.29 Outer Girder 8 Panels from Pier 18K during Live Load Test over Inner Girder, Comparison
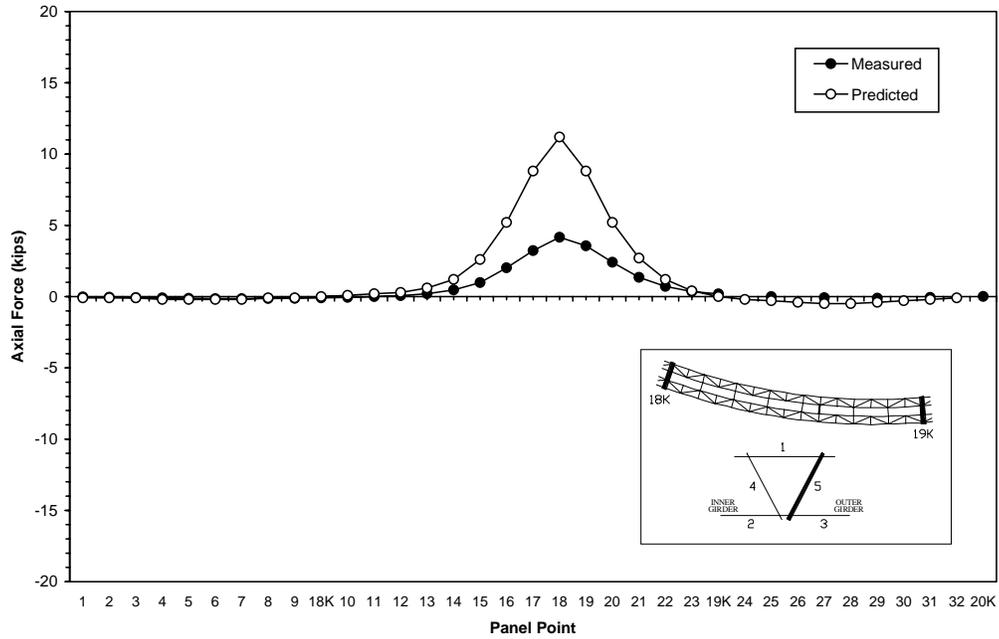
Figure 5.30 Diaphragm #18-5 during Live Load Test over Inner Girder, Comparison
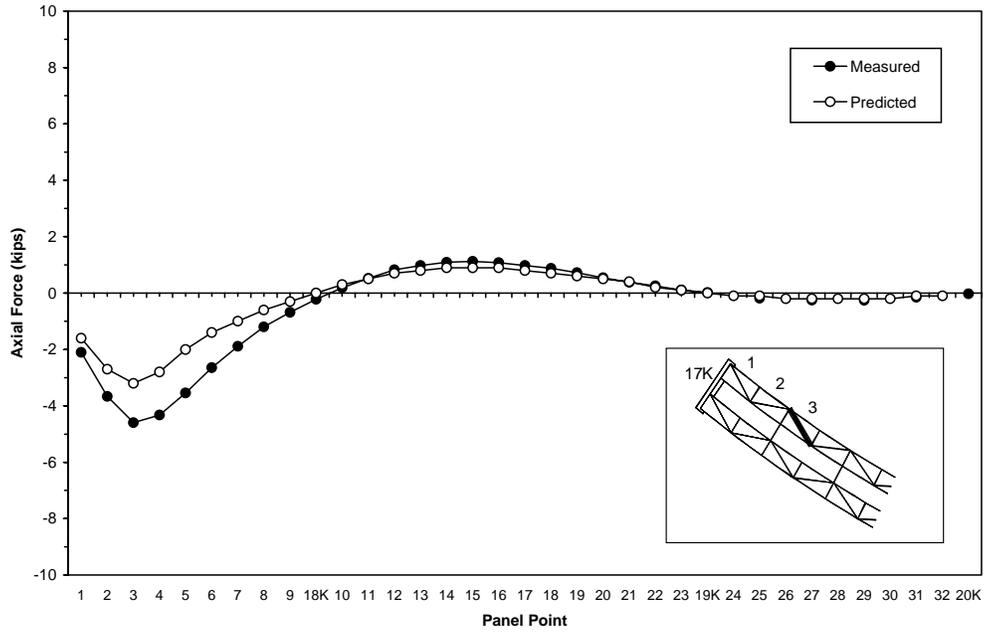
**Figure 5.31 Inner Girder Top Lateral 3 Panels from Pier 17K during
Live Load Test over Outer Girder, Comparison**

5.4 DISCUSSION OF Z-CONNECT RESULTS

The measured forces in the external diaphragm members during the truck load test were comparable to the magnitude of induced forces from temperature gradients in the bridge. The changes in temperature-induced forces were estimated as linear with time and were subtracted from the original data to calculate the forces caused only from the trucks. This approximation adds some uncertainty to the accuracy of the measured results.

The measured forces in diaphragms B and C were much lower than predicted in the FEM. The predicted forces did not change significantly with a reasonable change in the estimation of deck stiffness. One reason for the overestimation of forces could be due to the reduction in diaphragm stiffness caused by the connection detail, as discussed in Chapter 3. The reduced diaphragm stiffness will have a larger effect on predicting diaphragm forces on the composite bridge than it did before the deck was cast. This is because the girders are much stiffer as a closed section and less force is distributed between girders since the diaphragms are relatively flexible. The reduction in diaphragm stiffness due to the connection detail was not accounted for in the FEM. However, there may be other reasons for the large discrepancy between the predicted and measured results. Further investigation is required to achieve a more accurate prediction of the external diaphragm forces after the bridge is composite.

CHAPTER 6:
SUMMARY AND CONCLUSIONS

6.1 SUMMARY

Forces in the external diaphragms and top lateral-bracing members were measured during the construction of 3 three-span trapezoidal steel box girder bridges in Austin, Texas. The stresses in the bridge were monitored during three different loadings. A load test on one bridge was performed before the concrete placement using a crane equipped with a load cell. Measurements were taken on all bridges during the casting of concrete deck, the construction stage when the highest stresses are expected in the bracing and diaphragm members. The third loading used trucks that were moved along the length of bridge and also moved laterally across the deck on the two of the completed composite bridges. The measured forces in these members were compared to analysis using a Finite Element Model (FEM).

6.2 DIAPHRAGM FORCE MEASUREMENTS

The diaphragm used on the instrumented bridge consisted of singly symmetric angle members arranged as a K-frame. The angles were welded back-to-back which created an eccentric connection. Lab tests were performed on individual angle members and on a similar K-frame as used on the bridge to determine a reliable instrumentation configuration. It was found that the eccentricity of loading produced high bending stresses in the members when loaded axially. This reduced the accuracy of the angle force measurements since small errors in strain measurement or gage locations could lead to large errors in force calculations. It was estimated from the lab tests results that 10-15% reliability could be expected in the diaphragm measurements.

6.3 CRANE LOAD TEST RESULTS

The crane used an attachment to lift on the outer girder a fraction of the dead weight of the bridge. The test was performed as a reliable comparison between the measured and predicted forces with a known load. The FEM predicted the axial forces in the top lateral bracing members in both the inner and outer girders very well during the crane load test. The load can only be transmitted from the outer girder to the inner girder through the use of external diaphragms. However, the measured outer girder lateral forces were higher than predicted and the measured inner girder lateral forces were lower than predicted. This means that the distribution of load through the diaphragms was lower than expected.

The shear and moments in the diaphragm can be determined by measuring the axial forces in the diaphragm members. On one diaphragm, it was found during the crane load test that the measured shear and torsion transferred from the outer girder to the inner correlated very well with predicted results. Another diaphragm measured higher shear, but much less torsion than predicted. The third diaphragm was far away from the crane lift points and had very small forces as predicted.

6.4 CONCRETE DECK POUR

Early composite action was evident from measurements in the top lateral forces. The concrete deck provided significant stiffness to the bridge within hours after being poured. The partially hardened deck stiffens the girders by creating a closed composite section and provides a continuous connection between the girders increasing the sharing of the load between the two girders. The forces in the external diaphragm members were much less then predicted in the non-composite model of the bridge. This contribution is difficult to model since the concrete stiffness is uncertain and changes with time.

In general, the measured forces in the diaphragms were much lower than predicted with the FEM. The behavior of the diaphragms, namely the ratio of shear to moment transferred through the diaphragm, is

relatively the same as predicted by the FEM. When the pour was over the same span as the diaphragm, the diaphragm restrained the top of the girders from twisting away from the center of bridge curvature. The magnitude of restraint, both vertical displacement and twisting of the girders, was generally much smaller than predicted. This means that the ratio of girder stiffness to diaphragm stiffness was higher than predicted.

Overall, the FEM predicted the same behavioral response in the diaphragms as measured, although it generally overestimated the amount of contribution the external diaphragms have in restraining the girders. The maximum axial stress measured in all of the external diaphragm members due to the weight of the concrete was about 3ksi. In comparison, the top lateral members that were measured had axial stresses up to 7ksi from the concrete pour.

The measured stresses in the top lateral system during the staged casting of the concrete deck were substantially less than the results of the non-composite bridge analysis in all the bridges. The rapid hardening of the concrete raises the neutral axis of section reducing the stresses in the lateral change in length of the top flange. In addition, the hardened concrete closes the top of the box producing a closed box structure. The forces introduced into the lateral systems due to the torsional loading of the curved box are very small. Only the first pour produced significant forces in the laterals.

6.5   TRUCK LOAD TEST

Two trucks were positioned over several different points on the composite girder bridge. They were placed in a back-to-back configuration very close to the edge of the concrete deck to maximize the response out of the external diaphragms. Unfortunately, the test occurred over several hours during the day and the changes in diaphragm forces due to temperature were comparable to the forces due to the truck loads. This decreased the accuracy of the measured results since the temperature effects had to be estimated. However, it was clear that the diaphragm forces were still much less than predicted by the FEM. Again the behavior of the diaphragm action correlated well with the model, but the magnitude of forces were considerably less. The diaphragm forces measured during the load test were between 25-50% of the predicted forces.

6.6   FINITE ELEMENT MODEL

Generally, the finite element model overestimated the amount of force distributed from one box girder to the other. This means that the ratio of girder stiffness to diaphragm stiffness was higher than predicted. There are several possible reasons for the discrepancy in the measured and predicted results.

The connection detail from the diaphragm to each box girder caused a significant loss in diaphragm stiffness when the connection transferred tension. It was found that the WT stub that was bolted to the stiffened web of the girder could bend away from the girder when tensioned. This detail is difficult to model since the reduction in stiffness would only occur when the connection has net tension. If the diaphragms are prestressed (from temperature effects or stresses during erection), the connection will be in tension or compression during future loadings. If the connection has residual compression, a small tensile force on the angle would first relieve the compression and no loss in stiffness would occur at the connection. Conversely, if the connection has residual tension, even a compressive force would cause a reduction in stiffness in the diaphragm.

Another reason for the discrepancy is that the diaphragm in the model is connected to the girder at full depth. The real diaphragm is only about 70% of the depth of the girders. For the analysis to model the true depth of the diaphragm, a more detailed mesh would be required.

One other source of error is that the model does not consider any stiffness from the permanent metal deck forms that are placed between the top flanges of the girders. Although the forms are very thin, they can act as a shear diaphragm and provide additional bracing to the flanges. They also add torsional stiffness to the U-girders by closing the cross section.

REFERENCES

AASHTO LRFD Bridge Design Specifications, (1996), American Association of State Highway and Transportation Officials.

Basler, K., and Kollbrunner, C. F. (1969). *Torsion in Structures.* Springer-Verlag, Berlin, Germany, pp. 14-15.

Bridge Design Manual, (1991), Colorado Department of Transportation. Accessed through http://www.dot.state.co.us.

Chen, Brian S. (1999). "Buckling of U-Shaped Girders with Top-Flange Lateral Bracing," thesis presented to The University of Houston, in partial fulfillment of the requirements for the degree of Master of Science.

Cheplak, B.A. (2001). "Field Measurements of Intermediate External Diaphragms on a Trapezoidal Steel Box Girder Bridge," thesis presented to The University of Texas at Austin, in partial fulfillment of the requirements for the degree of Master of Science.

Davidson, J. S., Keller, M. A., Yoo, C. H. (1996). "Cross-Frame Spacing and Parametric Effects in Horizontally Curved I-Girder Bridges." *Journal of Structural Engineering,* Vol. 122, No. 9, September, pp. 1089-1096

Fan, Zhanfei. (1999). "Field and Computational Studies of Steel Trapezoidal Box Girder Bridges," thesis presented to The University of Houston, in partial fulfillment of the requirements for the degree of Doctor of Philosophy.

Fan, Zhanfei and Helwig, Todd A. (1999). "Behavior of Steel Box Girders with Top Flange Bracing." *Journal of Structural Engineering*, Vol. 125, No.8, August, pp. 829-837.

Guide Specifications for Horizontally Curved Highway Bridges. (1993) American Association of State Highway and Transportation Officials.

Lopez, Michael G. (1999). "Thermally-Induced Deformations and Stresses in a Steel Trapezoidal Twin-Box Girder Bridge," thesis presented to The University of Texas at Austin, in partial fulfillment of the requirements for the degree of Master of Science in Engineering.

Memberg, Matthew A. (2002). "A Design Procedure for Intermediate External Diaphragms on Curved Steel Trapezoidal Box Girder Bridges," thesis presented to The University of Texas at Austin, in partial fulfillment of the requirements for the degree of Master of Science in Engineering.

Recommended Specifications for Steel Curved-Girder Bridges, (1998), National Cooperative Highway Research Program, Transportation Research Board, National Research Council.

Topkaya, Cem. (2002). Behavior of Curved Steel Trapezoidal Box Girders during Construction, "Field Measurements of Intermediate External Diaphragms on a Trapezoidal Steel Box Girder Bridge," dissertation presented to The University of Texas at Austin, in partial fulfillment of the requirements for the degree of Doctor of Philosophy.

Zureick, A., Linzell, D., Leon, R. T., Burell, J. (2000). "Curved Steel I-Girder Bridges: Experimental and Analytical Studies." *Engineering Structures,* Vol. 22, No.2, pp. 180-190. Accessed through Elsevier Science Ltd.